

**DATING THE STONE AGE
AT ROSE COTTAGE CAVE
SOUTH AFRICA**

An exercise in optically dating cave sediments

BY

Marc Pienaar

Submitted in fulfillment of the requirements for the
degree of Master of Archaeology
in the Faculty of Humanities
University of Pretoria
Supervisor: Dr S Woodborne

6 October 2005

ABSTRACT

Results and analysis of Optically Stimulated Luminescence (OSL) dating of the Middle Stone Age (MSA) and Later Stone Age (LSA) sediments at Rose Cottage Cave (RCC) are presented. Seventeen luminescence samples taken over the last decade were used in this study. Fourteen of these samples were dated (eight in Pretoria and six in Risø, Denmark by A. S. Murray). The samples were taken from the entire sequence and gave age ranges from the bottom of the sequence up until the Oakhurst LSA industry.

The protocol that was used is the conventional single-aliquot regenerative (SAR) protocol, due to its ability to correct for behavioural problems associated with OSL dating. This study is primarily concerned with testing the validity of the conventional SAR protocol applied to South African archaeological sites. RCC presents problematic sediments for OSL dating because of a high feldspar component in the sediments at the site (OSL dating is preferably done on quartz grains due to a better understanding of the mechanisms of OSL production). Assessing the radiation dose samples received during their burial period was problematic due to the large presence of potassium rich feldspars. Assessing the radiation dose was problematic because the measurement of potassium (K) returned different values using several independent techniques. The mode of sediment deposition via different depositional mechanisms such as, fluvial, and clast spalling present difficult challenges in assessing the zero age value of a sample.

OSL ages were compared to a well defined radiocarbon chronology from RCC, and any inconsistencies would motivate closer sorting of the different dating techniques. In this study it was found that not all feldspar grains were removed from the quartz extracts during pretreatment procedures. The ability of the SAR protocol to pick out feldspar contamination was therefore not conclusive, and single grain measurements had to be used to differentiate quartz and feldspar grains.

The likelihood of age contamination from problematic depositional events was not supported and the results suggest that aeolian deposition was the main mechanism at the site. The vertical separation of depositional events i.e. the varying archaeological events, is very dense at RCC and this introduces the possibility of sample mixing during collection. For a few samples it is shown that sample mixing has occurred as mixing is usually evident in the degree of scatter in the OSL results.

After all the inconsistencies in OSL/Radiocarbon age correlations were worked out, a coherent OSL chronology was obtained. Certain issues surrounding dosimetry however, are still not resolved. These issues are beyond the scope of this study and so caution is advised when using OSL dates done with little or no dose-rate analysis.

The resulting dates provide a useful dataset for archaeologists who now have added resources to assess the Middle Stone Age (MSA) and better compare synchronous evidence from different sites in order to contribute to the debate surrounding the origins of modern humans and modern human behaviour. These results combined with the well established radiocarbon chronology give age ranges as follows: The Pre-Howiesons Poort (Pre-HP) MSA IIb industry is between 94 and 68 thousand years ago (ka); the Howiesons Poort (HP) industry is between 68 and 55 ka; the Post –HP MSA III dates to between 55 and 48 ka; the ‘almost sterile sands’ (which include the MSA IV industry) are between 48 and >27 ka; the MSA/LSA transition is between 27 and 20 ka; the Robberg LSA industry is between 20 and 10.5 ka; the Oakhurst LSA industry ranges from 10.5 to 8.5 ka; and the Wilton LSA industries are <8.5 ka.

OPSOMMING

Uitslae en ontleding van Opties-gestimuleerde Ligtingsdatering of “Optically-stimulated Luminescence Dating” (OSL) van die middel steentydperk (MSA) en latere steentydperk (LSA) sedimente by Rose Cottage Cave (RCC) word voorgelê. Sewentien ligtingsmonsters wat oor die afgelope dekade geneem is was in hierdie studie gebruik. Veertien hiervan was gedateer (agt in Pretoria en ses in Risø, Denemarke deur A.S. Murray). Die monsters was geneem uit die hele volgreeks en het ouderdomsreeks opgelewer vanaf die bodem van die reeks tot en met die Oakhurst laatsteentydperk (LSA) bedryf.

Die protokol wat gebruik is, is die konvensionele enkel-alikwot herskeppende of “single-aliquot regenerative” (SAR) protokol vanweë dié se vermoë om gedragsprobleme met OSL datering te korrigeer. Die studie is hoofsaaklik gemoeid met toetsing van die geldigheid van die konvensionele SAR protokol soos toegepas op Suid-Afrikaanse argeologiese terreine. RCC bied problematiese sedimente vir OSL datering as gevolg van ‘n groter feldspar komponent in die sedimente van die terrein (OSL datering word verkieslik gedoen op kwartskorrels as gevolg van ‘n beter begrip van die meganismes van OSL produksie). Raming van die bestralingsdosis wat monsters ontvang het in die tyd wat hulle begrawe was, is vergemoeilik deur die teenwoordigheid van groot hoeveelhede kaliumryke feldspar. Raming van die bestralingsdosis was problematies want die meting van kalium (K) het verskillende waardes gelewer wanner verskeie onafhanklike tegnieke gebruik is. Die wyse van neerlegging van sedimente deur middel van verskillende neerleggingsmeganismes soos fluviale en klast afsplintering bied moeilike uitdagings vir raming van die nul ouderdomswaarde van ‘n monster.

OSL ouderdomme is vergelyk met ‘n goedgedefinieerde radiokoolstof kronologie vanaf RCC en enige teenstrydighede sou dan motivering wees vir ‘n nadere sortering van die verskillende dateringstegnieke. In die studie is gevind dat nie alle feldsparkorrels uit die kwartsuittreksels verwyder is tydens

voorafbehandelingsprosedures nie. Die vermoë van die SAR protokol om felsparbesoedeling uit te lig is derhalwe nie onbetwisbaar bewys nie en enkelkorrel metings moes gedoen word om te onderskei tussen kwarts- en feldsparkorrels.

Die waarskynlikheid van besoedeling van ouderdomme in problematiese neerleggingsgebeurtenisse is nie ondersteun nie en die uitslae dui daarop dat eoliese neerlegging die hoof meganisme was by dié terrein. Die vertikale skeiding van neerleggingsgebeurtenisse dit wil sê die veranderende argeologiese gebeurtenisse is baie dig by RCC en dit bring die moontlikheid van monstervermenging tydens insameling te weeg. Vir 'n paar monsters word daar getoon dat sodanige vermenging wel plaasgevind het want vermenging is gewoonlik duidelik uit die mate van spreiding in die OSL uitslae.

Nadat al die teenstrydighede in OSL/Radiokoolstof ouderdomskorrelasies uitgewerk was, was 'n samehangende OSL kronologie verkry. Sekere kwessies rondom doseringsmeting ("dosimetry") is egter nog nie opgelos nie. Daardie kwessies val buite die omvang van hierdie studie en omsigtigheid word aangeraai waar OSL daterings gedoen word met min of geen doseerverhoudingsontleding ("dose-rate analysis").

Die resultate van die daterings lewer 'n bruikbare datastel vir argeoloë wat nou bykomende hulpbronne het om die middelsteentydperk (MSA) te assesser en beter vergelykings te tref tussen gelyktydige bewysmateriaal vanaf verskillende terreine en daardeur by te dra tot die debat rondom die oorsprong van die moderne mens en sy gedrag. Hierdie resultate gekombineer met die goedgevestigde Radiokoolstof kronologie lewer ouderdomsreekse soos volg: Die Pre-Howiesons Poort (Pre-HP) MSA IIb bedryf tussen 94 en 68 duisend jaar gelede (ka); die Howiesons Poort (HP) bedryf tussen 68 en 55 ka; die Post-HP MSA III tussen 55 en 48 ka; die 'amper steriele sandlae' (wat die MSA IV insluit) tussen 48 en >27 ka; die MSA/LSA oorgang tussen 27 en 20 ka; die Robberg LSA bedryf tussen 20

and 10.5 ka; die Oakhurst LSA bedryf wissel van 10.5 to 8.5 ka; en die Wilton LSA bedrywe is <8.5 ka.

ACKNOWLEDGMENTS

The direction of study that all students decide upon when confronted with the task of doing a Masters degree is a difficult one. This was a situation I found myself in, when the phone rang, and Dr. Stephan Woodborne asked if I was interested in being supervised in a field related to archaeological dating. All of a sudden a variety of study options presented themselves. Needless to say luminescence dating was the one that caught my attention.

I don't know how to thank Stephan enough. Not only has he shown the way that research should be done, but he has helped mould my life. Stephan has helped in getting financial aid, and has taught me life skills that have had profound effects during the last three years. Marrying my beautiful wife Fiona, and having our precious daughter Imogen Rose would not have been possible without financial support, life skills training and encouragement from the staff at QUADRU. To Fiona, her parents (Bob and Bev Harris), and my parents (Jacus and Fay Pienaar): I know it took a little longer than you expected, but I hope you will be proud. To Jason, my brother: sorry you beat me and finished your thesis first, but don't worry I'll beat you at something else (such as marriage).

Then there are the people who helped me gain the skills to understand and apply the dating technique. This is a huge thank you, Gill and Zenobia. Maybe someday I'll also have that sort of patience. Also to Lynn Wadley, who took the time to visit Rose Cottage Cave and help with the sampling. Thank you to Andrew Murray, who dated Rose Cottage Cave and in doing so provided a correlation dataset. Lastly I would like to thank the University of Pretoria and my fellow students from the Department of Anthropology and Archaeology for all the insight provided, and the fun we had together.

TABLE OF CONTENTS

ABSTRACT

ACKNOWLEDGEMENTS

1 INTRODUCTION	1
1.1 Purpose of study	1
1.2 Rose Cottage Cave	1
1.3 What is OSL?	2
1.4 Dating argument	3
1.5 Importance of study	6
2 ROSE COTTAGE CAVE	8
2.1 General Background	8
2.2 Palaeo-environmental reconstruction at Rose Cottage Cave	12
2.3 The archaeology of Rose Cottage Cave	14
2.4 Sampling strategy of Rose Cottage Cave sediments	18
2.5 Isolation of quartz from Rose Cottage Cave	20
3 OSL THEORY AND EQUIPMENT	21
3.1 OSL Theory	21
3.2 Calculation of the depositional age of sediments	24
3.3 Determination of trapped electron populations in the laboratory	24
3.4 Problems associated with OSL dating	26

3.5 OSL Instrumentation	28
3.6 D_e Determination	32
3.6.1 Additive and Regenerative dose protocols	32
3.7 The SAR Protocol	33
3.7.1 Advantages of the SAR protocol	37
3.8 D_e Distributions	39
3.9 Age models	44
4 OSL DOSIMETRY: THEORY AND EQUIPMENT	45
4.1 Dose rate determination	45
4.2 Alpha particle contribution	46
4.3 Beta, gamma and cosmic radiation	48
4.4 Instrumentation used to determine dose rates	51
4.4 Calculation of dose-rates	54
4.5.1 Dose-rate calculation – A worked example	55
5 THE SAR PROTOCOL APPLIED TO THE ROSE COTTAGE CAVE SAMPLES	57
5.1 Sample overview	57
5.2 Rejection criteria	58
5.2.1 Dose recovery experiment	58
5.2.2 Partial bleach test	61
5.2.3 IR-OSL depletion ratio test	63
5.2.4 Sensitivity change	68
5.2.5 Recycling Ratio (R-Ratio) test	73
5.2.6 Recuperation	77
5.2.7 D_e versus T – Preheat Plateau	78
6.3 Analysis of D_e values	82
6 DOSE RATE ANALYSIS	92

6.1 Introduction	92
6.2 Thorium and Uranium analysis	92
6.3 Potassium analysis	95
6.4 Dose-rates for Rose Cottage Cave	96
7 RESULTS, DISCUSSION AND CONCLUSION	101
7.1 Results	101
7.1.1 Resolving age discrepancies between OSL and radiocarbon	106
7.2 Discussion	108
7.3 Conclusion and recommendations	111
APPENDIX A: RADIOCARBON AGE CHRONOLOGY OF ROSE COTTAGE CAVE	113
APPENDIX B: GRAIN SIZE DISTRIBUTIONS OF RCC SAMPLES	116
APPENDIX C: RADIOACTIVITY AND DOSE-RATE DATA	117
C.1 TSAC calculation	117
C.2 Radioactive Decay chains	121
BIBLIOGRAPHY	124

LIST OF FIGURES

FIGURE 1. 1	LOCATION OF ROSE COTTAGE CAVE	2
FIGURE 1. 2	DIFFERENT AGES OF THE HOWIESONS POORT	6
FIGURE 2. 1	PLAN OF ROSE COTTAGE CAVE	11
FIGURE 2. 2	INTERPRETATIONS OF ROSE COTTAGE CAVE LITHOSTRATIGRAPHY	12
FIGURE 2. 3	SEA LEVEL CHANGES FOR THE LAST 150 KA	14
FIGURE 2. 4	CROSS SECTION OF MSA LEVELS FROM THE HARPER EXCAVATION	16
FIGURE 2. 5	LSA STRATIGRAPHY OF ROSE COTTAGE CAVE	18
FIGURE 3. 1	AITKEN'S ENERGY LEVEL DIAGRAM	22
FIGURE 3. 2	REPRESENTATION OF DECAY CURVES USING DIFFERENT PREHEAT TEMPERATURES.	25
FIGURE 3. 3	D_E DETERMINATION	26
FIGURE 3. 4	SCHEMATIC OF THE RISØ TL/OSL DA-15 READER	29
FIGURE 3. 5	SCHEMATIC OF SINGLE-GRAIN OSL ATTACHMENT	29
FIGURE 3. 6	RESULTS OF CALIBRATION QUARTZ	30
FIGURE 3. 7	HEATER PLATE TEST, SHOWING CHARGE TRANSFER	31
FIGURE 3. 8	GENERALISED SAR MEASUREMENT SEQUENCE	35
FIGURE 3. 9	A TYPICAL SAR GROWTH CURVE (L_x/T_x)	36
FIGURE 3. 10	SENSITIVITY CHANGES MONITORED BY THE RELATIONSHIP BETWEEN L_x/T_x AND T_x/T_N VS. SAR CYCLE NUMBER	37
FIGURE 3.11	GENERAL PRINCIPLE OF THE RADIAL PLOT	42
FIGURE 3.12	OVERDISPERSION VALUES FOR SAMPLE RCC 9	43
FIGURE 4. 1	AVERAGE ALPHA DOSE FOR QUARTZ GRAINS EMBEDDED IN A MATRIX THAT CONTAINS THORIUM AND URANIUM	47
FIGURE 4. 2	AVERAGE BETA DOSE FROM SURROUNDING MATRIX TO SPHERICAL GRAINS	49
FIGURE 4. 3	VARIATION OF GAMMA DOSE IN SOIL, EXPRESSED AS A % OF THE GAMMA DOSE AT INFINITE DEPTH	49
FIGURE 4. 4	SELF DOSE AT THE CENTRE OF A SPHERE FOR GAMMA RADIATION WITH ENERGY 2MEV	50

FIGURE 4. 5	VARIATION OF THE INTENSITY OF COSMIC RAYS WITH ALTITUDE, EXPRESSED AS A RATIO FOR WHICH THE CORRESPONDING ANNUAL DOSE IS 185 $\mu\text{Gy/a}$	50
FIGURE 4. 6	SPECTRUM DERIVED FROM A PORTABLE GAMMA SPECTROMETER	53
FIGURE 5. 1	VALUES OF RECOVERY DOSES OBTAINED BY SAR PROTOCOL	61
FIGURE 5. 2	$D_E(T)$ PLOTS DISPLAYING D_E VALUES QUOTED IN Gy OBTAINED AT DIFFERENT INTEGRATION CHANNELS	62
FIGURE 5. 3	IR OSL DEPLETION RATIO TESTS PERFORMED ON ALIQUOTS USING 5MM AND 2MM MASK SIZES AT DIFFERENT PREHEAT TEMPERATURES.	67
FIGURE 5. 4	SENSITIVITY CHANGES MONITORED BY THE RELATIONSHIP BETWEEN L_X/T_X AND T_X/T_N VS. SAR CYCLE NUMBER	72
FIGURE 5. 5	LOW AND HIGH DOSE RECYCLING RATIO (R-RATIO) TESTS PERFORMED ON ALIQUOTS USING DIFFERENT MASK SIZES	77
FIGURE 5. 6	PREHEAT PLATEAU RESULTS FOR RCC SAMPLES	81
FIGURE 5. 7	RADIAL PLOTS AND PD PLOTS SHOWING THE D_E DISTRIBUTIONS FOR THE RCC SAMPLES	90
FIGURE 6. 1	TH/U RATIOS FOR RCC SAMPLES	94
FIGURE 6. 2	TH/U RATIOS FOR RCC SAMPLES, ACCORDING TO DEPTH	94
FIGURE 6. 3	CONTRIBUTION OF ^{40}K , ^{232}Th AND NATURAL U TO THE BETA AND GAMMA DOSE RATES OF ROSE COTTAGE CAVE	98
FIGURE 6. 4	DOSE-RATES OBTAINED FOR RCC USING ALL THE AVAILABLE TECHNIQUES	99
FIGURE 7. 1	COMPARISON BETWEEN OSL DATING AND OTHER DATING TECHNIQUES PERFORMED AT RCC	104
FIGURE 7. 2	AGE SEQUENCE FOR RCC	105
FIGURE 7. 3	RADIAL PLOTS SHOWING ALL THE GRAINS FROM SAMPLE RCC 21	106
FIGURE 7. 4	THE EFFECTS OF MOISTURE CONTENT AND %K ON A SAMPLE	109

LIST OF TABLES

TABLE 2.1	SAMPLING STRATEGY	19
TABLE 4.1	CONVERSION FACTORS USED FOR DOSE RATE CALCULATION	54
TABLE 4.2	EXTERNAL ATTENUATION FACTORS	54
TABLE 4.3	RAW DATA FOR SAMPLE RCC 10	55
TABLE 4.4	DRY DOSE-RATES (G _y /ka) FOR SAMPLE RCC 10	55
TABLE 5.1	RCC SAMPLES IN DEPTH ORDER	58
TABLE 5.2	VALUES OF RECOVERY DOSES OBTAINED BY SAR PROTOCOL	59
TABLE 5.3	SUMMARY OF D _E VALUES OBTAINED FROM RCC SAMPLES	91
TABLE 6.1	TH AND U PPM COMPARISONS	93
TABLE 6.2	RATIOS OF %K FROM XRG AND FGS MEASUREMENTS	95
TABLE 6.3	FRACTIONAL COMPONENTS OF DOSE-RATES TO ROSE COTTAGE CAVE	97
TABLE 6.4	DOSE-RATES OBTAINED FOR RCC USING THE BEST TH/U RATIO AND BOTH (WHEN AVAILABLE) MEASUREMENTS OF K%	100
TABLE 7.1	D _E VALUES AND DOSE-RATES USED IN AGE DETERMINATION FOR ROSE COTTAGE CAVE	102
TABLE 7.2	PRELIMINARY RESULTS FOR ROSE COTTAGE CAVE	103
TABLE 7.3	MOST PROBABLE AGE RANGES FOR THE ROSE COTTAGE CAVE SEQUENCE	110
TABLE 7.4	RESULTS FOR ROSE COTTAGE CAVE	111

LIST OF ABBREVIATIONS

Bq:	Becquerel, 1 Bq = 1 decay/sec
Ci:	Curie, 1 Ci = 37×10^9 Bq
CW-OSL:	Continuous-wave optically stimulated luminescence
D_e:	Equivalent laboratory dose
ELSA:	Early Later Stone Age
ESA:	Early Stone Age
FBP:	Fast bleaching TL peak
FGS:	Field gamma spectrometer
Gy:	Gray, 1 Gy = 1 joule/kg
HF Acid:	Hydrofluoric acid
HP:	Howiesons Poort
IR:	Infrared
IRSL:	Infrared Stimulated Luminescence
K:	Potassium
ka:	kilo year (1 year $\times 10^3$)
LED:	Light Emitting Diode
LGM:	Last Glacial Maximum
LSA:	Later Stone Age
L_x:	Luminescence regenerative dose
MeV:	Mega Electron-volt
MSA:	Middle Stone Age
mW:	Mega-watt
OIS:	Oxygen Isotope Stage
OSL:	Optically Stimulated Luminescence
ppm:	Parts per million
Rb:	Rubidium
RCC:	Rose Cottage Cave
SAR:	Single aliquot regenerative (protocol)
SBP:	Slow bleaching TL peak
Th:	Thorium
TL:	Thermoluminescence
TSAC:	Thick Source Alpha Counting
T_x:	Luminescence test dose
U:	Uranium
WAV:	Weighted average
α:	Alpha (radiation)
β:	Beta (radiation)
γ:	Gamma (radiation)

1 INTRODUCTION

1.1 Purpose of study

The Middle Stone Age (MSA) began in southern Africa possibly more than 200 000 years ago and ended between 30 000 and 20 000 years ago (Deacon & Deacon, 1999). The period contains key elements of change in the human species. It was during this time that key aspects of modern behaviour emerged and possibly the first anatomically modern skeletal morphology. Luminescence techniques are among the most promising methods for dating the MSA at present, and it is likely that the methods could be employed to establish an absolute chronology for the MSA. Only a handful of archaeological sites have produced luminescence chronologies (Feathers & Bush, 2000; Feathers, 2002; Jacobs *et al.*, 2003a, 2003b; Tribolo, 2003; Wadley & Jacobs, 2004). Progress towards creating reliable Optically Stimulated Luminescence (OSL) dating protocols have advanced greatly (Murray & Wintle, 2000; Jacobs, 2004; Jacobs *et al.*, *in press.*). The key protocol used is the single aliquot regenerative (SAR) protocol (Murray & Wintle, 2000). The purpose of this study is to test the reliability of SAR protocol (by comparison between OSL and radiocarbon dates) as applied to date in South Africa in order to establish a coherent chronology for the MSA at Rose Cottage Cave (RCC).

1.2 Rose Cottage Cave

RCC is situated on the Platberg (29°13' S, 27° 28' E) near the town of Ladybrand in the eastern Free State (Wadley, 1997). It lies within the Caledon River corridor, a sub-humid, summer rainfall area about 50 km wide, that extends from the town of Clarens in the north-east to the confluence of the Orange and Caledon Rivers (Wadley *et al.*, 1992). It is located in a series of karoo sandstone hills protruding from the underlying shale (Herries & Latham, 2002). The cave is about 20 m long and 10 m wide and according to Butzer (1984a; 1984b) was formed by mechanical weathering of the sandstone strata. A large section of collapsed roof has blocked its entrance, restricting access to narrow east and

west corridors (figure 1.1). The site contains a well defined stratified sequence that extends from the Late Pleistocene (Wadley, 1997; Wadley *et al.*, 1992) in a well defined pre Howiesons Poort MSA industry (Harper, 1997; Wadley & Harper, 1989) until recent times including many of the Middle Stone Age (MSA) and Late Stone Age (LSA) industries found in southern Africa.

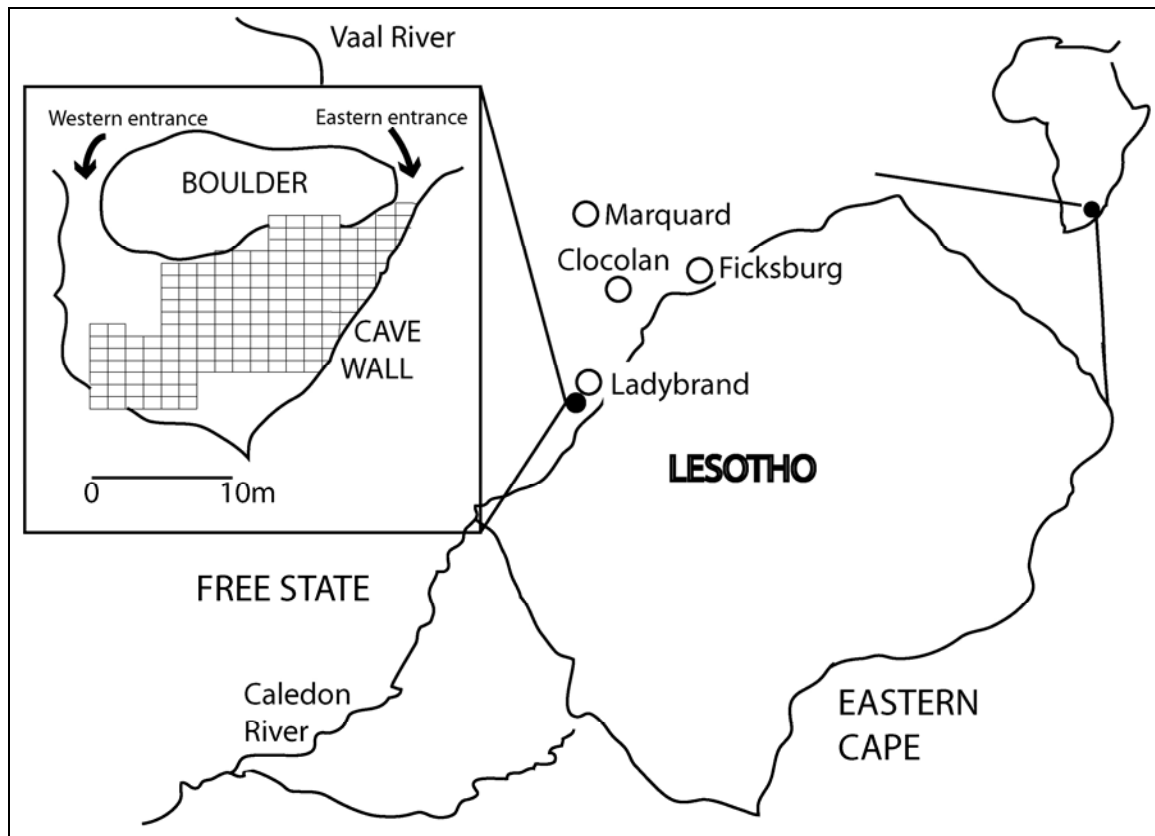


Figure 1.1 Location of Rose Cottage Cave (modified from Wadley, 1997).

1.3 What is OSL?

OSL dating is based on the storage and release of radiation energy in crystalline mineral structures. The two principal minerals used are quartz and 'high potassium' feldspars, both of which are found in greater or lesser quantities in most sediment. The preferred mineral used to determine the age of sedimentary deposits is quartz due to a better understanding of the mechanisms of OSL production inside the crystal structure (Bøtter-Jensen *et al.*, 2003).

During the 1960s Thermoluminescence (TL) was developed at Oxford University for archaeological dating (Aitken, 1985) of pottery (Fleming, 1979). In southern Africa luminescence techniques have only recently been applied to archaeological sediments (Wintle, 1999). In 1985 the first thermoluminescence (TL) measurements were published for South Africa (Vogel, 1985). In the same year a new means of dating depositional ages was introduced by Huntley *et al.* (1985) when they introduced optically stimulated luminescence (OSL) dating using the 514 nm line from an argon laser to stimulate luminescence from quartz. The OSL technique offers an alternative method to radiocarbon dating which can be used to obtain reliable depositional ages of up to 200 000 years in the right environment (Huntley *et al.*, 1985).

1.4 Dating argument

RCC contains over six meters of deposit with a relatively even distribution of quartz and feldspar grains in most archaeological layers. The deposits at RCC consist of predominantly sandstone clast's produced through weathering or rock spalling of the cave roof and walls and laminated sediments brought in by water through faults and cracks at the rear of the cave (Butzer, 1984a, 1984b). Although the mineralogy of the sediments is well suited to OSL dating, such sediments are generally problematic due to contamination from roof and wall spalling (Fullagar *et al.*, 1996; Roberts *et al.*, 1998, 1999) and water lain sediments. Both of these mechanisms can introduce inadequately bleached grains that have the effect of changing the average OSL age of the sediment. The SAR protocol in conjunction with other checks should eliminate such contamination as well as that caused by high feldspar concentrations. Although the application of the SAR protocol in the dating of archaeological cave occupations is theoretically feasible, the approach has yet to be empirically tested. OSL dates obtained from RCC using the SAR protocol can be cross checked with known chronologies.

The most obvious test is an internal one achieved by OSL dating RCC sediments that already have a well established radiocarbon chronology. The radiocarbon chronology from RCC is one of the best in southern Africa (Butzer, 1984a;

Wadley, 1991; Wadley & Vogel, 1991), and while the true advantage of OSL dating lies in the ability to date beyond the practical limit of radiocarbon dating, some attention is given in this thesis to dating sediments with associated radiocarbon dates. For the most part the relevant radiocarbon dates conform to a regional chronology complemented by associated studies in Lesotho, particularly at Sehonghong Shelter (Mitchell, 1994). However the comparison between radiocarbon dates and OSL dates is not simple. It will become clear in the discussion on OSL dating theory that OSL dates are calculated in true calendar years, and the date is reported relative to the calendar date of the analysis. Radiocarbon dates, in contrast, are calculated relative to the year AD 1950, and the age is calculated using the Libby half-life for ^{14}C which is known to be in error by approximately 3% (Stuiver & Polach, 1977). This means that radiocarbon years are not the same as calendar years. An additional level of complexity arises from natural fluctuations in the production of ^{14}C in the atmosphere.

Both the secular variation in ^{14}C and the error resulting from the incorrect half-life used in radiocarbon dating are accommodated in the “calibration” of radiocarbon dates. In this process the measured radiocarbon date is compared with radiocarbon dates from known age tree rings in order to determine the calendar age of the sample. Recently it became clear that differences in carbon cycling in the northern and southern Hemispheres gives an approximate 40 year apparent age to the southern Hemisphere. This has to be taken into account in the calibration step for radiocarbon dates because the tree ring calibration dataset derives entirely from the northern Hemisphere. McCormac *et al.* (2004) have shown that using a fixed offset between the northern and southern hemisphere is erroneous and calibration of the southern hemisphere is therefore best achieved on dendro-chronologically dated wood. Unfortunately no such dataset exist for the southern hemisphere for the period before 1000 years ago. Furthermore, the calibration record between 26 ka and 50 ka is constructed from a variety of datasets such as laminated lake sediments, corals and speleothems. Van der Plicht *et al.* (2004) have noted that offsets greater than 2000 years exist between these datasets and recommend that this period should not be used in radiocarbon calibration.

The RCC radiocarbon dates in this study were calibrated using the Southern Hemisphere 1998 calibration dataset (SH98) (Stuiver *et al.*, 1998a). It should be noted that this dataset is interpolated on relatively few measurements (Talma & Vogel, 1992, 1993) combined with a average 40 year offset from the northern hemisphere 1998 dataset (INTACAL 98) (Stuiver *et al.*, 1998b).

The calibration issues around radiocarbon are complex and they result in several different representations of the dates. The radiocarbon dates are initially reported as dates “BP” or Before Present which is defined as the year AD 1950. After calibration the date is presented in the form of Julian Calendar years AD or BC. In order to compare these dates with OSL dates it is necessary to consider AD calibrated radiocarbon dates as negative, BC calibrated radiocarbon dates as positive, and to add to this the year in which the OSL date was determined.

Another test of the OSL approach is to compare the dates from RCC with those from other sites derived using other methods, or even using OSL methods under different circumstances. RCC is one of only seven known MSA sites to contain a well stratified Howiesons Poort (HP) assemblage (Wadley, 1997; Harper, 1997; Wadley & Harper, 1989) that can be cross-checked by an emerging HP chronology based on other archaeological sites shown in figure 1.2.

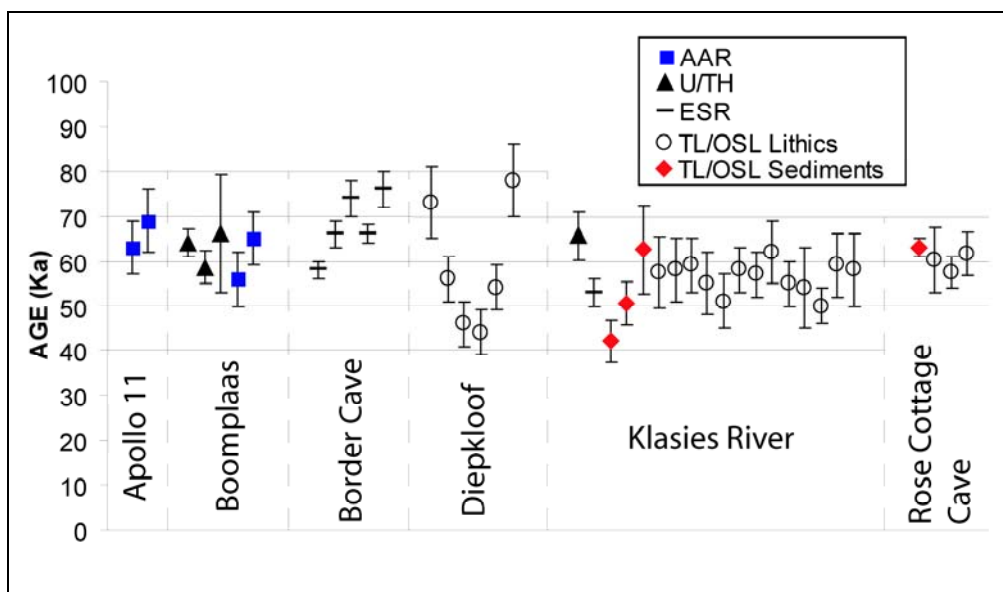


Figure 1.2 Different ages of the Howiesons Poort. The general consensus age occurs between 50 Ka and 70 Ka. (Tribolo, 2003; Feathers, 2002; Grün & Beaumont, 2001; Vogel, 2000; Miller *et al.*, 1999; Grün *et al.*, 1990; Murray pers. comm.).

1.5 Importance of study

The development of chronometric dating techniques in recent years has helped to establish absolute chronologies and re-construct paleo-climates. If it can be shown that OSL dating, using the SAR protocol, can establish a coherent MSA chronology at RCC, especially for the HP, then it will be possible to illustrate the link between technological adaptation and changing environments. This would aid development of archaeological and evolutionary thinking, as well as prove the reliability of previous OSL results. If on the other hand it is found that the SAR protocol cannot be used reliably at RCC, the problems need to be identified, and an alternative dating protocol needs to be applied to RCC and OSL dates obtained at other archaeological sites.

A more specific issue that needs to be addressed is the chronology of the MSA/LSA transition. At Border Cave (BC) Beaumont defines the Early Later Stone Age (ELSA) and he also classified the pre-Robberg levels at RCC as ELSA (Beaumont 1978). Wadley (1991) and Wadley & Vogel (1991) argue that the RCC layers predating 26 900 \pm 550 (Pta 6303) (uncalibrated BP) (Layers stratified below and including layer Ruth) are typologically MSA in nature. This implies that Beaumont's ELSA classification is too broad and it includes both the terminal MSA and the MSA/LSA transition assemblages. To some extent this argument is typological, but it is essential that similar age assemblages be compared between RCC and BC. The relevant BC assemblage derives from a layer known as the 1WA that has been subsequently dated to 38.5 ka (uncalibrated BP) (Bird *et al.*, 2003). In the same way that the OSL dates provide an independent chronology for the pre-26 000 year old deposits (i.e. for the layers in which radiocarbon calibration becomes problematic), so too the Electron Spin Resonance dates for BC provide an independent chronology for this site. The ELSA at BC is placed between 41 ka and 30 ka (calibrated relative to AD 2001) (Grün & Beaumont, 2001). The key contribution in this study is to identify the corresponding age layers at RCC in order that a direct comparison can be made between the relevant stone tool assemblages.

Detailed explanations of OSL theory is explained in the course of this study. These explanations are divided into two sections the first focuses on the numerator in the OSL age equation, including the equipment that is used and, the second focuses on the denominator in the OSL age equation. These two aspects are analysed separately in this thesis and brought together in the final chapter. The calculations in the final chapter uses the most probable values in the OSL age equation and are then compared to an existing radiocarbon age chronology for RCC.

2 ROSE COTTAGE CAVE

2.1 General Background

The first excavations at RCC were conducted under the supervision of B. D. Malan, a former student of A. J. H. Goodwin in the 1940s (Malan, 1952). From 1943 till 1946 he excavated RCC in what was probably the longest excavation in South African archaeology at the time (Mason, 1989). The primary aims of his excavations were:

- To ascertain the cultural stratigraphy of the Free State Wilton and Modderpoort cultures
- To study the MSA/LSA transition
- To establish the relationship between the various phases of rock art represented on the cave wall.

In the 1920s South African archaeology had broken away from European stone tool typological nomenclature largely due to the work of A.J.H. Goodwin and C. Van Riet Lowe (Goodwin & Van Riet Lowe, 1929; Goodwin, 1935). In 1929 the term Middle Stone Age (MSA) had been adopted due to the emerging variability in the Early Stone Age (ESA) and Later Stone Age (LSA) and it had been interpreted as a 'Mousterian' influence that had diffused into southern Africa. The MSA was characterised by the Levallois technique and broadly defined by Goodwin & Van Riet Lowe (1929) as a flake tool industry. The Howiesons Poort (HP) MSA sub-stage was seen as similar to the Magosian and by 1947 was accepted by the Pan African Congress on Prehistory, as the final phase of the MSA (Malan, 1952).

It was in this context that Malan divided the RCC sequence into a Modderpoort industry (basal layers), which he classified as a sub unit of the 'South African Magosian'. This was followed by about 2.1m of almost sterile sand topped by 1.7m of 'grey ash' near the top of the sequence which he associated with the LSA (Malan, 1952). Without the aid of absolute dating, the 'Magosian' material from RCC seemed an ideal candidate for a MSA/LSA

transitional industry. Malan subsequently became influential in extending the term 'Magosian' to the rest of southern Africa. Hoffman, one of Malan's associates, classified the levels above the 'Magosian' (Howiesons Poort levels) into three different 'cultures'. From base to top these were termed the 'Koning culture' (MSA IV), an unnamed blade culture and a Wilton industry (Wadley, 1991). Breuil (Wadley, 1991) identified the unnamed blade culture as a unique assemblage that could represent a new stone tool industry in southern Africa. Later excavations would confirm that Breuil had identified the first occurrence of the Robberg industry in South Africa (Wadley, 1991).

Prior to the 1950s the MSA was thought to begin around 4000 years ago followed by the LSA 2000 years later (Goodwin & Van Riet Lowe, 1929). By the mid 1950s the three age classification scheme (ESA, MSA, LSA) expanded to include the First and Second Intermediate stages (Deacon, 1990). The Magosian became the second intermediate phase. This was due to a paradigm shift that recognised the environment as a driver of cultural change. A great contribution to this paradigm came from the work of J. D. Clark in his synthesis '*The prehistory of southern Africa*' (1959). Central to Clark's work was the notion of Climato-stratigraphic dating, a relative dating technique based on the 'Pluvial Hypothesis' (Leakey & Solomon, 1929) in which the advance and retreat of alpine glaciers could be used as climatic indicators. In Africa, pluvial succession was proposed on Rift Valley lake deposition (Deacon, 1983) and the entire MSA was placed within a period of increased rainfall called the Gamblian Pluvial, the equivalent of the Würm Glacial in Europe (Clark, 1959).

The advent of radiocarbon dating of archaeological sites (Libby *et al.*, 1949) had a profound effect on South African archaeology. The first proposed ^{14}C chronology for southern Africa (Clark, 1959) provided a ^{14}C date of 60 000 B.P. from an Acheulian level (ESA) at Kalambo Falls, Zambia (Clark, 1969) and suggested that the MSA lasted between 38 000 BP and 6000 BP, while the LSA post-dated 6000 BP. In 1962 P. B. Beaumont, who was working under R. J. Mason at the time, re-excavated RCC with the specific aim of collecting charcoal samples for dating (Wadley, 1991). Several ^{14}C dates were

obtained by Beaumont from the LSA layers. He also collected material from the almost sterile sands that produced infinite dates of greater than 50 000 years and confirmed for the first time the real antiquity of the cave deposits (Butzer 1984b; Mason, 1962, 1969, 1989; Wadley & Vogel 1991; Wadley, 1991).

In 1972 a revised ^{14}C chronology for southern Africa was published (Vogel & Beaumont, 1972a, 1972b) that suggested that the MSA probably lasted between 100 000 years ago and 35 000 years ago. This framework was later augmented by palaeo-environmental reconstruction based on evidence emerging from other MSA sites. At RCC, Beaumont introduced a new industrial term which he called the Early Later Stone Age (ELSA). His RCC sequence was grouped into the Magosian followed by the ELSA and topped by a three phase Wilton and 'Pre-Wilton' industry in the upper ash layers (Wadley & Vogel, 1991). He recognised Hoffman's unnamed blade culture to be representative of a Robberg-like Industry which he grouped along with the 'Koning culture' and Malan's final MSA into the ELSA (Beaumont, 1978).

In the late 1970s and early 1980s, K. W Butzer visited RCC and collected further ^{14}C samples (Wadley & Vogel, 1991; Butzer, 1984b) from both the LSA and MSA levels of Malan and Beaumont's excavations. The ages he obtained were associated with material classified according to Beaumont's scheme. The main purpose of Butzer's visit however, was not to try and resolve a chronological framework for the stone age, but rather to study the processes of sedimentary deposition (Butzer, 1984a; 1984b; Wadley, 1991). Butzer (1984a, 1984b) recognized the climatic implications of the RCC sedimentology, and interpreted the well-laminated water-lain sediments to be a result of heavy and protracted rains, while silt and clay-sized grains indicate lower rainfall (Herries & Latham, 2002). His environmental model at RCC is controversial and does not correlate to other environmental studies performed at the site (Wadley, 1997).

In 1987 new excavations started at RCC under L. Wadley, who excavated through the LSA to the top of the sterile sands (Wadley, 1991, 1995, 1996,

1997). P. T Harper excavated through exposed MSA sections left after the Malan and Beaumont excavations (Harper, 1997; Wadley, 1997). The work by Wadley and her team produced a coherent well-defined LSA sequence. The Wadley excavations lasted from 1987 till 1997 and focused primarily on the spatial analyses of the occupation levels and reconstruction of past environments (Avery, 1997; Engela, 1995; Esterhuysen, 1996; Esterhuysen & Smith, 2003; Herries & Latham, 2002; Plug & Engela, 1992; Scott, 1989; Wadley *et al.*, 1992). Figure 2.1 depicts the spatial orientation of RCC showing the major excavated areas and Figure 2.2 shows the development of the lithostratigraphic sequence from 1943 till Wadley's excavation.

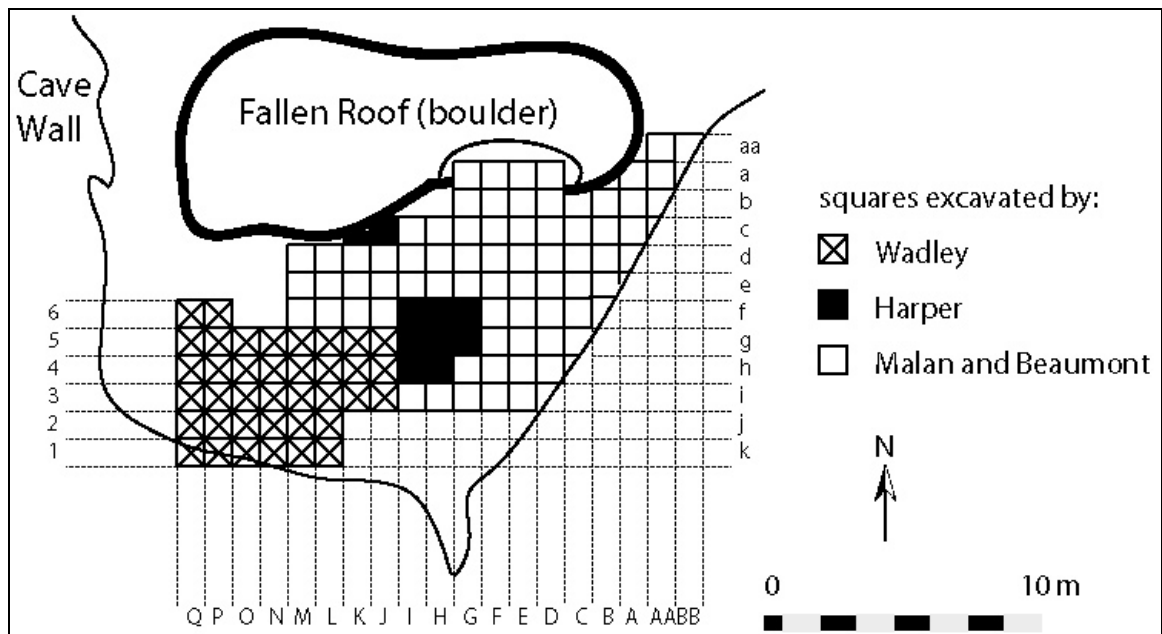


Figure 2.1 Plan of Rose Cottage Cave after Wadley 1997

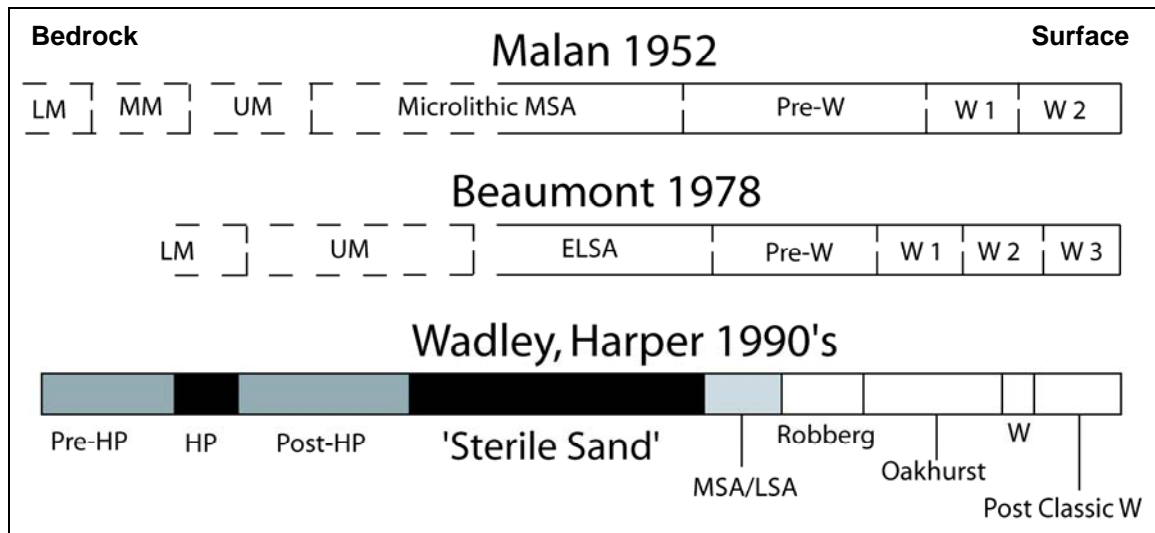


Figure 2.2 Interpretations of Rose Cottage Cave Lithostratigraphy. LM – Lower Magosian, MM – Middle Magosian, UM – Upper Magosian, HP – Howiesons Poort, W – Wilton. After (Wadley & Harper, 1989; Wadley, 1991; Wadley & Vogel, 1991).

2.2 Palaeo-environmental reconstruction at Rose Cottage Cave

Human adaptive strategies recorded in archaeological sites must in some way accommodate climatic and ecological changes. Currently the best evidence for environmental change during the Quaternary is provided by data recovered from Antarctic ice cores such as the Vostok core (Tyson *et al.*, 2001). Other climatic variations are observable through oxygen isotope variations in foraminifera from deep-sea cores (Pillans *et al.*, 1998) and define the major warm-cold transitions that characterised the movements of ice sheets derived from the Milankovitch Astronomical Theory (Milankovitch, 1941).

The majority of the environmental evidence from RCC dates between 23 000 years ago and the present. Charcoal and faunal assemblages from RCC (Engela, 1995; Esterhuysen, 1996) provide a basis for our contemporary understanding of palaeo-environmental change in the Caledon river valley (Mitchell *et al.*, 1998). The charcoal analysis shows two vegetation regimes: heathland vegetation during the Pleistocene suggesting cooler dry conditions

and woodland vegetation typical of the Holocene (Wadley *et al.*, 1992). This is complemented by an environmental archaeomagnetic proxy record that suggests an oscillating cooler climate for the late Pleistocene levels with the lowest temperatures occurring during the Last Glacial Maximum (LGM) (Herries & Latham, 2002). The Holocene presents woodland species probably found on the hillsides, and grassland similar to today (Wadley, 1997). Micromammal samples taken from levels dating from 8 500 years ago until 500 years ago indicate an early Holocene wet phase, a climatic optimum in the mid Holocene, and oscillating events in the late Holocene including the Little Ice Age (Avery, 1997).

Pollen spectra from the sites of Elim, Graigrossie and Cornelia near the town of Clarens, approximately 100 km north-east of RCC, suggest a cooler wetter climate between 23 000 and 20 000 years ago (Scott, 1989, Scott *et al.*, 1995, 1997). Studies at both RCC and Tloutle shelter in Lesotho have yielded a proxy climatic history from 13 500 years ago to 5 000 years ago for the Caledon river valley (Esterhuysen & Smith, 2003). Although the period is regarded as a warming interval, data from these two sites suggests a series of oscillating warming and cooling events (Esterhuysen & Smith, 2003).

The opportunity now exists to extend the understanding of palaeoenvironments and climates in the Caledon river valley past the limit of the radiocarbon dating technique. With the developments in OSL dating correlation between archaeological and environmental chronologies can be achieved by cross-checking absolute dates against oxygen isotope stages. A basic outline of the oxygen isotope stages is presented in figure 2.3. The last glacial/interglacial cycle according to variations in foraminifera reveals that a regional manifestation of global warming occurred around 125 000 years ago in the western Indian ocean (Tyson & Partridge, 2000) known as Oxygen Isotope Stage (OIS) 5e. A general trend of cooling occurred thereafter, reaching full maturity about 18 000 years ago in the Last Glacial Maximum (LGM) (Pillans *et al.*, 1998). Complementary evidence for post glacial warming in southern Africa after the LGM comes from local speleothem data (Holmgren *et al.*, 2003) confirmed for RCC by proxy pollen records from the

surrounding area (Van Zinderen Bakker, 1976; Wadley *et al.*, 1992) and charcoal / faunal analysis from the site itself.

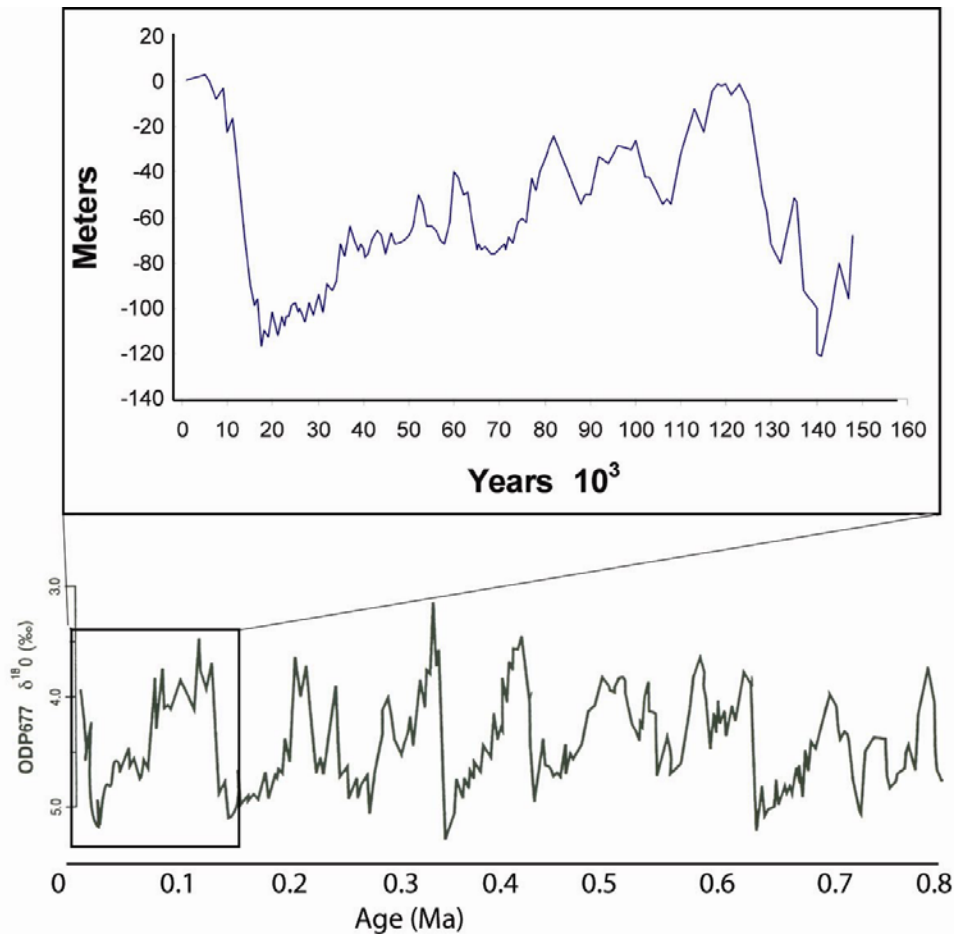


Figure 2.3 (top) Sea level changes for the last 150 ka derived from core V19-30 isotope record, Huon Peninsula. (Bottom) isotope record of ODP Site 677 (modified from Pillans *et al.*, 1998).

2.3 The archaeology of Rose Cottage Cave

The currently accepted Stone Age sequence for RCC is that derived by P.N. Harper and L. Wadley, who excavated through the remaining sections of Malan's excavation to bedrock, a depth of over 6.5 metres. The MSA lithic classification used at RCC by Wadley and Harper is after Singer & Wymer (1982). The sequence, taken from squares If, Ig, Hf, Hg and Hf (see Figure 2.1) begins with a pre-Howiesons Poort MSA II stone tool assemblage (layers LEN, KUA and KUB) consisting of a few points, knives and some scrapers.

They are however, near sterile in artefact accumulation (Harper, 1997). The overlying 15 levels (EMD to SUZ) present backed tools characteristic of the Howiesons Poort (Wadley, 1997) and are representative of a relatively continuous and intense occupation at the cave. Harper (1997) interprets the replacement of formal MSA tools in the pre-HP layers as technological discontinuity, and according to him technological continuity is only regained in the post-HP levels.

The post-Howiesons Poort or MSA III (levels ANN to THO) show a decline in the production of flake blades and an increase in end flake production (Wadley, 1997). Above the post-HP are the 'almost sterile' orange sands (levels MAD to KAR), that span over a metre of deposit (Harper, 1997). Samples taken by K.W. Butzer in 1977 indicate a ^{14}C date of 23 000 B.C. for the top of the sterile layers. Beaumont and Mason submitted samples all dating to > 40 000 years ago and Wadley obtained two dates for the 'orange sands' of 34 375 B.C. and 36 609 B.C. (see Appendix A). The ^{14}C data then suggests a period from 23 000 to > 40 000 years ago for the sterile sands (Wadley & Vogel, 1991). Figure 2.4 presents the stratigraphic horizons of the MSA sequence and shows the positions from where OSL samples were taken.

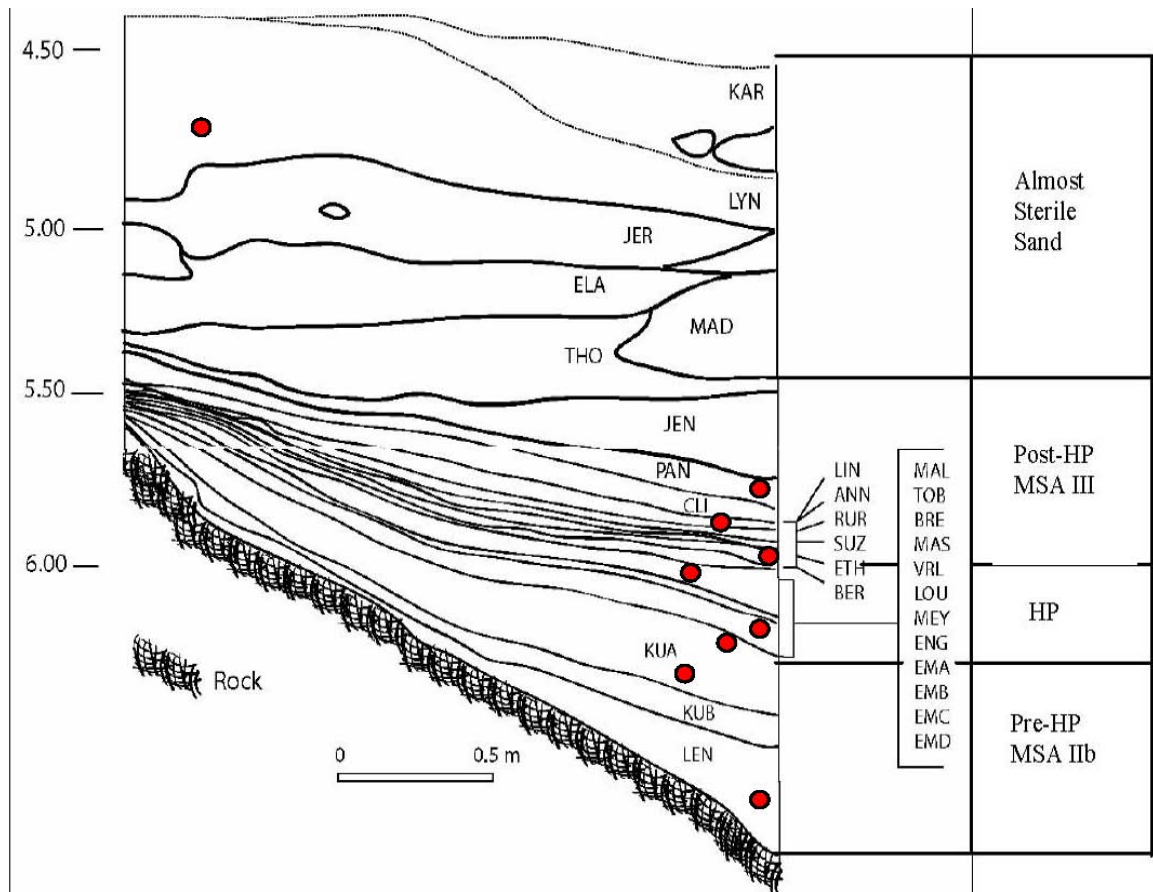


Figure 2.3 Cross section of MSA levels from the Harper excavation, squares If, Ig and Ih, modified from Harper, 1997. Note the finely stratified Howiesons Poort layers.

The layers directly above the ‘sterile sands’, up until and including layer Ru, are recognised as the final MSA phase. Layers G2 and G represent a MSA/LSA transition (Clark, 1999, 1997a, 1997b; Wadley, 1997) and contain more than 65 000 stone artefacts, representing one of the largest assemblages of this type in southern Africa. This assemblage is similar to a transitional assemblage at Sehonghong shelter (Clark, 1997a; 1997b) and radiocarbon dates to 21 735 B.C. with a one sigma range (21 921 – 21 549 B.C.) (see Pta 5598 Appendix A).

The LSA layers at RCC are well-stratified into the Robberg, Oakhurst, Wilton and post-classic Wilton industries (Clark, 1997a; Wadley, 1991; 1997). These layers have a chronological radiocarbon sequence (see Appendix A) and form the basis for testing the OSL protocols. Wadley (1991) excavated a 32m² area in the western portion of the cave. Levels Db, Lb and DCM contain the first

clear evidence for a Robberg industry (Clark, 1997b). The industry was first officially recognised in Nelson Bay Cave on the Robberg Peninsula (Klein, 1974). It was however, first observed in South Africa at RCC by Abbé Henri Breuil in the 1950s (Wadley, 1996). The age of the Robberg Industry in South Africa is between 22 000 and 12 000 years ago (Deacon & Deacon, 1999), ending just before the Pleistocene/Holocene transition. The Robberg at RCC however, is thought to end roughly 10 000 years ago (Wadley, 1991).

The majority of the formal stone tool assemblage of the Robberg Industry consists of thin parallel-sided bladelets (Wadley, 1997). Binneman (1997) suggests that the bladelets at RCC were produced by bipolar flaking and usewear traces along the lateral surface indicate that they were used predominantly for cutting or sawing. The majority of the molecular residues found on these tools suggest they were used for delicate work on plant material rather than meat (Williamson, 1997). The Industry also contains the earliest bone points found at RCC, as well as very few ostrich eggshell fragments (Wadley, 1996). Wadley (2000) suggests a more structured use of space in the Robberg levels as compared to the MSA/LSA transition. A variety of hearths create an arc around the entrance boulder where they are protected from natural weather processes (Wadley, 1996).

Above the Robberg industry is the Oakhurst (levels Ja, Ph, Cm, H and O) (see Figure 2.5) characterized by a variety of scrapers and microlithic side struck flakes (Wadley, 1991). At other sites in South Africa the Oakhurst commences about 12 000 years ago and ends about 8 000 years ago. With the late transition from the Robberg at RCC, the Oakhurst begins roughly 10 000 years ago and ends 2 000 years later (see Appendix A). There is a marked increase in trade material in the Oakhurst (Wadley, 1991). This is overlain by the 'Classic Wilton' (level Pt) and 'post-Classic Wilton' (levels Mn, A2 and A). The post-Classic Wilton contains assemblages with pottery and ostrich eggshells, and has a high frequency of retouched tools (Wadley, 1997). The presence of a cowrie shell and interpretations of the rock art indicate contact with coastal peoples. Thorp's (1997, 2000) analysis of the pottery from layers Mn and A suggests interaction with Sotho-speaking

groups. Figure 2.5 presents the stratigraphic horizons of the LSA sequence taken from the Wadley excavation. The dots indicate the positions from where luminescence samples were taken and cover the entire LSA lithostratigraphic sequence.

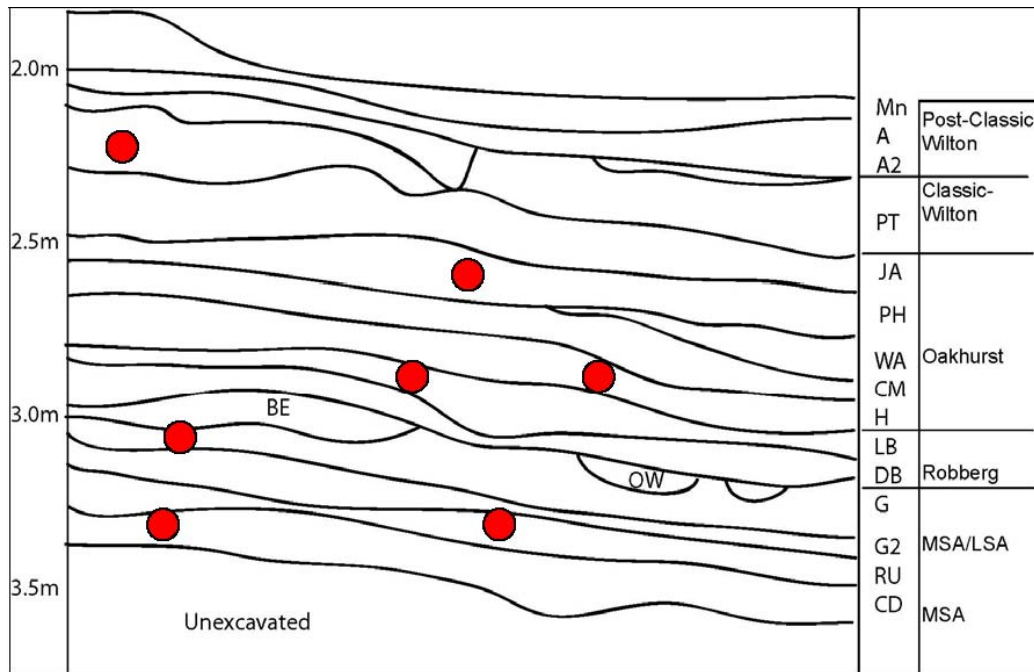


Figure 2. 4 LSA stratigraphy of Rose Cottage Cave, north section, squares O5 and N5, modified from Clark (1997b).

2.4 Sampling strategy of Rose Cottage Cave sediments

A total of 16 OSL samples were taken from the base of the excavation up to the top of the excavation, but due to time constraints and machine availability only 14 were dated. 11 samples were taken from the MSA section up to the base of the ‘sterile sands’ and cover the main archeological periods. Five samples were taken from the LSA layers. These samples were taken from layers associated with radiocarbon dates so that correlation between dating methods could be checked. Three prior luminescence dating studies have been conducted at the site focusing on the MSA deposits with the main aim of establishing an age for the HP. These include TL dating of sediments (Woodborne & Vogel, 1997; *pers. comm.*), TL dating of burnt lithics by H.

Tribolo and H. Valladas (Tribolo, 2003), and OSL dating of sedimentary deposits by A. S. Murray (*pers. comm.*). These studies place the upper levels of the 'sterile sands' at 33 000 years ago, the post-HP between 44 000 and 60 000 years ago, the HP to between 60 000 and 70 000 years ago and, the pre-HP as >70 000 years ago. Table 2.1 presents a schematic outline of where the luminescence samples were taken from

Table 2.1 Sampling strategy for Rose Cottage Cave samples

RCC OSL samples			
Depth (m)	Layer	Sample	Lithostratigraphy
	MN A A2		<i>Post-Classic Wilton</i>
	PT	RCC 17	Classic Wilton
2.5	JA PH CM H	RCC 22 RCC 21	Oakhurst
	LB DB BE	RCC 20 RCC 10	Robberg
	G G2	RCC 19	MSA/LSA Transition
3	RU CD	RCC 9 RCC 18	MSA IV
4.8	LYN	RCC 16	Almost "sterile" sand
6.8	CLI ANN	RCC 6	Post-HP MSA III
6.9	ETH BER EMC	RCC 14 RCC 7 RCC 13	HP
6.5	KUA KUA LEN	RCC 12 RCC 8 RCC 11	Pre-HP MSA IIb

Sampling must be carried out in a manner that prevents the stimulation of trapped electron populations in quartz grains (Murray & Wintle, 2000). During sample collection at Rose Cottage Cave sample tubes (50 mm diameter) were inserted into the stratigraphy under a light-tight tarpaulin using a subdued red light filtered torch.

2.5 Isolation of quartz from Rose Cottage Cave

In the laboratory the sediment samples underwent chemical treatment to remove carbonates and organic matter, and then physical separation to isolate a single mineral fraction (quartz or high potassium feldspars). The process of quartz purification is given in detail by Aitken (1985), Stokes (1992), Huntley *et al.* (1993), and Roberts *et al.* (1994).

In this study the samples were suspended in concentrated hydrochloric acid to remove the carbonates (CaCO_3) and Iron (Fe). Organics were removed by adding either NaOH or H_2O_2 , then dried and bulk sieved into different size fractions. Magnetic particles were removed using a Franz magnetic separator. The size fraction used in this study was determined by the grain size distribution of the sample and generally corresponded to 106-150 μm and 180-212 μm (see Appendix B). Quartz and potassium feldspars were then separated on the basis of density by suspension in heavy liquids (Mejdahl, 1985). A sodium polytungstate solution of specific gravity 2.62 was used for the isolation of quartz (Stokes, 1992; Huntley *et al.*, 1993; Roberts *et al.*, 1994). The samples were then etched in 40% hydrofluoric acid (HF) to remove any contribution from alpha radiation and any remaining plagioclase feldspars.

3 OSL DOSE DETERMINATION: THEORY AND EQUIPMENT

3.1 OSL Theory

The production of OSL dates using quartz is based on three criteria:

- A flux of energy from natural radioactivity
- A reproducible luminescence response to radiation by the mineral (a natural dosimeter)
- A zeroing event.

Minerals that make up sedimentary deposits, such as quartz and feldspar grains act as natural dosimeters. They absorb and store energy from the decay of natural radioactivity found in the surrounding environment. This energy is produced by trace amounts of uranium (U), thorium (Th) and potassium (K) found in the surrounding soil matrix. The decays relevant to luminescence dating consist of alpha (α), beta (β), gamma (γ) and cosmic radiations. Energy from these decays force valence electrons inside the quartz crystals to diffuse to higher energy “traps”. The process whereby stored electrons are released is called zeroing or “bleaching” and occurs naturally during sediment mobilisation (exposure to sunlight), or through heat, that could be related to archaeological phenomena such as hearths. The basis of this process is simplified in Aitken’s (1985) schematic of the transfer, storage and release of energy in a quartz grain (figure 3.1).

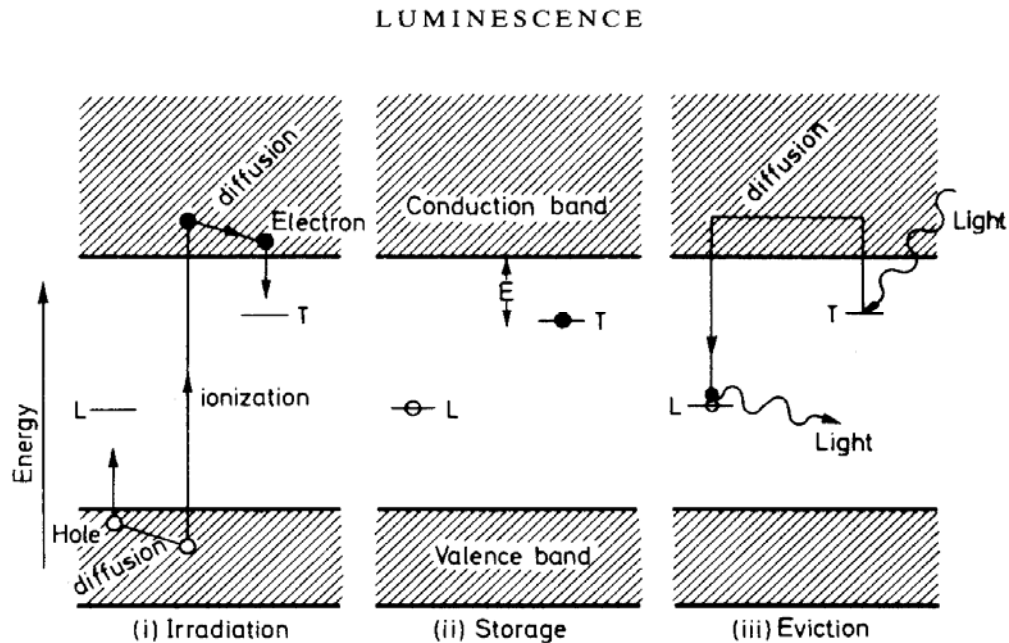


Figure 3. 1 Radiation energy causes valence electrons to be transferred to the conduction band. In this process positively charged ‘holes’ are formed in the valence band. The holes assume a high energy state because of their electron deficiency. After diffusion the electrons either recombine with holes or get trapped at defects or impurities within the mineral lattice. These traps occur at different energy levels and have different thermal stability. When trapped electrons are stimulated by either light or heat they diffuse in the conduction band and recombine with the holes. The resulting energy emission can be in the form of heat or light. Holes that produce light during electron recombination are known as luminescence centres (Aitken, 1998:44).

Figure 3.1 can be used to explain that radiation energy from the surrounding environment is transferred to the valence electrons in a quartz grain. These electrons diffuse to a high energy state called the “conduction band” (Bøtter-Jensen, 1997). The movement of an electron out of the valence band is associated with the formation of a positively charged “hole” that has a higher energy state than the valence band. Diffusion of high energy electrons in the conduction band causes them either to recombine immediately with the holes, or they become trapped in local energy minima caused by defects or impurities in the crystal lattice. The mechanism of electron trapping in quartz grains is dependent on the radiation dose rate that derives from the surrounding matrix. If this is constant, then the accumulation of trapped electrons will be a time dependent function. An energy input in the form of

heat or light transfers sufficient energy to the trapped electrons for them to escape the trap. These electrons either recombine with trapped holes called luminescence centres and release energy in the form of light or recombine with 'hole' traps that do not result in photon emission; these are called non-radioactive centres. The accumulative light that is released is called luminescence and is a direct measure of the de-trapped electron population.

There are many different electron trap types relating to different impurities within a crystal lattice. These traps have varying energy levels that have different thermal stabilities and optical depletion rates. Three easily identifiable trap populations in quartz correspond to thermal treatment at 110°C, 325°C and 375°C (Spooner *et al.*, 1988) respectively. Wintle & Murray (1998) have shown that the major proportion of a luminescence signal is produced by the charge responsible for the 325°C TL peak. These energy traps exhibit different bleaching behaviour: the 375°C peak bleaches more slowly than the 325°C peak and is referred to as the slow bleaching peak (SBP). The 325°C peak is a faster bleaching peak (FBP) and has been used extensively in dating (Huntley *et al.*, 1993). It has been demonstrated (Murray & Wintle, 1999a) that samples dominated by a fast bleaching component from the 325° TL peak (lifetime of 10^8 years at 20°C) can produce ages with little complications. Optically stimulated luminescence obtained from quartz using light stimulation between 420 and 520 nm yields a peak luminescence emission at 340 nm. This is comparable to the emission of the 110°C and 325 °C TL traps in the ultra-violet region and the 375 °C TL trap in the blue region (Bøtter-Jensen & Duller, 1992). Infra-red stimulation using a wavelength at around 880 nm does not significantly affect quartz (Stokes, 1992; Duller, 2003) although it does stimulate a luminescence signal in feldspars; the signal that is produced is called infra-red stimulated luminescence (IRSL).

3.2 Calculation of the depositional age of sediments

The depositional age of sediments is calculated as the time since electron traps were previously emptied or bleached until the present. The rate at which these traps are repopulated is determined by the environmental dose rate expressed in Gy/ka (radiation dose received per unit time). Several methods can be employed to evaluate the dose-rate. In this study the radionuclide concentration (ppm) of Th and U were determined in the laboratory by Thick Source Alpha Counting (TSAC), and ⁴⁰K was determined by XRF, then converted into Gy/ka. In the field, in situ gamma measurements were performed with the aid of a portable field gamma spectrometer (FGS). The dose rate can then be compared with the accumulated dose (D_e) of the sample to calculate the age using the *age equation*:

$$Age (ka) = \frac{Equivalent\ laboratory\ dose\ (D_e)\ (Gy)}{Dose\ rate\ (Gy / ka)} \quad \text{Equation 3. 1}$$

3.3 Determination of trapped electron populations in the laboratory

The measurement of the trapped electron population in the laboratory is accomplished by a similar mechanism to the zeroing event. The quartz is stimulated (with heat or light) with sufficient energy to de-trap the electrons. In OSL dating of quartz, isolated grains are stimulated using continuous wave OSL (CW-OSL), using blue LEDs for 40 seconds at 90% power i.e the wavelength and illumination intensity are fixed. The signal created by the recombination of electrons with luminescence centres results in an OSL decay curve (figure 3.2).

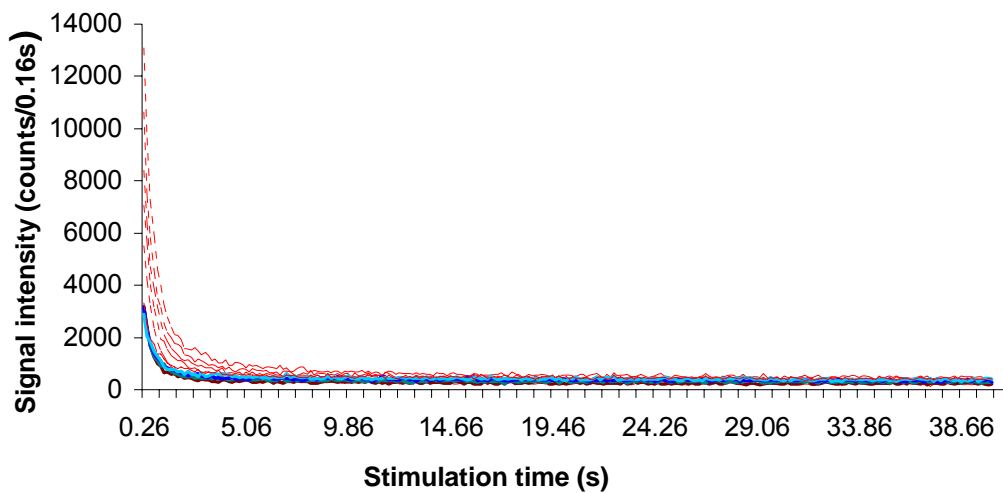


Figure 3. 2 Representation of eight decays from the same sample using different preheat temperatures. The two red bars indicate the area of integration for the signal and background. The blue line represents stimulation carried out after a 300°C preheat indicating partial depletion of the 325°C trap.

The resulting luminescence signal observable in these OSL decay curves is a direct measure of the trapped electron population and is proportional to the charge trapped since the last depositional event. This measurement can be used to establish the radiation dose (*Equivalent Dose, D_e*) the sample received since burial, by reproducing the amount of radiation that is required in the laboratory to match the natural OSL signal. The D_e is then determined by comparing the natural OSL signal with an OSL signal produced from a range of artificial irradiations administered in the laboratory. In this study samples were irradiated using a calibrated ^{90}Sr beta source positioned 5mm from the sample when in the irradiation position (Bøtter-Jensen *et al.*, 2000) and delivering a dose rate of more than 10 Gy/min (0.18 Gy/sec).

The reconstructed growth of the luminescence signal in relation to the applied dose is called the *dose response curve* or the *growth curve*. Artificially created decay curves are converted into dose response curves that are used to project the natural OSL measurement onto a radiation axis. Figure 3.3 below shows a representation of a dose-response curve that can be used to assess the D_e of a sample.

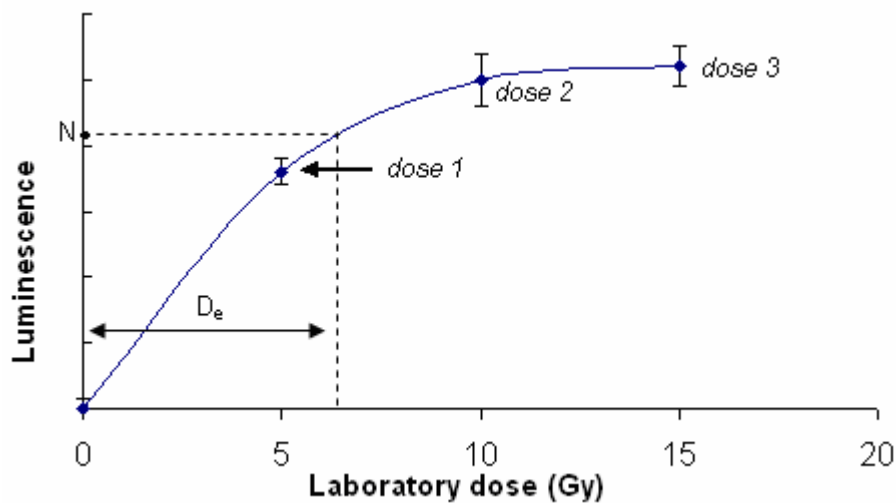


Figure 3.3 Regenerative growth curve. Each data point has been given a laboratory dose after the aliquot was bleached. The D_e is determined as the intercept between the natural measurement (N) and the dose response curve (modified from Aitken, 1998).

3.4 Problems associated with OSL dating

Several problems exist in OSL dating of sediments. These relate to the history of the sedimentary grains (adequate light exposure prior to deposition, contamination) and the physical properties of the quartz grains at a particular site. One problem in particular with archaeological sites is associated with a mixture of grains from adjacent stratigraphic layers or contamination from roof and wall disintegration. Jimmium Rock Shelter in northern Australia is a good example of how contamination can lead to an overestimation of the depositional age of the sediments (Fullagar *et al.*, 1996; Roberts *et al.*, 1998, 1999). At Rose Cottage Cave sediments were assumed to have been deposited by a mixing of water lain sediments, wind blown sediments and eroded cave roof and wall material (Butzer, 1984a, 1984b).

For these sediments analytical approaches used to determine the bleaching history of the grains (Bailey, 2003a, 2003b; Bailey *et al.*, 2003) were a critical requirement of the dating process. An assumption is that the quartz OSL signal consists of components defined in terms of the speed at which they bleach (Bailey *et al.*, 1997, Jain *et al.*, 2003). In most quartz grains there are a

minimum of three OSL components (Bailey *et al.*, 1997), namely the slow, medium, and fast components. Jain *et al.* (2003) have identified at least seven OSL components in quartz, referred to as the UltraFast (UF), Fast (F), Medium (M), Slow 1 (S_1), Slow 2 (S_2), Slow 3 (S_3) and Slow 4 (S_4) components. Samples that are dominated by a medium or slow component have a disadvantage in that partial bleaching is more probable.

Two commonly used methods to detect partial bleaching are categorised as distribution methods and signal analyses methods (Bailey, 2003a; 2003b). Distribution methods rely on the interpretation of the spread of D_e values, whereas the signal analysis method compares various components within the decay of individual OSL signals. The use of a signal analysis protocol to identify incomplete signal resetting has been used in this study. The method uses a single aliquot procedure (Duller, 1991) and calculates D_e as a function of time ($D_e(t)$), where time is defined as the stimulation time of the blue diodes in the reader, and gives a time dependent depletion characteristic of the signal. In the $D_e(t)$ method of Bailey (2003a, 2003b) the OSL signal must consist of thermally stable fast bleaching and a slow bleaching components. The assumption is that if all the OSL components were adequately zeroed, then a consistent age would be obtained from all portions of the signal. If the sample is partially bleached then a slower bleaching component (medium component) would yield a greater residual signal i.e. indicate a greater age.

Problems associated with the physical characteristics of quartz are commonly called luminescence sensitivity changes and they manifest as variability in the dose response curve. Changes in OSL sensitivity are related to the characteristics and behavior of OSL traps. Sensitivity changes that occur during D_e determination can be observed as a function of preheating as well as measurement cycle and relate to the distribution of charge among the different kinds of traps. The sensitivity changes found in shallower TL traps are removed by thermal treatment. The use of a preheat range between 160°C and 300°C has been suggested (Murray *et al.*, 1997) in order to isolate a signal derived from thermally stable traps and to equalize sensitivity between the natural and laboratory irradiated measurements.

3.5 OSL Instrumentation

An increasing demand to produce large amounts of measurements has driven the need for automated luminescence systems, and advances in understanding luminescence behaviour (particularly in quartz) has led to improved accuracy and precision through improved laboratory protocols. The development of the conventional SAR protocol (Murray & Wintle, 2000) (discussed in chapter four) and the introduction of single grain dating (Lamothe *et al.*, 1994) has recently led to the development of automated single aliquot/single grain systems. These systems need to fulfil the following requirements:

- A calibrated beta irradiation source
- A heater element with exceptional temperature control
- An optical stimulation system
- A single grain XY attachment unit, and
- A light emission detection unit (photomultiplier).

The Risø automated OSL/TL DA-15 (figure 3.4) unit meets these criteria and was used in this study. It is fitted with a standard photomultiplier (PM) tube, an OSL XY unit for single grain measurements, four optical stimulation systems, a thermal stimulation system, and an internal beta irradiation source. The OSL attachment is built up of 10 clusters of blue LEDs, positioned 20 mm in distance from the sample. The LEDs are arranged in four clusters each containing six LEDs and deliver $> 40 \text{ mW/cm}^2$ at the sample position. To minimise scatter a green long-pass GG-420 filter is placed in front of each cluster (Bøtter-Jensen *et al.*, 2003). A second stimulation system comprising 24 IR LEDs (875 nm) are arranged in six clusters in between the blue LEDs. They deliver approximately 135 mW/cm^2 at the sample position. Both IR and blue diode arrays are equipped with optical feedback systems that are used to stabilise their emission power (Bøtter-Jensen *et al.*, 2003).

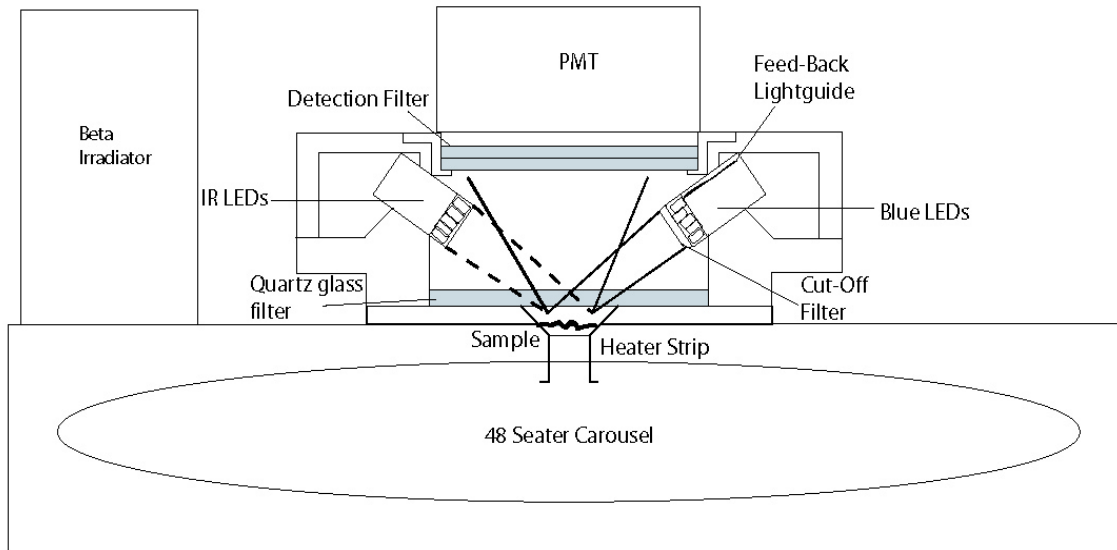


Figure 3. 4 Schematic of the Risø TL/OSL DA-15 reader with new IR/Blue LED OSL unit attachment (after Bøtter-Jensen *et al.*, 2003).

The XY single grain attachment (see figure 3.5) comprises of a 150 mW IR (830 nm) laser and a 10 mW (532 nm) green laser (Bøtter-Jensen *et al.*, 2003). This enables the user to perform routine measurements on single grains of quartz or feldspar. The grains are arranged in an aluminium disc, consisting of a 10 x 10 hole matrix, each hole being approximately 300 μm wide and 300 μm deep. The laser focuses on a 50 μm spot on each grain as required when performing measurements.

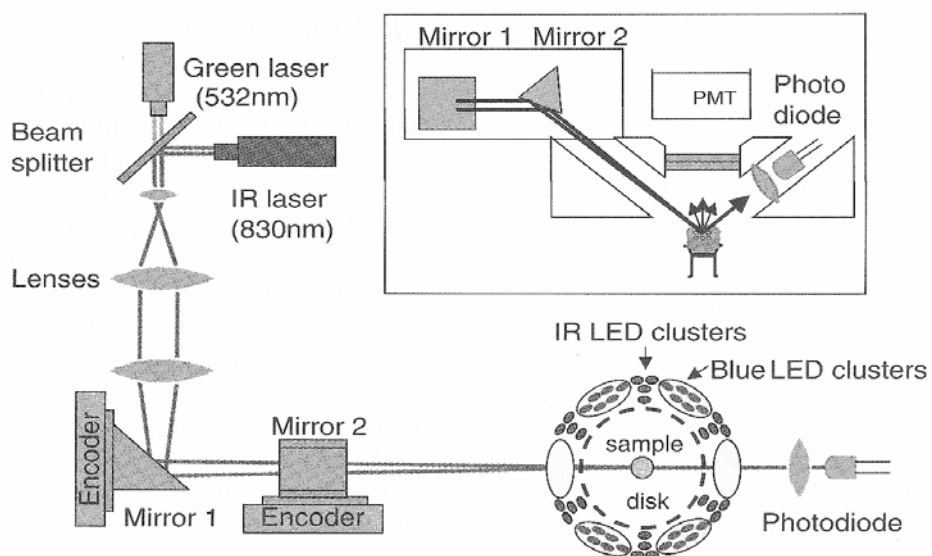


Figure 3. 5 Schematic of single-grain OSL attachment (from Bøtter-Jensen *et al.*, 2003).

The beta irradiation attachment on the Risø TL/OSL DA-15 reader is positioned 5mm above a sample in the irradiation position (Bøtter-Jensen *et al.*, 2000) and is fitted with a ^{90}Sr source with activity 1.48 GBq (40 mCi). This source is a 0.5 MeV beta emitter with a half-life of 28.5 years. Its daughter is ^{90}Y , a 3 MeV beta emitter with a half-life of 64.1 hours and a 230 keV/480 keV gamma emitter with a half life of three hours. The final product is stable Zirconium 90 (^{90}Zr). Although the typical strength of such a source is ~ 5 Gy/min (0.1 Gy/sec) at the sample irradiation position (Bøtter-Jensen *et al.*, 2000), the QUADRU ^{90}Sr source delivers a dose rate of more than 10 Gy/min (0.18 Gy/sec). A consequence of such a strong irradiation source is the effect of 'cross-talk' to neighbouring discs on the carousel. The cross-talk is defined as the radiation dose to samples in the vicinity of the intended sample. The extent of cross-talk or 'cross-irradiation' to adjacent samples can be as high as 0.1735 ± 0.0004 % (Bøtter-Jensen *et al.*, 2000). However, Bray *et al.* (2002) have reported $0.0055 \pm 0.012\%$ less than Bøtter-Jensen *et al.* (2000) by 2 orders of magnitude.

The beta source was calibrated by using gamma-irradiated (5 Gy) calibration quartz (180-212 μm) provided by A.S. Murray. A total of 35 aliquots were measured using a standard SAR protocol (Murray & Wintle, 2000). The results are presented in figure 3.6 in the form of a radial plot and a probability density plot displaying how a D_e of 5 Gy relates to the ^{90}Sr source in terms of s , where s is defined as the stimulation time of the beta source in the reader, in seconds irradiation.

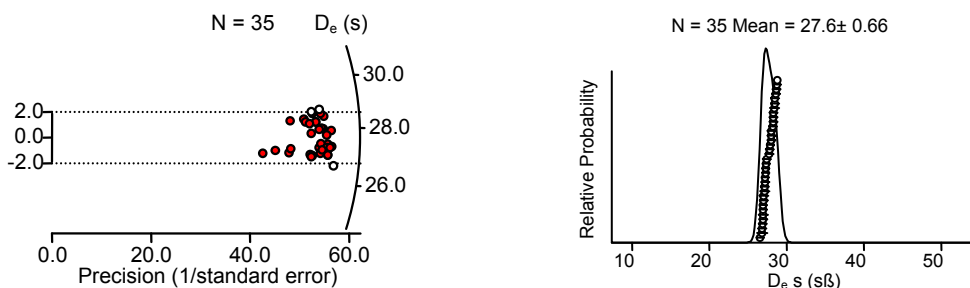


Figure 3.6 Results of calibration quartz having a gamma dose of 5 Gy. Measurements were performed on 180-212 μm quartz fractions using a 5mm mask size.

The heater strip in the Risø TL/OSL DA-15 reader is made of high resistance alloys. Temperature feedback is achieved using a thermocouple welded to the heater strip (Bøtter-Jensen, 1997), and rapid cooling is done with the use of nitrogen that flushes the measurement chamber. To test the accuracy of the heater plate and stability of preheating, a measurement protocol was carried out using a 180-212 μm fraction of bleached calibration quartz. The results presented in figure 3.7 were performed on one aliquot, 6 mm in diameter, that was given a dose of 9 Gy and a test dose of 1.8 Gy, repeated for ten measurement cycles. Stimulation was carried out at 125 °C. The sensitivity corrected luminescence signal (L_x) divided by the test signal (T_x) shows the effects of charge transfer from the 110 °C trap and depletion of the 325 °C trap at higher preheat temperatures. This is similar to sensitivity changes observed by Aitken & Smith (1988) when preheating between 220 °C and 300 °C. The results display thermal stability between 160 °C and 260 °C, causing the least amount of thermal erosion to the 325 °C OSL trap and providing a good indication that the heater plate is working adequately.

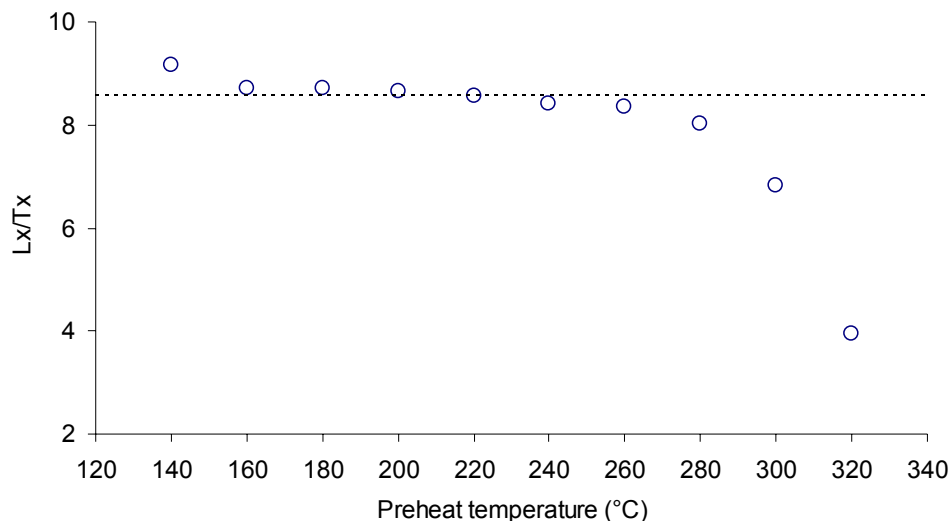


Figure 3.7 Heater plate test, showing charge transfer before 160 °C and after 260 °C on a typical quartz sample.

A systematic error was calculated for the Risø TL/OSL DA-15 reader by repeatedly irradiating, preheating and stimulating the same aliquot ten times. Preheating was carried out at 260°C and OSL stimulation was measured at

125°C. A linear trend was fitted through the data points. The scatter above and below the line represented the standard deviation of the data from the trend line. The relative standard error arising from instrumental uncertainty is therefore the error arising from variability around the fitted line minus the error that arises from counting statistics and was calculated as 1.8% and was subsequently used for all calculations in this study.

3.6 D_e Determination

3.6.1 Additive and Regenerative dose protocols

The protocols for measuring the equivalent dose (D_e) comprise two approaches: the additive dose and regenerative dose methods (Aitken, 1998). Both approaches begin with the determination of the natural luminescence signal, and then simulate the growth of the luminescence signal using a calibrated laboratory radiation source. In the regenerative approach, however, samples are first bleached to near zero before each dose is administered to stimulate the shape of the luminescence growth curve.

In both methods measurements are carried out on aliquots of pre-treated mineral extracts mounted on silicate that is sprayed onto the discs (steel or aluminium) through a predetermined mask size. This limits the area of oil application, and hence the number of grains that will adhere to the disc. Both additive and regenerative approaches have employed multiple and single aliquot protocols in order to obtain accurate estimates of D_e. The determination of D_e is then the use of laboratory protocols that can be employed to establish the equivalent laboratory dose the sample received since deposition until the present. In the single aliquot approach first developed by Duller (1991) for feldspar dating, all measurements are carried out on the same aliquot (Aitken, 1998). This has an advantage over multiple aliquots by avoiding the need to normalise inter-aliquot variability. The single aliquot regenerative dose (SAR) protocol (Murray & Roberts, 1998; Murray & Wintle, 2000) was used in this study as a means to determine D_e values.

The main concern in D_e determination is related to OSL sensitivity changes between natural and laboratory induced irradiations (Wintle & Murray, 1998; Murray & Wintle, 1999b). Sensitivity changes are attributed to the change in luminescence efficiency (OSL per evicted electron) (Aitken, 1998) and the rate of trap filling per unit irradiation (Murray & Wintle, 2000). It has been shown that sensitivity changes are proportional to the intensity of the 110°C TL peak (Aitken & Smith, 1988) in quartz. Zimmerman (1971) created a model for sensitisation of the 110°C TL peak and demonstrated how high temperature annealing can activate sensitivity changes. Most of this type of charge transfer observable in shallow energy traps (Murray & Wintle, 1999) can be removed through preheating. Precaution must be taken, however, due to an increase in recuperation or “charge transfer” at higher preheat temperatures by thermally stimulating higher energy traps (Aitken & Smith, 1988).

3.7 The SAR Protocol

During each measurement cycle in the SAR protocol three thermal treatments are applied, namely: Preheating, heating during stimulation and a cutheat before each test dose. Preheating is used to redistribute charge in order to compare the natural and irradiated signals. This type of transfer is known as thermal transfer or recuperation and reflects the presence of unstable (slowly bleaching) traps or centres (Wintle & Murray, 1999). Murray & Wintle (2000) recommend that stimulation be carried out at 125°C with a heating rate of 5°C/s to eliminate the influence of charge transfer from the 110°C peak. The cutheat is administered at a low enough temperature as to avoid sensitivity changes in deeper traps and at the same time eliminates unstable charge from the 110°C trap. If an Ultra-Fast luminescence component is detected, Murray & Wintle (2003) have suggested a higher cutheat temperature (e.g. 200° C) to remove this component. The effects of recuperation, monitored with the use of a zero dose measurement (Murray & Olley, 2002), may also be removed with high temperature stimulation such as 240° C for 100s (Jacobs, 2004).

The major advancement brought about by the SAR protocol is the incorporation of a test dose used to correct for sensitivity changes during measurement cycles. Sensitivity corrected dose response curves are created by administering a small test, roughly (10%) of the natural D_e (T_x), is used to monitor sensitivity changes (although the test dose can be any size), followed by a regenerative dose (L_x). Normalisation of this response provides a reasonable correction for sensitivity changes. A generalised measurement sequence, illustrated in figure 3.8 is as follows:

- Aliquots of the sample are divided into eight groups of three and given a dose (D_i) followed by a range of preheat temperatures between 160° and 300°, for ~ 10 seconds. In the first measurement cycle the applied dose is zero and this measurement yields the natural luminescence signal.
- After preheating, the OSL signal (L_x) is measured at 125°C (Murray & Olley, 2002). Note that during the first OSL measurement or natural, no dose (D_i) is given.
- A test dose, in the order of 10% of the natural is administered after each L_x measurement to correct for sensitivity changes. The test dose (D_t) is heated to 160°C to removed unwanted components of the 110°C TL trap (cut heat) and the OSL signal (T_x) is measured at 125°C.
- The cycle is repeated using several different doses for each cycle.

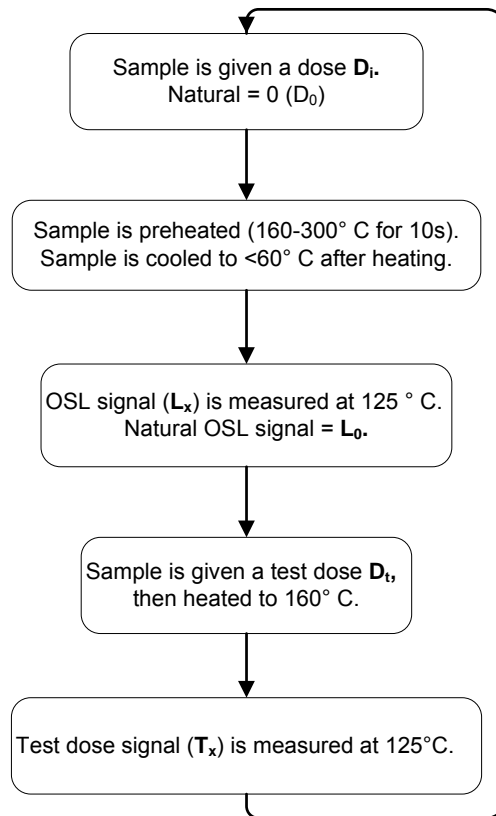


Figure 3.8 Generalised SAR measurement sequence modified from Murray & Wintle (2000)

A sensitivity corrected dose response curve shown in figure 3.9 compares the regenerative dose (L_x) and test dose (T_x) and can be explained by

$$L_{x\text{cont.}} = \frac{L_x - L_{x\text{bg}}}{T_x - T_{x\text{bg}}} \quad \text{Equation 3.1}$$

Where:

L_x is the OSL from the regenerated SAR cycle (typically the first 0.2-0.8s of stimulation),

$L_{x\text{bg}}$ is the background (slowly depleting portion of the OSL signal).

T_x and $T_{x\text{bg}}$ are the test dose signal and background (Stokes *et al.*, 2000).

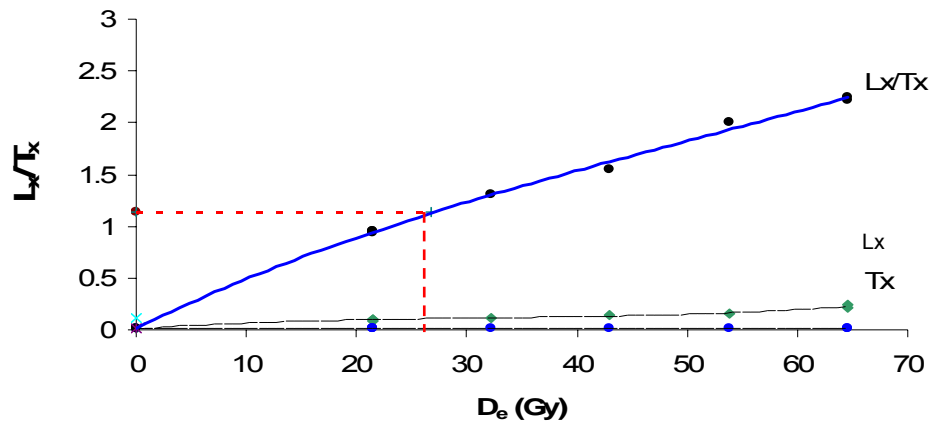


Figure 3.9 A typical SAR growth curve (L_x/T_x), having a D_e intercept of 26 Gy. Note the OSL measurement (L_x) and the test dose (T_x) have been normalised to zero. The ratio between these two measurements is used to construct the corrected (L_x/T_x) dose response curve.

From Figure 3.9 we assume that the signal from the test dose (T_x) uses the same electron traps responsible for the main OSL signal (L_x), therefore giving a good indication of sensitivity change. The test dose uses the OSL of the 110°C TL peak to monitor sensitivity changes associated with temperature and time that occur after irradiation (Murray & Roberts, 1998; Wintle & Murray, 1999; Murray & Wintle, 2000). As noted earlier the use of a preheat range between 160°C and 300°C has been suggested (Murray *et al.*, 1997) in order to isolate a signal derived from thermally stable traps.

Murray & Mejdahl (1999) demonstrated that the relationship between the OSL test dose and the OSL regenerative dose must be linear for sensitivity to be adequately corrected. This linear relationship is demonstrated for quartz (Murray & Mejdahl, 1999; Murray & Roberts, 1998; Murray & Wintle, 2000) by the relationship between the test doses (T_x) and the regenerative doses (L_x). Figure 3.10a below is an example of values of L_x are plotted against T_x for a series of preheat measurements and shows the relationship between two regenerative dose points. In figure 3.10b sensitivity changes that occur in the 110°C TL trap for the same set of data is represented. The regenerative test dose values (T_x) are normalized to T_n (the test dose administered after measurement of the natural) and show the sensitisation process that occurs

during a typical SAR process. There is an initial decrease in sensitivity for the lower preheat temperatures (160°C - 240°C) and an initial increase in sensitivity for the higher preheat temperature (260°C - 300°C).

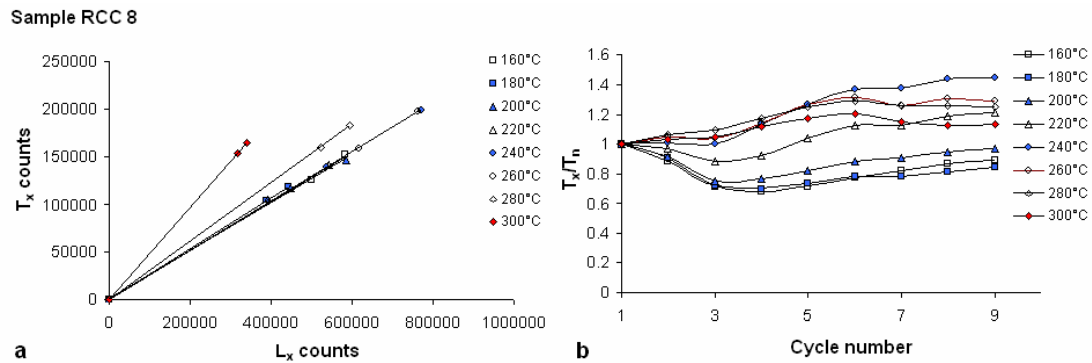


Figure 3.10 Sensitivity changes monitored by the relationship between L_x/T_x and T_x/T_n vs. SAR cycle number. The checks are performed on aliquots using large mask sizes (5mm). The repeated dose points representing L_x/T_x values were obtained through recycling low dose data points. Each paired value is taken as averages from eight different preheat temperatures. The 300°C values in figure 4.2a deviate from the main trend due to thermal depletion of the L_x measurement. For all the temperatures L_x vs. T_x values present a linear relationship. In figure 3.10b the values of T_x are normalized to T_n , the lower preheat temperatures show a decrease in sensitivity for the first few measurement cycles. The higher preheat temperatures have an increase in sensitivity for the first few measurement cycles.

3.7.1 Advantages of the SAR protocol

Murray & Wintle (1999a, 2000) demonstrated that a quartz dose response curve is not greatly affected by choice of preheat, provided that sensitivity changes are corrected. Two tests have been suggested (Murray & Roberts 1998, Wintle & Murray, 1999; Murray & Wintle, 2000; Wallinga *et al.*, 2001) to check the reproducibility (Murray & Wintle, 2000) of sensitivity corrected dose curves. The first and probably the most important check is termed the *dose recovery test* (Wallinga *et al.*, 2001). In this test the sample is first bleached to near zero, then given a known laboratory dose thought to be representative of the natural D_e . The SAR protocol is applied to the sample with the first preheat measurement applied after the initial dose administration. Preheat

temperature ranges between 220°C and 260°C are used due to their thermal stability. If the SAR protocol does not yield the applied dose (the dose is not recovered) there is a high probability that the D_e of the natural dose will be inaccurate.

The second test is called the recycling ratio or R-ratio test (Murray & Wintle, 2000). This test is used to check reproducibility (Murray & Wintle, 2000). The R-ratio acts as a simple test to check the reliability of sensitivity corrected dose measurements, i.e. inaccuracies may be detected by the deviated values of these recycled points (Bailey, 2000). Usually two recycled measurements are repeated in the SAR protocol: one with a low dosage to mimic the first regenerative point in which most sensitivity changes take place; and a second with a high dosage. The two recycling ratios $[(L_{x1}/T_{x1})/(L_{x2}/T_{x2})]$ should be very close to unity if appropriate sensitivity corrections during a SAR measurement cycle are applied. In practice less than two standard deviations from unity is acceptable (Murray & Wintle, 2000).

A similar test that was suggested to identify the occurrence of feldspars within a quartz sample (Duller, 2003) is termed the OSL IR depletion ratio test. It is in effect similar to the R-ratio test as it involves two replicate measurements. The first measurement (L_1/T_1) consists of a typical regenerative dose, usually the first regenerative point. The second measurement (L_2/T_2) is a replicate of the first measurement, but before the second measurement the sample is stimulated with infra-red (IR) diodes. As quartz is not affected by IR stimulation, any depletion of the signal measured during L_2/T_2 would be the result of bleaching of any feldspar contamination. A reduction criteria of more than two standard deviations from unity is used to determine an acceptable ratio of $[(L_1/T_1)/(L_2/T_2)]$ (Jacobs *et al.*, 2003a). Anything below this rejection criterion is assumed to be feldspar and is omitted from the analysis. In summary the accuracy of the SAR protocol is tested by a series of prescribed checks. These tests check the validity of the sample by

- Removing and transferring unwanted components of an OSL signal through thermal treatment

- Monitoring the sensitivity of both the Natural signal and regenerated signals (R-ratio)
- Assessing sample contamination.

3.8 D_e Distributions

Single grain analysis demonstrates that relatively few grains contribute to the total luminescence signal obtained from aliquot dating (Jacobs, *in press*). McFee & Tite (1994) relate this to varying levels of dose absorption experienced by individual grains. The single aliquot disc-to-disc scatter experienced by grouping large numbers of grains in aliquots is reduced by averaging out the combined D_e values of many single grains. A good practice is to carry out measurements on a limited grain size fraction and to use size specific masks for each aliquot. Smaller mask sizes result in fewer grains on the aliquot, and the inter-aliquot scatter in OSL measurements may increase because fewer D_e values are averaged. This is not always the case however, and other reasons for scatter could include sample mixing through contamination e.g. roof spall, partially bleached samples and microdosimetry. Microdosimetry relates to grains that lie next to highly radioactive particles such as zircon or the grains themselves could contain radioactive inclusions with higher radioactivity (Wintle, 1997). For these reasons a large number of aliquots are used in D_e determination, 24 in this study, and the D_e values for each aliquot is determined. After aliquots have been rejected using the criteria outlined above the true D_e value is calculated from the combined D_e values of the remaining aliquots.

Correct curve fitting in the dose response analysis allows “true apparent” D_e values to be assessed and any cause of scatter may be a result of other factors mentioned above. In a typical quartz sample the shape of a dose response curve starts to become non-linear as electron traps start to saturate and linear curve fitting may be incorrect in these situations. In this study dose response curves were constructed using regenerative dose points fitted to either an exponential or an exponential plus linear term. This was done by using *Analysis Pro* developed by Geoff Duller. Exponential curve fittings were

used due to the exponential saturation levels experienced in quartz grains (Wintle, 1997). The curves were fitted according to the average error of the fit where the smallest error constituted the best fit. The equation used to describe the term exponential is shown in equation 3.2.

$$I = I_0 + I_{\max} (I - e^{-D/D_0}) \quad \text{Equation 3.2}$$

Where:

I is the L_x/T_x ratio,

I_0 indicates the initial part of the luminescence signal,

I_{\max} is the upper limit of the luminescence signal,

D is the regenerated laboratory dose,

D_0 is a constant and controls the rate of trap filling.

The equation used for an additional linear term was used when additional traps were created by an administered dose and is shown in equation 3.3

$$I = I_0 + I_{\max} (I - e^{-D/D_0}) + k.D \quad \text{Equation 3.3}$$

Where:

k is the additional linear term added to the exponential function represented by a constant.

Once all the D_e values from a specific sample have been acquired, graphic displays may be used to determine whether a single dose population or some other factor evident in overdispersion controls the values of D_e . Two types of plots to represent D_e values are used in this study: a probability density plot (PD plot) and a Radial Plot. The measurement errors obtained through general statistics indicate which type of plot to use.

The PD plots uses each individual D_e values and represents them on a Gaussian curve; the central value is the D_e . The Gaussian curves from the

different grains are summed to create a probability density function. PD plots do not represent true age variation according to measurement precision, whereas radial plots do (Galbraith, 1998). In OSL dating it is preferred to plot D_e estimates with clear reference to their precision (Galbraith, 1990, 1994). Galbraith (1988) suggested the radial plot, where the precisions are clearly plotted on one axis (Figure 3.11). All data on a radial plot is relative to a central value taken as the weighted average by,

$$Z_0 = \left\{ \sum_{i=1}^n z_i / \sigma_i^2 \right\} / \left\{ \sum_{i=1}^n 1 / \sigma_i^2 \right\} \quad \text{Equation 3.4}$$

Where:

Z_0 is the weighted average of all the L_x measurements

Z is the individual L_x measurements and

σ is the standard deviation of each aliquot.

Once the weighted average (WAV) is obtained an x,y scatter plot is constructed. The precision of the sample is displayed on the x axis by $1/\sigma$ and the data points relative to their precision are displayed on the y axis by $(Z - Z_0)/\sigma$. $(Z - Z_0)$ is the slope of the data relative to the WAV (Galbraith, 1990). A third axis, the 'radial axis' represents the individual D_e values from a specific sample. The area in which the data will be represented can be limited by drawing a 2 sigma band around the central value on the y axis. 95% of the points should fall within this band in an ideal sample. When more than 5% of D_e values lie outside the 2 sigma range, the dose distribution is overdispersed. To add a radial or circular scale to the plot, an arc is drawn using a suitable radius and the x, y coordinates are plotted using a suitable reference value by

$$x = r_0 / \left\{ 1 + h^2 (Z - Z_0)^2 \right\}^{1/2}, \quad y = (Z - Z_0)x \quad \text{Equation 3.5}$$

(Galbraith, 1990)

Where:

r_0 is the radius centered at $x=0, y=0$

h is the length of 1 unit of x divided by the length of 1 unit of y

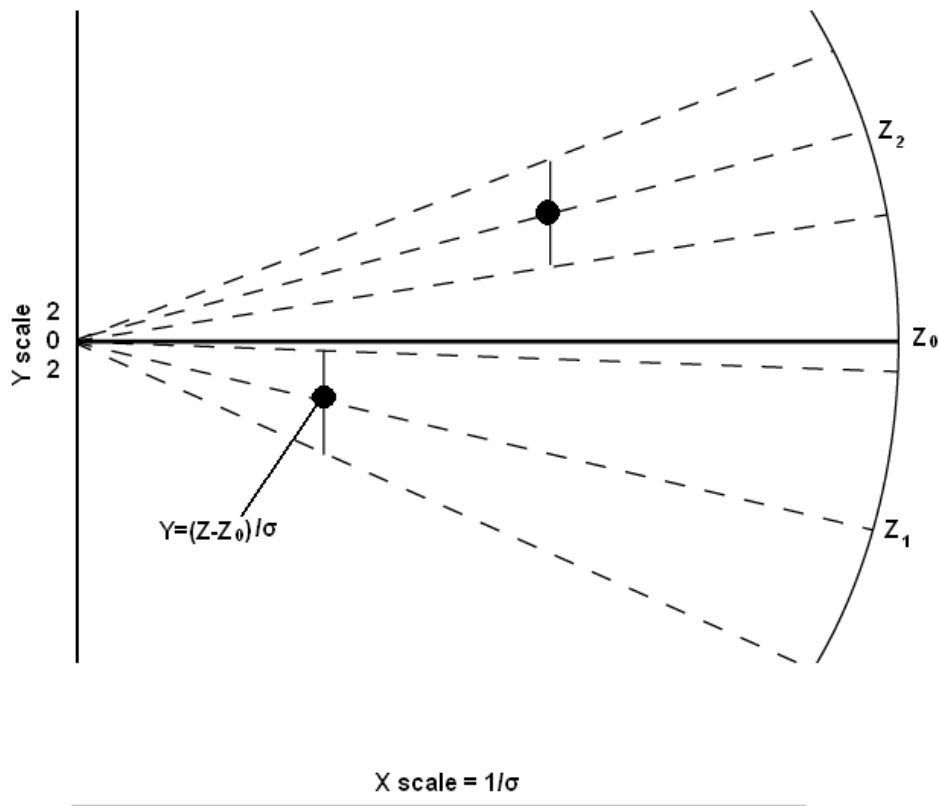


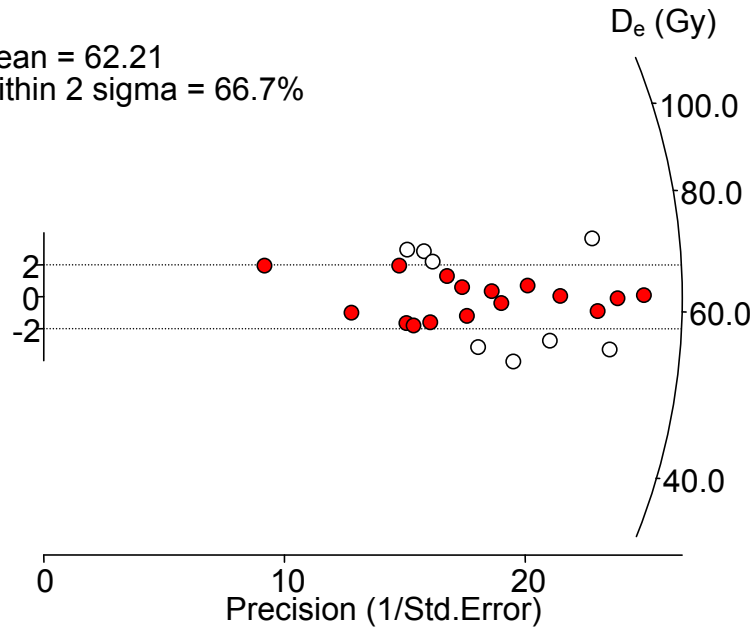
Figure 3.11 General principle of the Radial Plot. Each estimate has a unit standard error on the y scale. Points with larger x i.e. the further to the right points appear the more precise they are. The y values appear on the radial axis and samples that fall within 2 standard deviations from unity are detected on the y axis (Galbraith, 1990).

Overdispersion of D_e values in a radial plot refers to an increased number of data points that lie outside of the two standard deviation bars from a central D_e value (Galbraith *et al.*, 1999). The % overdispersion can be used to determine whether sample mixing has occurred and what type of age model to use in age calculation. Figure 3.12 shows the overdispersion values obtained on a large and small mask size for the same sample.

Sample: RCC 9
 Mask size: 5mm
 Etched: No

Overdispersion: 9.78%

Mean = 62.21
 Within 2 sigma = 66.7%



Sample: RCC 9
 Mask size: 2mm
 Etched: No

Overdispersion: 16.61%

Mean = 60.95
 Within 2 sigma = 35.7%

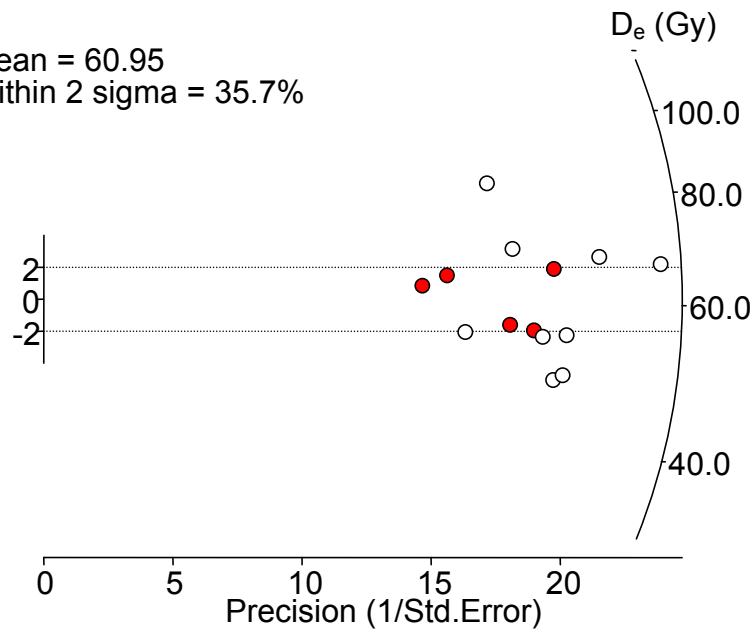


Figure 3.12 Overdispersion values for sample RCC 9 using: a 5mm (top) and 2mm (bottom) mask size.

3.9 Age models

The statistical analysis of D_e values obtained by measuring quartz gives an estimate of the log D_e values and their standard errors. In an ideal sample all aliquots should give consistent estimates of D_e . In some incidences a central estimate of D_e is not the case. Galbraith *et al.* (1999) have suggested the use of three different “age models” that may be used to assess a single D_e value. The models are called the *common age model*, the *central age model* and the *minimum age model*. In the common age model the D_e estimates would be consistent with a common value. If the log D_e values are not consistent with a common value a central age model may be used. In the central age model the D_e values are random and form a normal distribution and the central age can be calculated as the maximum likelihood of the sample. The minimum age model is used to obtain a minimum age of the sample and is used when parameters such as partial bleaching have occurred.

4 OSL DOSIMETRY: THEORY AND EQUIPMENT

4.1 Dose rate determination

The radiation that is relevant to luminescence dating has a broad emission range and is categorized into light and heavy ionizing radiation (Aitken, 1998). It is possible to calculate the overall absorbed radiation dose by assuming a balanced energy system. This implies that the matrix surrounding the sample is greater than the range of the internal radiation. The overall energy absorption is therefore equal to the energy emission. The radiation to which grains are exposed can be divided into an internal and external dose contribution. The internal dose comprises alpha and beta radiation from within the sample grains. The external dose is derived from alpha, beta and gamma radiation from the surrounding matrix, as well as cosmic radiation. The ionising radiation from these elements is provided by daughter isotopes found in radioactive decay chains (see Appendix C). In these chains the half-lives of the isotopes Th, U and K are in the order of 10^9 years, these along with their daughters provide a constant influx of radiation in a soil matrix. Valence electrons in quartz (and other mineral grains in the sediment) absorb this radiation and diffuse into higher energy traps. The result is the accumulation of trapped electrons through time. The rate at which sediments are irradiated during deposition is called the environmental dose rate, and the total absorbed energy is called the equivalent dose (determined in the laboratory as D_e). The equation used to resolve for time becomes

$$AGE = \frac{\text{EquivalentDose } (D_E)}{D_\alpha + D_\beta + D_\gamma + D_C} \quad (\text{Aitken, 1985; 1998})$$

Equation 4.1

Where:

$D_\alpha + D_\beta + D_\gamma + D_C$ are alpha, beta, gamma and cosmic dose rates.

4.2 Alpha particle contribution

Alpha radiation is less efficient than beta and gamma radiation in the trapping of electrons due to its high ionising density. The alpha particle range is very short and only affects the outer rind of sand-sized grains. Alpha particles consist of 2 neutrons and 2 protons, with 2 units of positive charge (${}^4_2\text{He}$) and they are emitted by Th and U (see appendix C). Their contribution is predominantly external in quartz grains, but consideration must be given to the possible inclusion of these elements in quartz. An estimated internal alpha contribution from Th and U for HF etched quartz was calculated to be 0.586 ppm and 0.169 ppm respectively (Jacobs *pers. comm.*). In coarse grain dating (i.e. the quartz inclusion technique developed by Fleming (1966, 1970)) sand-sized grains are selected and etched with 40% Hydrofluoric Acid (HF) typically removing the outer 9µm which is effected by alpha radiation. This has the advantage, if the internal alpha contribution is negligible, of avoiding the need to determine the alpha radiation effectiveness.

If the quartz grains are not etched during laboratory pre-treatment the alpha particle contribution has to be taken into consideration. The alpha particle effectiveness or range that has been affected by alpha radiation for normal sand sized grains is within the range 0.04 to 0.1 mm (Stokes *et al.*, 2003), for a 195 µm sized grain the total alpha contribution will be within the 4-12% range (Aitken, 1985). The grain dependant size attenuation of alpha particles in quartz was first calculated by Fleming (1966). Bell (1980) later calculated the alpha attenuation in grain sizes ranging from 1 µm to 1mm showing alpha penetration in fine grains to be < 90% of the total grain. Figure 4.1 shows that the average alpha dose received by grains in the diameter of 195 µm is below 20%.

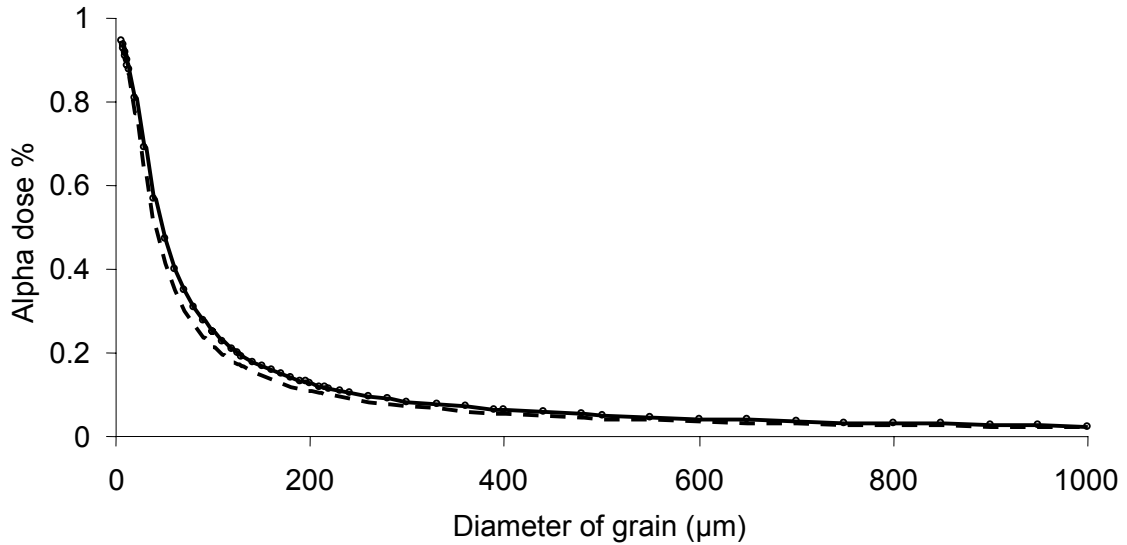


Figure 4. 1 Average alpha dose for quartz grains embedded in a matrix that contains thorium and uranium (after Bell, 1980). The dashed line represents the alpha contribution from Th, the solid line represents the alpha contribution from U. The attenuation factor is derived for uranium using a linear regression formula of $19.602 \times \text{grain size}^{-0.9811}$ and for thorium $22.701 \times \text{grain size}^{-0.9802}$.

Two factors affect the absorption of alpha radiation. First, the alpha absorption coefficient is proportional to the effective track length, as the energy loss of the alpha particle increases per unit length as the particle slows down (Aitken, 1985). Second, the moisture in the soil matrix attenuates the alpha contribution. The moisture content of a sample can vary from 1% to 40%, the upper limit being the saturation level (Aitken, 1985). The alpha particle contribution for samples from RCC was calculated using an alpha effectiveness of 0.04, and attenuation factors for un-etched material was taken into account using values obtained from figure 4.1. The dry alpha dose rates were also corrected for moisture content using equation 4.2 (Aitken, 1985).

$$D_{\alpha} = \frac{D_{\alpha, dry}}{1 + 1.50WF} \quad \text{Equation 4.4 (Aitken, 1985)}$$

Where:

D_{α} is the effective 'dry' alpha dose rate.

W is the saturated moisture content of the sample (expressed as the ratio between the weight of “wet” sample and the weight of sample after it has been dried).

F is the average level of saturation over the sample’s burial period.

4.3 Beta, gamma and cosmic radiation

The beta and gamma radiation relevant to luminescence dating are emitted by K, U, Th and a small contribution from Rb. They have longer ionising ranges and any absorbed dose is predominantly from an external source. In soil beta particles have a typical range of 2mm, gammas roughly an order of magnitude higher than beta’s, and cosmic radiation can reach a few metres into the soil (figure 4.3) (Aitken, 1985). The overall environmental dose rate consists of roughly two thirds beta irradiation (Mejdahl, 1979) (see figure 4.2). Gamma rays are the second largest contributors to the dose-rate. Gamma rays from the decay of ^{40}K also make a small contribution to the internal dose of a grain. Self dose percentage is used as a concept to describe the internal gamma dose rate and constitutes a small percent of the total gamma dose rate (see figure 4.4). The equation for the D_γ component becomes:

$$D_\gamma = \frac{P}{100} D_\gamma^i + \left(1 - \frac{P}{100}\right) D_\gamma^e \quad (\text{Aitken, 1985})$$

Equation 4.3

Where:

P is the average gamma dose in the sample (expressed as a percentage),

D_γ^i and D_γ^e are the internal and external gamma dose rates.

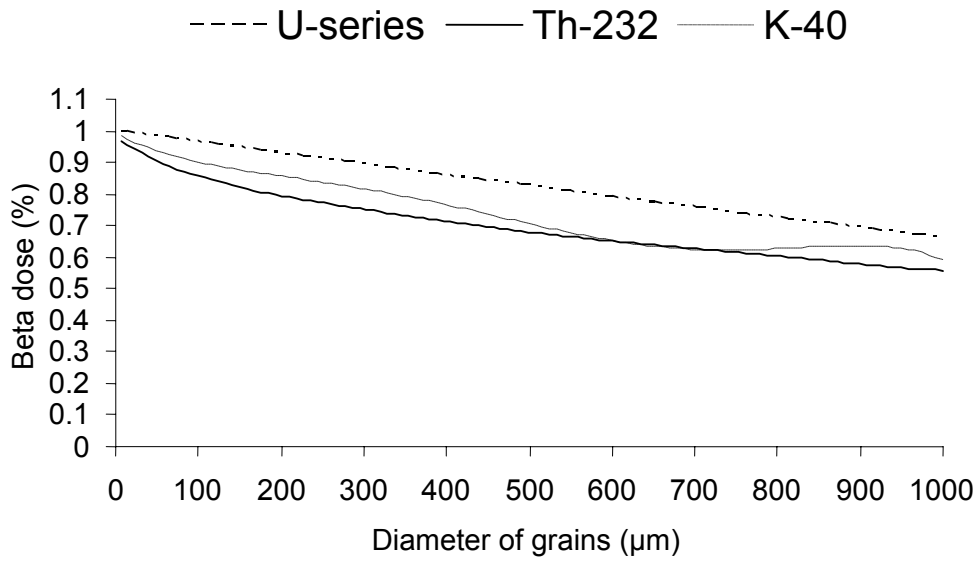


Figure 4. 2 Average beta dose from surrounding matrix to spherical grains (after Mejdahl, 1979).

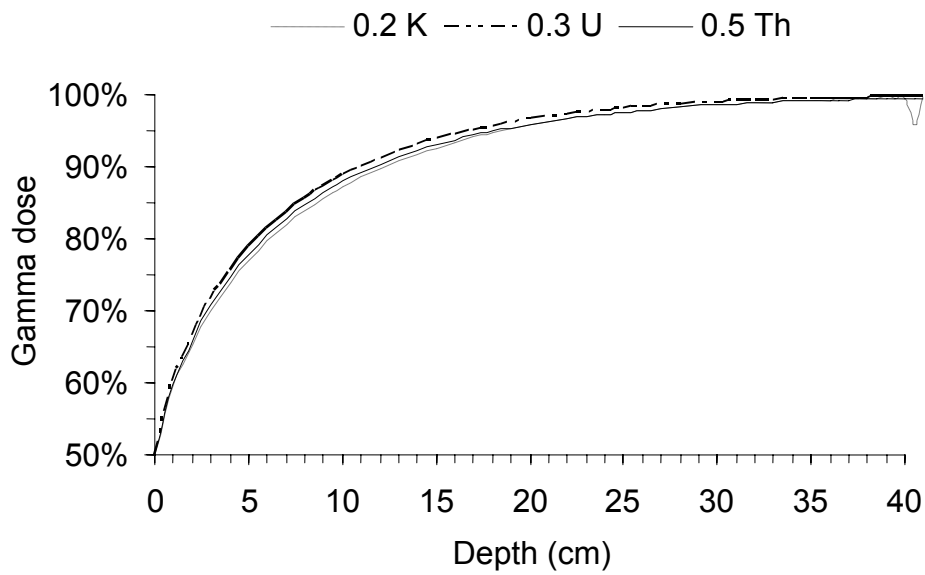


Figure 4. 3 Variation of gamma dose in soil, expressed as a % of the gamma dose at infinite depth (from computation by Løvborg in Aitken, 1985).

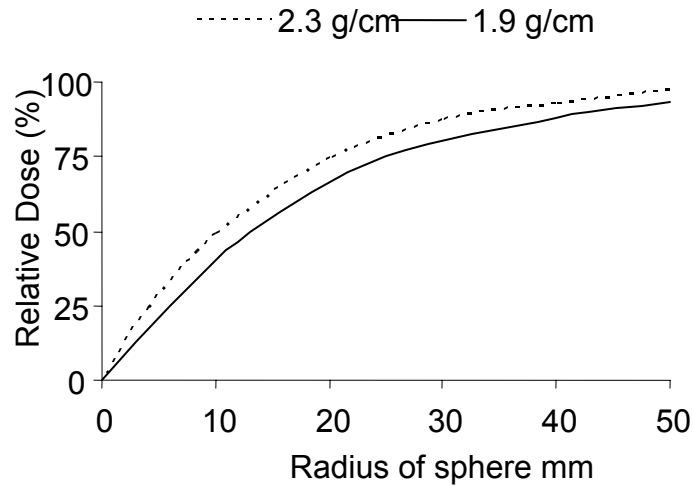


Figure 4. 4 Self dose at the centre of a sphere for gamma radiation with energy 2MeV (from Aitken, 1985).

The cosmic ray contribution constitutes a small fraction of the total environmental dose rate. The value used to define the cosmic ray contribution needs to be adjusted for overburden and altitude (Aitken, 1985). Cosmic rays are made up of ‘soft’ and ‘hard’ components. The soft component, consisting mostly of electrons, is absorbed by the first half metre of soil. The hard component, also used in assessing the dose rate, comprising mostly of muons (Aitken, 1985). The muons can be observed with decreasing intensity at substantial depths (Prescott & Hutton, 1994) (Figure 4.5). The cosmic contribution to the dose rate is also affected by latitude and altitude.

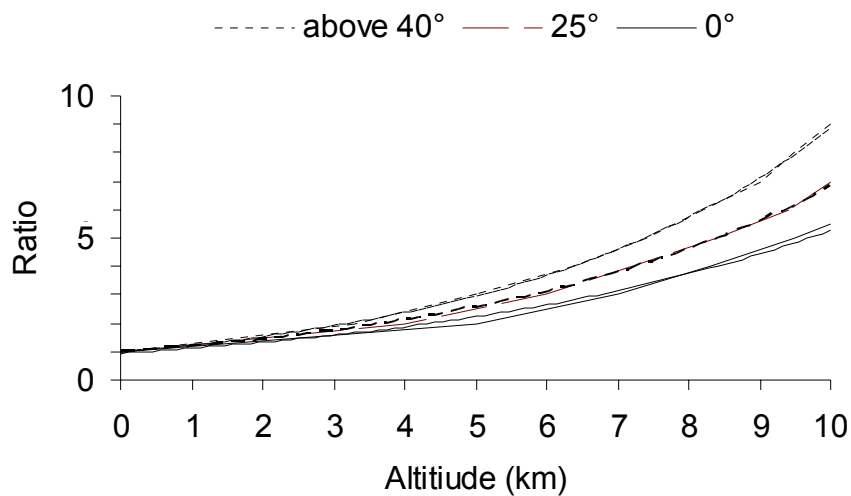


Figure 4. 5 Variation of the intensity of cosmic rays with altitude, expressed as a ratio for which the corresponding annual dose is 185 $\mu\text{Gy/a}$ (from Aitken, 1985).

The dry dose rates from beta particles and gamma rays must also be corrected for moisture attenuation unless *in situ* gamma measurements are performed. The moisture content correction is made in terms of WF , where:

$$W = (\text{saturation wet weight-dry weight}) / (\text{dry weight})$$

$$F = (\text{average water content}) / (\text{saturation water content}) \quad (\text{Aitken, 1985}).$$

The value used for F is usually estimated and is expressed as a fraction of the saturated water content. It has also been estimated (Zimmerman, 1971) that the absorption coefficient is 50% higher for alpha radiation, 25% for beta radiation and 14% for gamma radiation. Then to obtain the true or 'Wet' dose rates the actual values are given by

$$D_{\beta} = \frac{D_{\beta, \text{dry}}}{1 + 1.25WF}$$

$$D_{\gamma} = \frac{D_{\gamma, \text{dry}}}{1 + 1.14WF}$$

Equations 4.3

4.4 Instrumentation used to determine dose rates

Dose rates were determined by Thick Source Alpha Counting (TSAC) combined with X-ray Fluorescence measures of K as well as *in situ* gamma measurements. Alpha counting was done using a Daybreak 583 thick source alpha counter. TSAC measures paired activity of U and Th assuming that all the daughters are present in equilibrium. The instrument has a 0.02 to 0.4 s window in which it is able to measure 'slow pairs'. Slow pairs reflect the decay of ^{216}Po (half-life 0.145 s) into ^{212}Pb in the Th chain (see appendix C). By factoring the probability of detecting a slow pair, the pairs count can be used to calculate the contribution of the Th chain to the total alpha count. The remaining alpha counts are presumed to derive from the U chain (Aitken, 1985).

The samples are measured in a 42mm diameter holder (area = 1385 mm²). The sample holder contains a zinc sulphide (ZnS) screen that produces scintillations when struck by alpha particles. The scintillation events can be measured accurately with modern photomultiplier tubes (Aitken, 1985). The output from the daybreak TSAC is in the form of raw ppm concentrations of U and Th, but the output values could not be replicated manually using the standard approach. In this study the values were calculated using the raw counts (see appendix C).

Determination of the external dose rate can be problematic due to the heterogeneity of the sample matrix. A solution to the problem is to measure the gamma radiation contribution *in situ* using a portable gamma spectrometer. This method is relatively fast but has the disadvantage of having to auger a hole in the sample site that is wider than the detector and at least 30 cm in depth. For archaeologically sensitive sites, such as RCC, the auger hole could overlap the desired layer, as well as destroy site information. When using a portable gamma spectrometer, the individual dose rate contributions from Th, U and K are determined (Aitken, 1985). The spectrometer used in this study was an Aptec portable gamma spectrometer with a 2 inch NaI crystal, doped with thallium (TI) as an activator. Scintillations produced by gamma rays are measured by a photomultiplier tube (one pulse per gamma ray) and produces a corresponding electrical pulse. The electron has the same energy as the gamma photon and dissipates its energy in the crystal (Aitken, 1985). Figure 4.6 taken from sample RCC 10 shows the spectrum from a typical RCC soil sample.

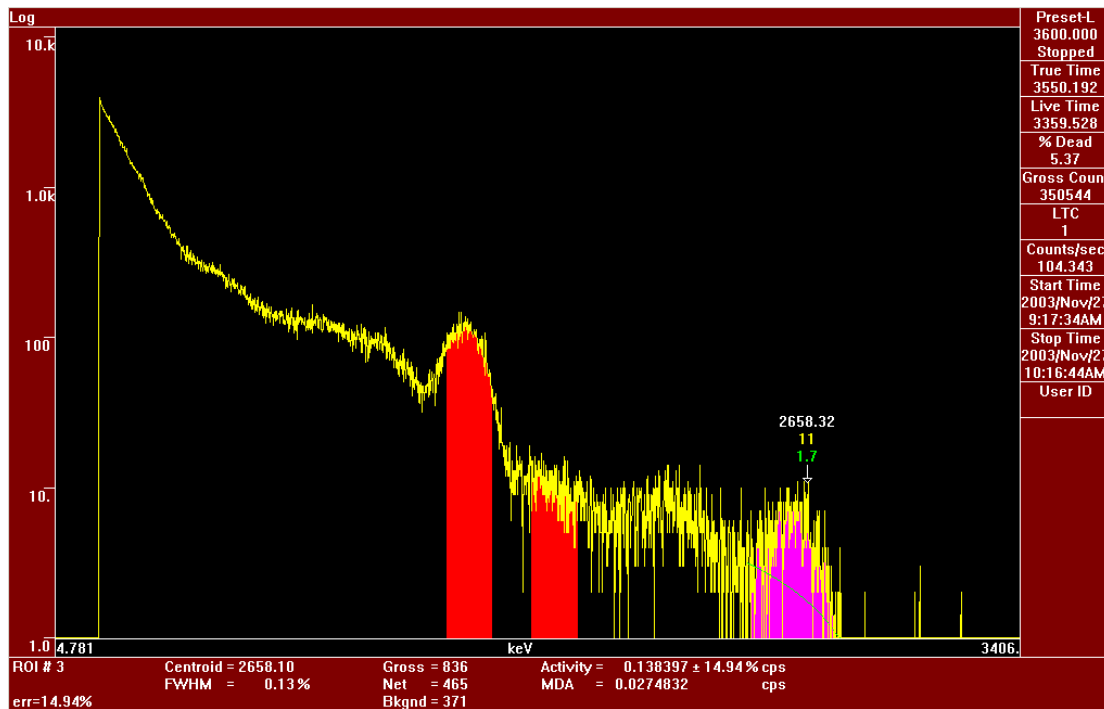


Figure 4. 6 Spectrum derived from a portable gamma spectrometer showing the energy range or photopeaks for the main radioactive elements used in luminescence dating.

With the gamma spectrometer used in this study a full spectrum of gamma radiation pulses are measured, and an acceptance 'window' is generated centred on the range of pulse heights concerned with each radioactive peak (Aitken, 1985). For ^{40}K the peak is 1.46 MeV and the corresponding integration is between 1.38 and 1.53 MeV. For uranium the peak is 1.76 MeV, and is integrated between 1.69 and 1.84 MeV, and for thorium the peak is at 2.61 MeV and is integrated between 2.46 and 2.76 MeV. The system was calibrated using the calibration blocks at Oxford University, and the same integration windows were used.

In order to obtain acceptable precision on the detection counts, the field measurements were conducted for a minimum of 40 minutes, but where time allowed a minimum of 60 minutes was used. Multiple peak identification was used to calibrate the energy scale of the spectrometer and to compensate for any drift that may occur during field measurements.

4.5 Calculation of dose-rates

The dose rates derived in this thesis are from the measurement of element concentrations (ppm) by means of conversion factors calculated by Adamiec & Aitken (1998). The 'Dry dose rates' expressed as a direct conversion from elemental concentration to dose rates need to be corrected for attenuation controlled by moisture content and the effective alpha particle contribution. The conversion factors taken from Adamiec & Aitken (1998) are shown in table 4.1

Table 4.1 Conversion factors used for dose rate calculation (Adamiec & Aitken, 1998).

	²³² Th	²³⁸ U	²³⁵ U	Natural U	⁴⁰ K
Abundance by weight	100%	99.29%	0.71%	-	-
Half-life	14.05	4.468	0.704	-	1.277
Parent activity (Bq/mg)	4.06	12.4	80	12.9	
<i>Dose-rate (Gy/ka) per ppm</i>					
Alpha, full series	0.732	2.685	16.6	2.78	0
Beta, full series	0.0273	0.143	0.515	0.146	0.782
Gamma, full series	0.0476	0.112	0.269	0.113	0.243

Dry dose rates were corrected for attenuation affects on grain size, then by the effects of moisture. Values used for the two grain sizes used for analysis are given in table 4.2 below.

Table 4.2 External attenuation factors

	Average grain Size	
	126µm	195µm
<i>Alpha attenuation</i>		
Th	0.199	0.130
U	0.171	0.111
<i>Beta attenuation</i>		
Th	0.891	0.856
U	0.838	0.797
K	0.955	0.932

4.5.1 Dose-rate calculation – A worked example

The calculations are taken from data obtained for sample RCC 10 shown in table 4.3. The example below was chosen as it comprises alpha attenuation calculations, for etched samples this step was simply ignored.

Table 4.3 Raw data for sample RCC 10

	Raw data	Error
²³² Th ppm	3.4264	0.3889
²³⁸ U ppm	1.2551	0.0413
K%	1.45	
Cosmic contribution	60	20
Moisture content	10	2
Grain size (µm)	195	
Alpha efficiency	0.04	0.02

The Th, U and K concentrations are multiplied by their corresponding conversion factors given in table C1 to obtain the 'Dry dose rate (Gy/ka)', and then corrected for grain size attenuation using values taken from table 4.2. See table 4.4 below.

Table 4.4 Dry dose rates (Gy/ka) for sample RCC 10

	Alphas	Betas	Gammas
Th	2.508 ± 0.285	0.094 ± 0.011	0.163 ± 0.019
U	3.489 ± 0.115	0.183 ± 0.006	0.142 ± 0.005
K		1.134	0.352
Corrected for grain size attenuation			
Th	0.324 ± 0.037	0.080 ± 0.009	.0163 ± 0.019
U	0.387 ± 0.013	1.146 ± 0.005	0.142 ± 0.005
K		1.058	0.352

The dry dose rates are added together and corrected for moisture content however, the alpha contribution from Th and U needs to first be corrected by the alpha efficiency factor of 0.04. The dry dose rate then becomes,

Alpha: 0.028 ± 0.002

Beta: 1.284 ± 0.014

Gamma: 0.657 ± 0.023

Example 4.1

The 'wet' dose-rates or true dose rates become:

Alpha: 0.024 ± 0.002

Beta: 1.126 ± 0.014

Gamma: 0.583 ± 0.023

Total dose-rate: 1793.25 ± 38.25 Gy/Ka

Example 4.2

5.0 THE SAR PROTOCOL APPLIED TO THE ROSE COTTAGE CAVE SAMPLES

5.1 Sample overview

In this chapter the OSL analyses of quartz aliquots from Rose Cottage Cave are presented. Seventeen luminescence samples, taken over the last decade, were used in this study. Fourteen of these samples were dated. In 1996 S. M Woodborne collected six luminescence samples (RCC 5-10) from the Harper excavation for part of a post-doctoral study into the MSA (Woodborne & Vogel, 1997). A total of twelve further OSL samples (RCC 11-22) were collected from RCC during 1999 and 2003 from the Wadley and Harper excavations by S. M. Woodborne and M. Pienaar. Table 5.1 presents the pretreatment affiliations of all the dated RCC samples. A total of eight of these samples were dated in Pretoria and six in Risø, Denmark by A. S. Murray. Samples RCC 6-10 were used to characterise the OSL behaviour of samples by using two mask sizes (5mm and 2mm) and etched and un-etched quartz.

The conventional SAR protocol (Murray & Wintle, 2000) (chapter 3) was used for all the RCC samples using a preheat range between 160°C and 300°C for 10 s with a cut-heat of 160°C for 0s. The L_x and T_x measurements were acquired through a range of regenerative OSL measurements each stimulated at 125°C for 40 s with blue LEDs at 90% power. All measurements were carried out on an automated Risø TL/OSL DA 15 reader with a measured systematic error of 1.8%. Behavioural controls inherent to the conventional SAR protocol were administered to each sample and depositional factors such as partial bleaching were assessed using signal analysis methods (Bailey, 2003a, 2003b). The grain size was chosen based on the distribution of isolated quartz extracts.

Table 5. 1 RCC samples in depth order showing grain size fractions and mask sizes used in dating

RCC OSL SAMPLES		
Sample name	Size Fraction	Mask size
RCC 17		
RCC 22		
RCC 21	180-212 μ m	2mm
RCC 20		
RCC 10	180-212 μ m	5mm & 2mm
RCC 19	180-212 μ m	2mm
RCC 9	180-212 μ m	5mm & 2mm
RCC 18	180-212 μ m	2mm
RCC 16	180-212 μ m	Measured at Risoe
RCC 6	106-150 μ m	5mm & 2mm
RCC 15	180-212 μ m	Measured at Risoe
RCC 14	180-212 μ m	Measured at Risoe
RCC 7	180-212 μ m	5mm & 2mm
RCC 13	180-212 μ m	Measured at Risoe
RCC 12	180-212 μ m	Measured at Risoe
RCC 8	106-150 μ m	5mm & 2mm
RCC 11	180-212 μ m	Measured at Risoe

5.2 Rejection criteria

The aliquots were assessed against OSL rejection criteria that were assumed to eliminate most errors with the OSL behaviour and sedimentary history of the grains. The following rejection tests were applied in order to obtain correct D_e values:

- A dose recovery experiment
- A partial bleach test
- A feldspar elimination test (IR-OSL depletion ratio)
- Sensitivity correction in regeneration analysis
- A recycling ratio Test (RR)
- A test for recuperation (charge transfer), and
- Must present a preheat plateau.

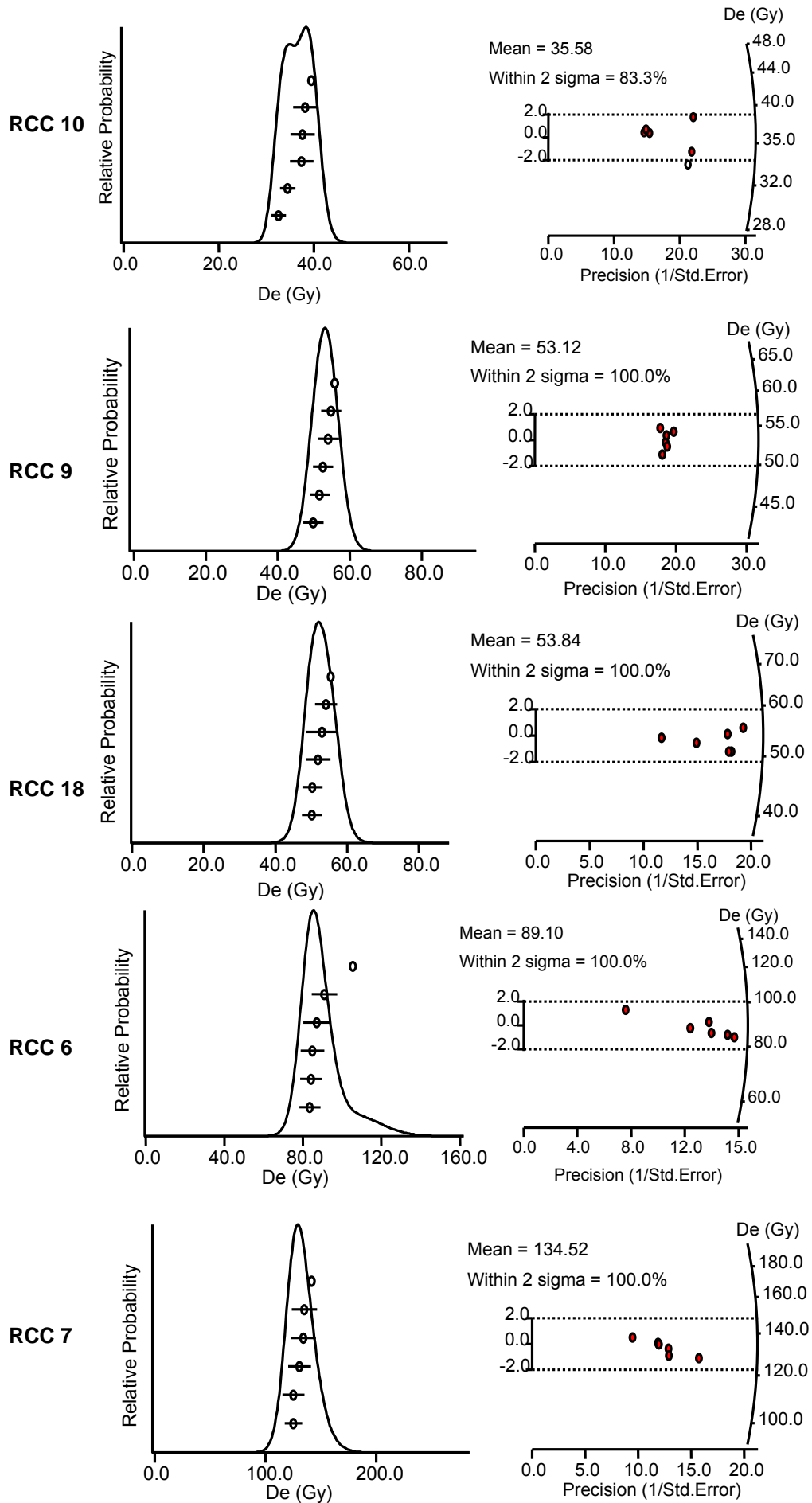
5.2.1 Dose recovery experiment

Dose recovery experiments (Murray & Roberts, 1998; Roberts *et al.*, 1999) were performed on six aliquots per sample. The aliquots were optically bleached using blue LEDs for 40s at 125°C. After zeroing, a known laboratory dose assumed to be

representative of the natural dose, was administered and a conventional SAR protocol was performed to see if the dose could be recovered. The test is an independent verification of the SAR protocol and any sensitivity changes that could occur from the natural OSL signal are detected. The test does not re-create time-dependent effects that occur naturally and could therefore result in slight differences between the natural dose and the recovered dose. The test does, however, give a good indication of the reproducibility of the D_e value and the appropriateness of using sensitivity corrected dose response curves throughout a SAR measurement sequence. Samples RCC 6-10 and RCC 18 were used as general indicators for all the Rose Cottage Cave material in this experiment. Table 5.2 shows the results of dose recovery experiments, where the average recovered dose vs. the given dose is quoted. All values recovered well and it was assumed that all RCC samples have little if any sensitivity changes in the natural OSL measurement. Graphical displays in the form of radial plots and relative probability plots are shown in figure 5.1

Table 5. 2 Values of recovery doses obtained by SAR protocol for known doses using a dose recovery experiment (Murray & Roberts, 1998; Roberts *et al.*, 1999). Samples are presented in order of decreasing depth.

Sample Name	Administered Dose	Recovered Dose	% Dose Recovery
RCC 10	35.8 Gy	35.6 Gy	97.8%
RCC 9	53.8 Gy	53.1 Gy	98.7%
RCC 18	53.8 Gy	53.8 Gy	100.0%
RCC 6	89.6 Gy	89.1 Gy	99.4%
RCC 7	134.4 Gy	134.5 Gy	99.9%
RCC 8	134.4 Gy	123.6 Gy	92.0%



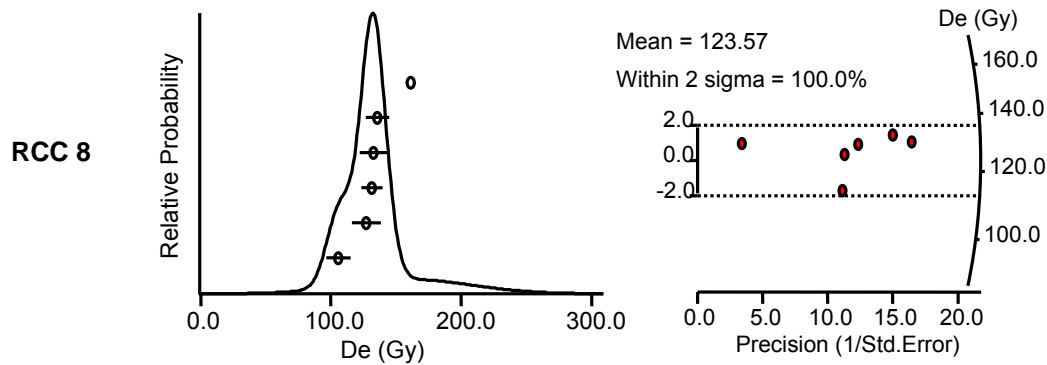


Figure 5. 1 Values of recovery doses obtained by SAR protocol for known doses using a dose recovery experiment (Murray & Roberts, 1998; Roberts *et al.*, 1999). Samples are presented in order of decreasing depth.

5.2.2 Partial bleach test

Both Butzer (1984a, 1984b) and Herries & Latham (2002) have suggested that the deposit in Rose Cottage Cave derives from material detached from the cave roof and walls, introduced through a major joint intersection at the back of the cave that was enlarged by water erosion. Butzer suggested that the deposition of the cave consists of predominantly weathered sandstone klasts, produced through weathering or rock spalling of the cave roof and walls and laminated sediments brought in by water. The possibility of incomplete signal resetting needs to be assessed. In this study signal analysis methods (discussed in chapter 2) were used to determine incomplete signal resetting (Bailey, 2003a, 2003b). The $D_e(t)$ method of Bailey was performed on samples RCC 6-10, 18, 19 and 21. Ten random aliquots representative of a preheat range between 160°C and 300°C were used for each sample.

The method requires that the OSL signal comprise a thermally stable fast bleaching and a slow bleaching component. If the sample is partially bleached then a slower bleaching components would yield a greater residual signal i.e. yield a greater age. Stimulation was carried out at 125°C for 40s using blue LEDs at 90% power. Values of D_e were obtained for each aliquot using approximately 0.5 second integration channels and are shown in stratigraphic order in figure 5.2. The downward right trend in figure 5.2 indicates that the fast component could not

have been preferentially bleached. This is based on the assumption that if partial bleaching occurs, the fast component would bleach first and there would be a higher residual signal from an integration channel in the medium component. This is not characteristic of fluvial or spalled material and could indicate aeolian deposition.

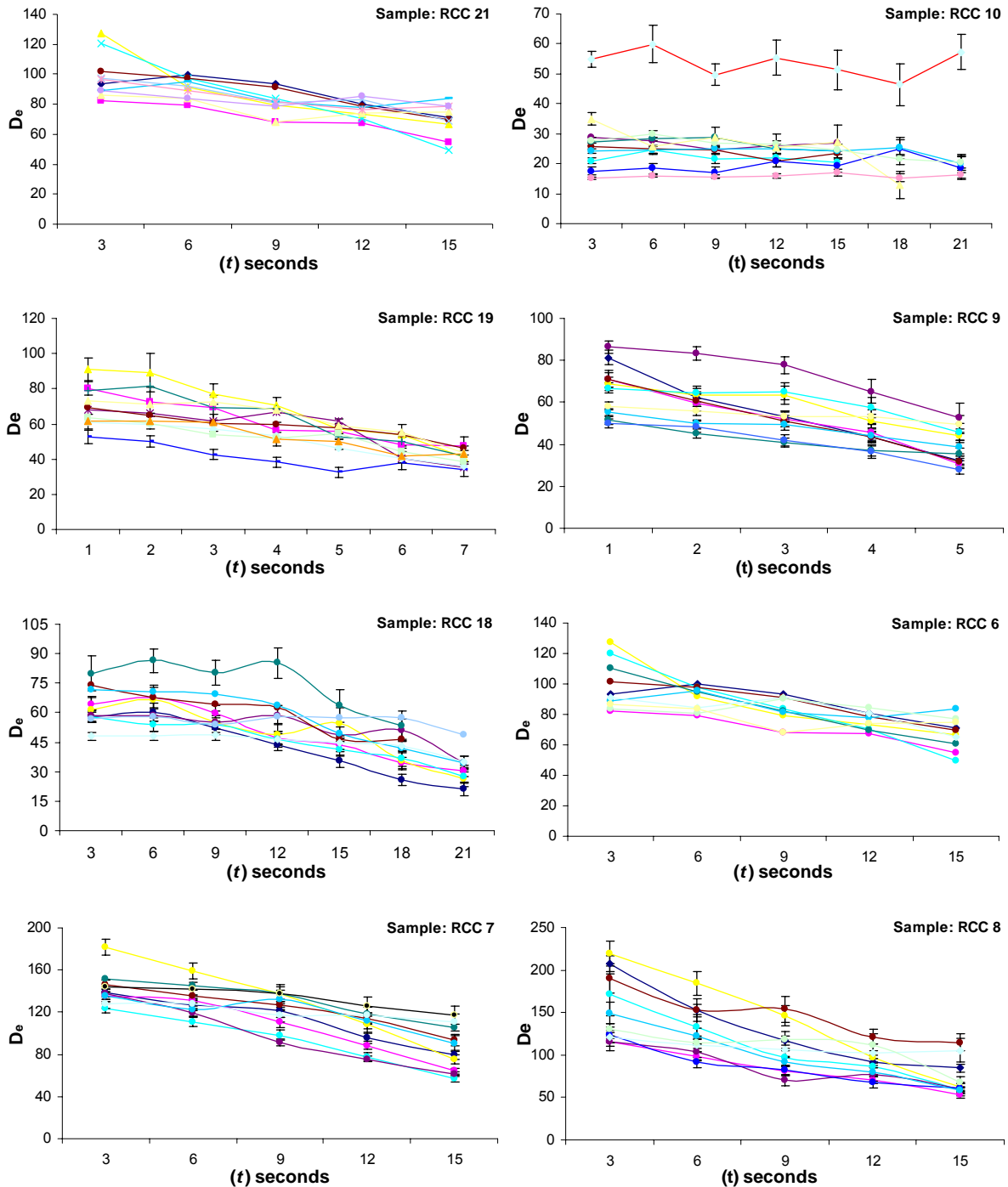


Figure 5.2 $D_e(t)$ plots displaying D_e values quoted in Gy obtained at different integration channels (Bailey, 2003a).

5.2.3 IR-OSL depletion ratio test

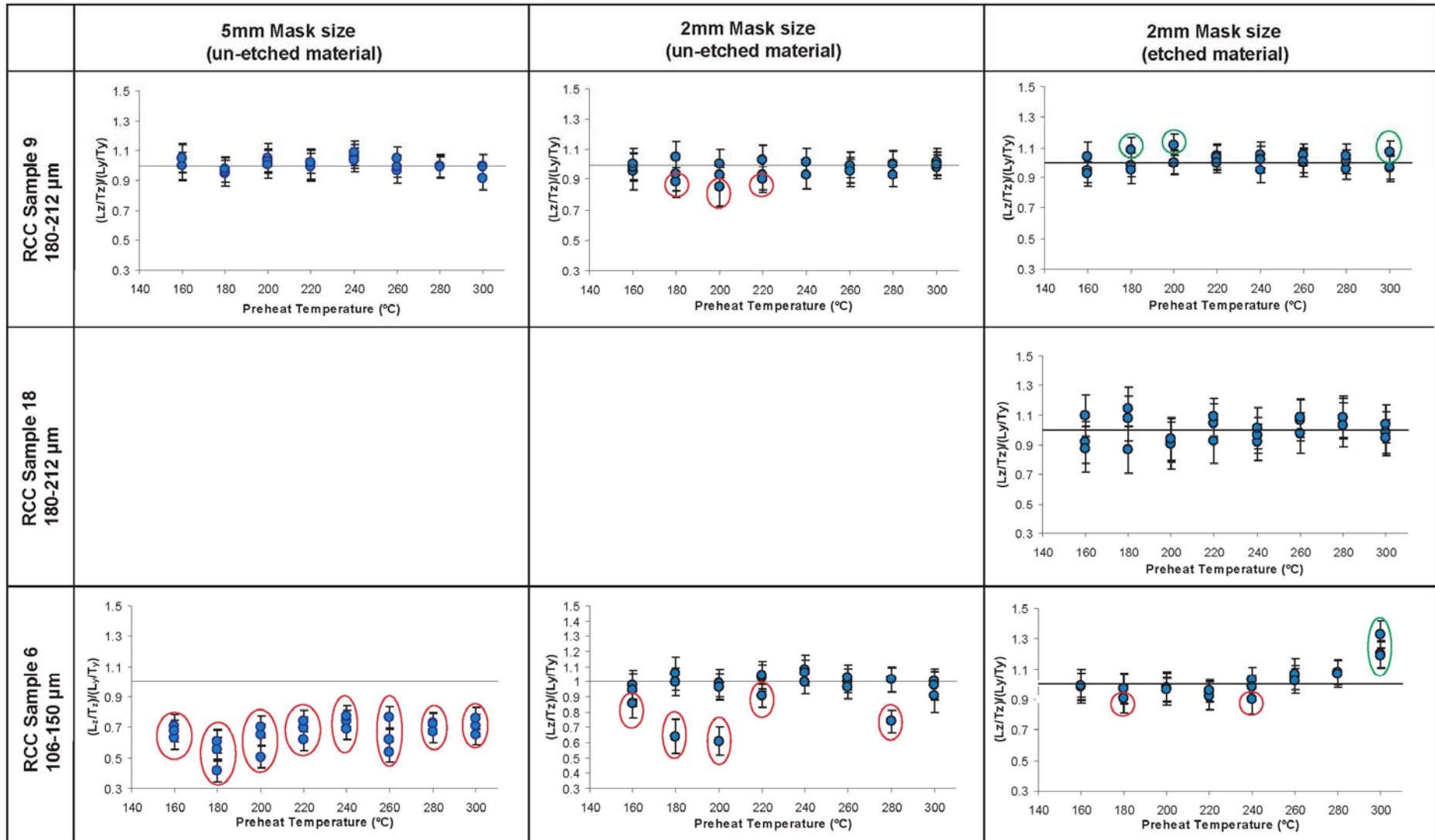
Feldspar contamination in quartz aliquots usually results in higher D_e value estimates in OSL measurements. This is due to an internal potassium contribution that increases the internal dose but is not considered in the dosimetry or is the result of highly sensitive feldspars that have not been eradicated through pre-treatment techniques. If random trap emptying synonymous with feldspars, also known as anomalous fading, occurs (Aitken, 1998), then feldspar contamination could also result in an underestimation of D_e . It is therefore important to assess whether scatter in the equivalent dose measurements is a result of feldspar contamination. The IR OSL depletion ratio test consists of 3 measurement cycles. The first measurement (L_1/T_1) consists of a typical regenerative dose, usually the first regenerative point. The second measurement (L_2/T_2) is a repeat of the first measurement. Typically the ratio between these two measurements would fall within unity if no other measurement is applied. Before the second measurement however, the sample is stimulated with IR diodes. IR stimulation at approximately 880 nm does not significantly affect quartz (Stokes, 1992; Duller, 2003) and any depletion of the signal measured during L_2/T_2 would be the result of feldspar contamination.

Figure 5.3 shows the OSL IR depletion ratio test using large (5mm) mask sizes, 2mm mask sizes and the results of samples that were etched in HF acid. The initial dose was 18 Gy measured with blue LEDs for 40s. A repeat dose of 18 Gy was stimulated using IR diodes at 90% power for 100s followed by stimulation from blue LEDs for 40s. Where the depletion ratio deviated from normality by more than 2σ , calculated from the measurement precision, the aliquots were rejected from further analysis (Jacobs *et al.*, 2003a). Figure 5.3 shows the results with two standard deviation error bars. The red circles indicate aliquots that were rejected due to feldspar contamination; the green circles represent aliquots that were rejected due to unexplained recycling ratio behaviour.

Out of a total of 408 aliquots, 101 or 25% of the aliquots were rejected due to feldspar contamination. If the etched material is not included then a total of 98 out of 240 aliquots (41%) of the aliquots would have been rejected. This implies that in

a feldspar rich site such as RCC not all feldspars are removed by mineral separation, or there is the possibility of internal feldspar inclusions. It is therefore crucial that the samples are etched in HF. The accepted samples, except for the 5mm mask sized samples RCC 10, 6, and 7 however, statistically constitute a large enough population to accept further analyses.

	5mm Mask size (un-etched material)	2mm Mask size (un-etched material)	2mm Mask size (etched material)
RCC Sample 21 180-212 μm			
RCC Sample 10 180-212 μm			
RCC Sample 19 180-212 μm			



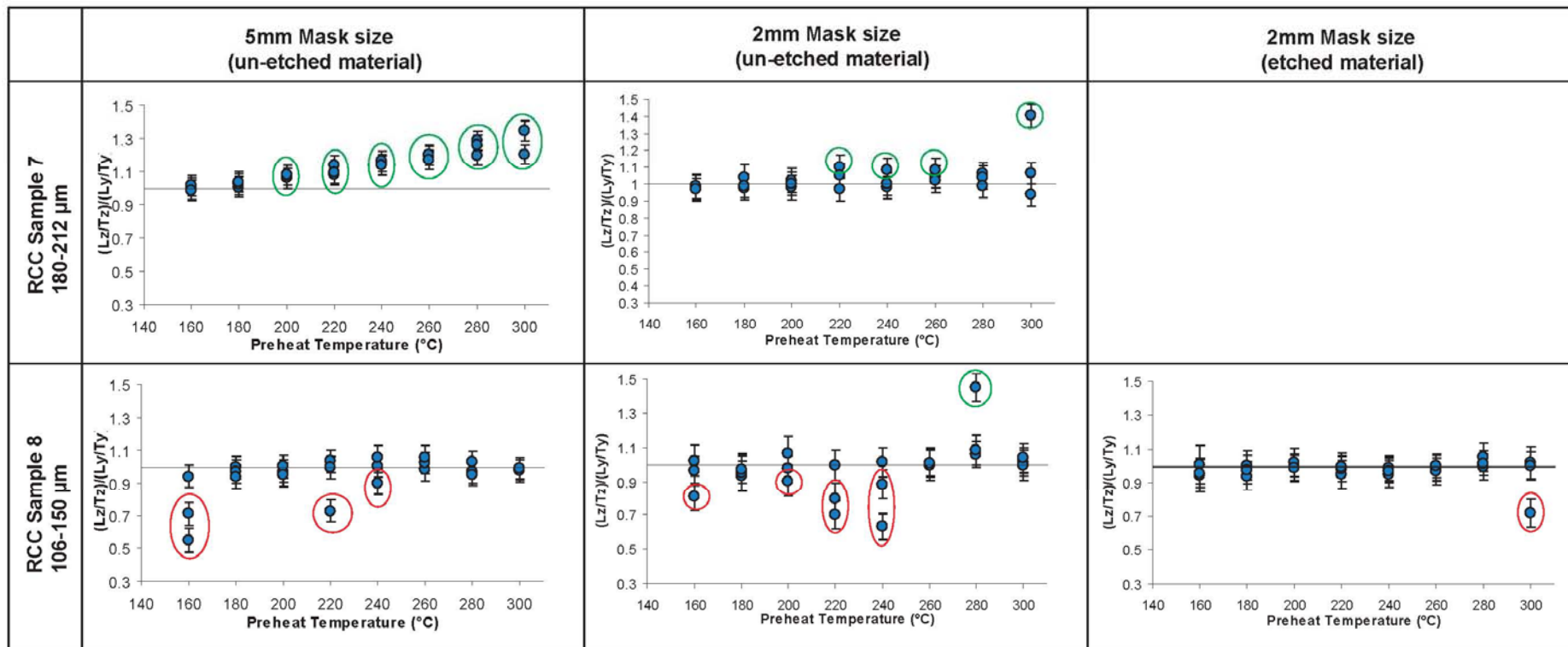


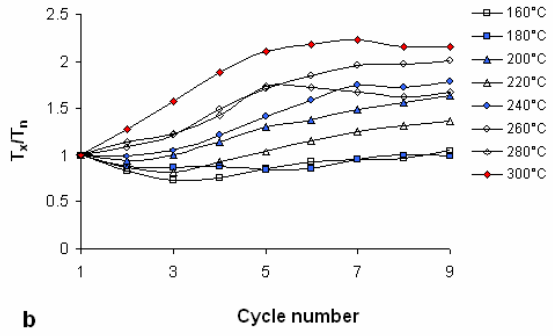
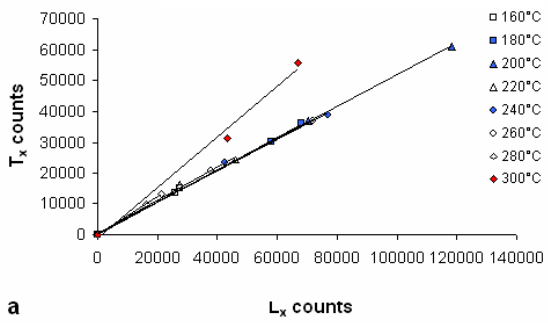
Figure 5.3 IR OSL Depletion Ratio tests performed on aliquots using 5mm and 2mm mask sizes at different preheat temperatures. The IR OSL Ratio is given as $[(L_z/T_z)/(L_y/T_y)]$, where L and T are the regenerated OSL intensity of the given dose and the test dose. Large mask size samples RCC 6, 7 and 10 were completely rejected as measurement ratios deviated substantially between recycled points, resulting in a very low ratio. The reduction in mask size from 5mm to 2mm shows the effect of feldspar elimination. On average 20% of the aliquots were rejected from 2mm mask size samples. Samples that were etched have an average of 7% rejections.

5.2.4 Sensitivity change

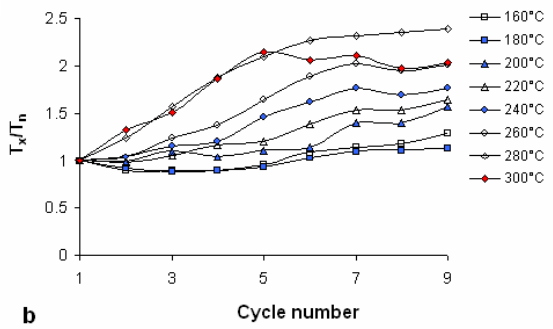
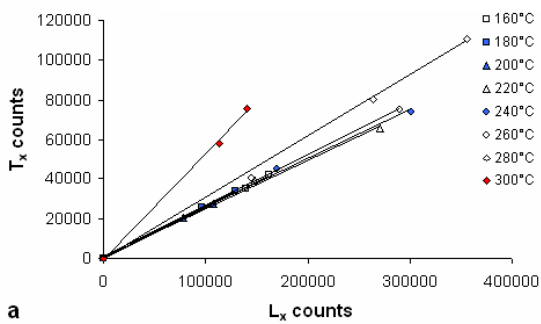
In this test a small test dose (roughly 10% of the natural D_e) is administered into a measurement sequence (Murray & Roberts, 1998; Wintle & Murray, 1999; Murray & Wintle, 2000). The test dose is used to normalize a L_x measurement. Any sensitivity changes relate to the transfer of charge produced by laboratory irradiation and preheating. Sensitivity changes can be observed as a function of preheating as well as measurement cycle. The use of a preheat range between 160°C and 300°C is used (Murray *et al.*, 1997) in order to isolate a signal derived from thermally stable traps and to equalize sensitivity between the natural and laboratory irradiated measurements. Murray & Mejdahl (1999) demonstrated that the relationship between the OSL test dose and an OSL regenerative dose must be linear for sensitivity to be corrected.

The linear relationship between L_x and T_x is shown in figure 5.2 using large and small mask sizes and a range of preheat temperatures between 160°C and 300°C. The values of L_x are plotted against T_x for two regenerative dose cycles, the values of T_x are then normalized to T_n (the test dose administered after measurement of the natural) and show the sensitisation process that occurs during a typical SAR measurement cycle. There is an initial decrease in sensitivity for the lower preheat temperatures (160°C - 240°C) and an initial increase in sensitivity for the higher preheat temperature (260°C - 300°C). If the values increase and decrease by about 25% to 35% they demonstrate typical behaviour (Jacobs *et al.*, 2003a) and it can be assumed that sensitivity changes are corrected successfully. Note only samples that have been accepted after the feldspar contamination test are shown in figure 5.4, and that all the samples show typical OSL quartz behaviour.

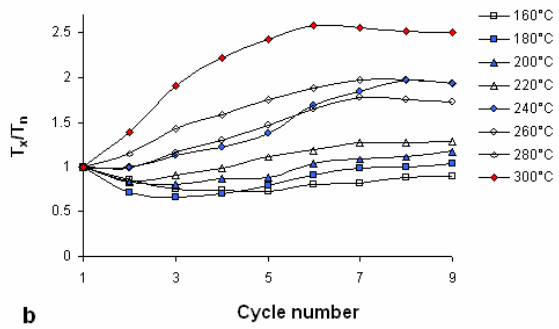
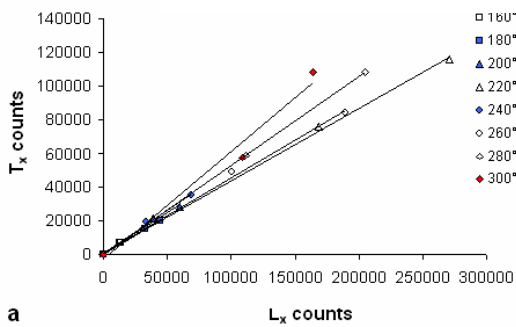
Sample RCC 21 2mm mask size (etched material)



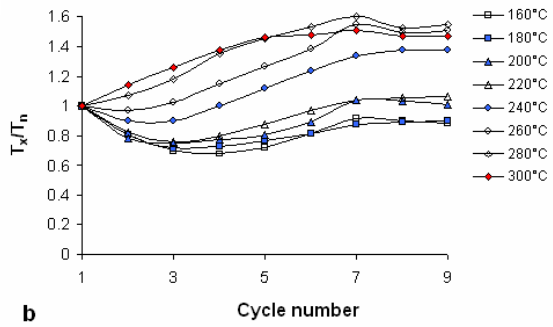
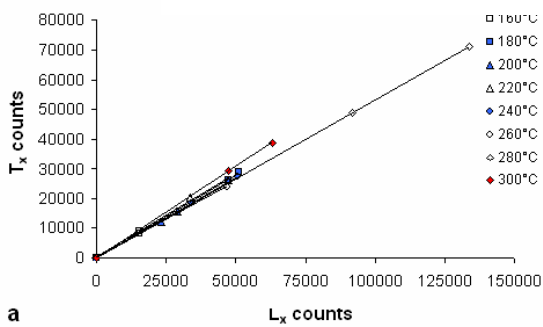
Sample RCC 10 2mm mask size (un-etched material)



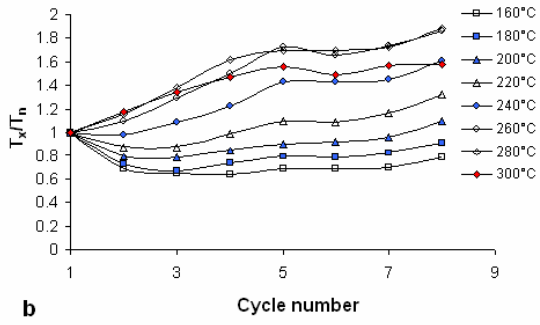
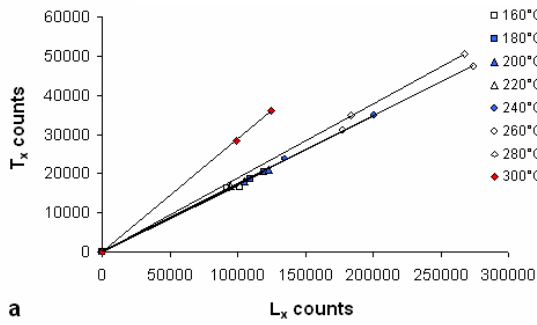
Sample RCC 10 2mm mask size (etched material)



Sample RCC 19 2mm mask size (etched material)



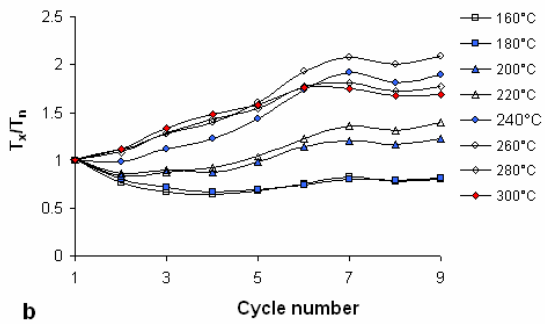
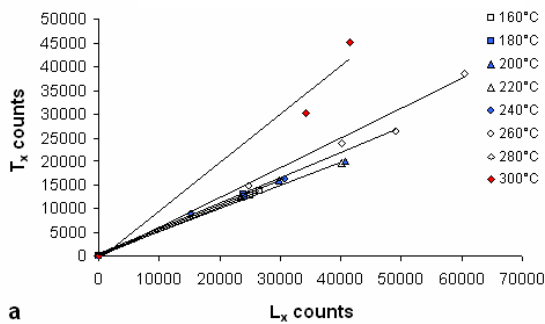
Sample RCC 9 5mm mask size (un-etched material)



a

b

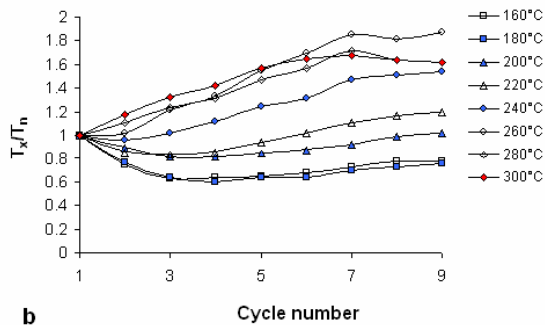
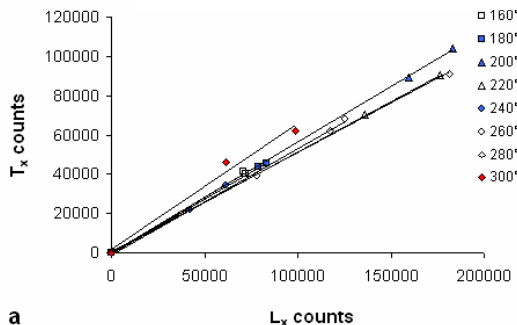
Sample RCC 9 2mm mask size (un-etched material)



a

b

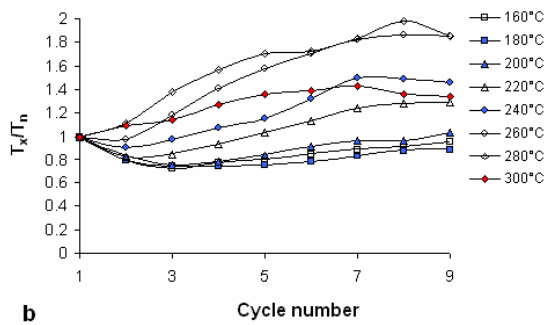
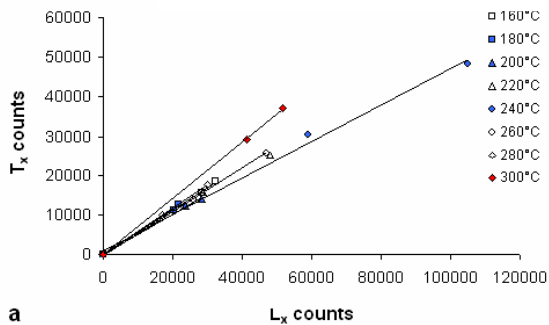
Sample RCC 9 2mm mask size (etched material)



a

b

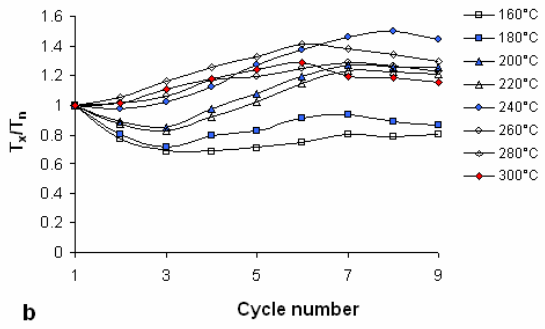
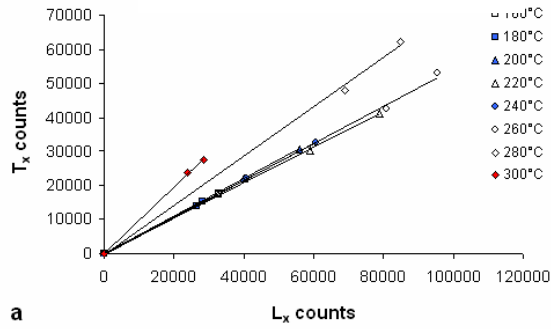
Sample RCC 18 2mm mask size (etched material)



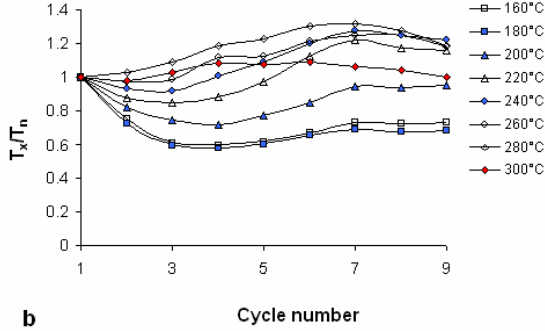
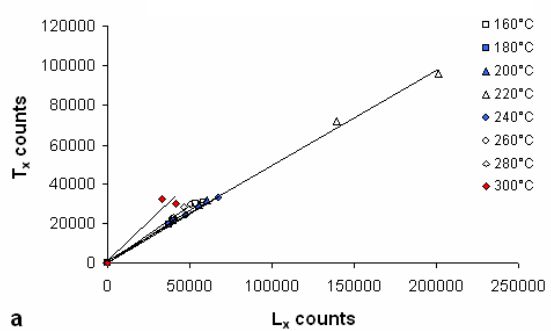
a

b

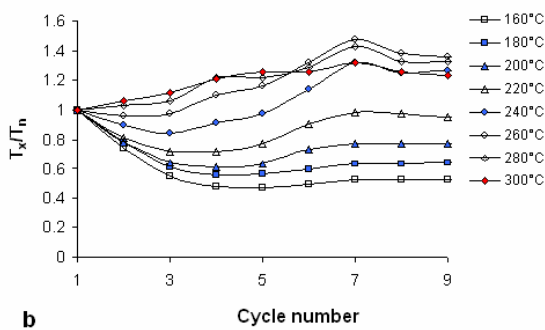
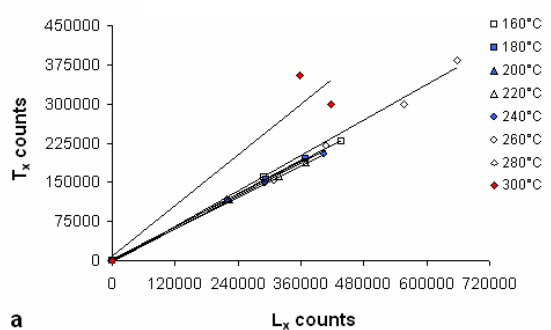
Sample RCC 6 2mm mask size (un-etched material)



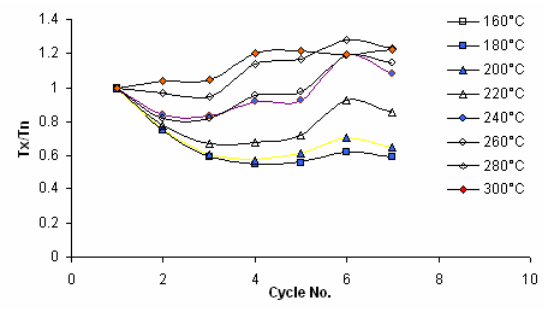
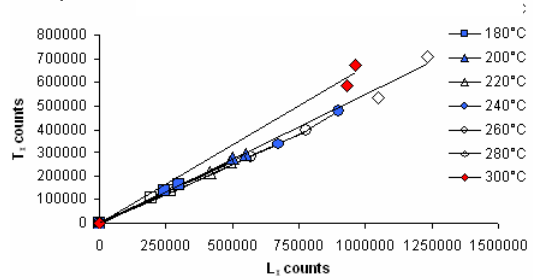
Sample RCC 6 2mm mask size (etched material)



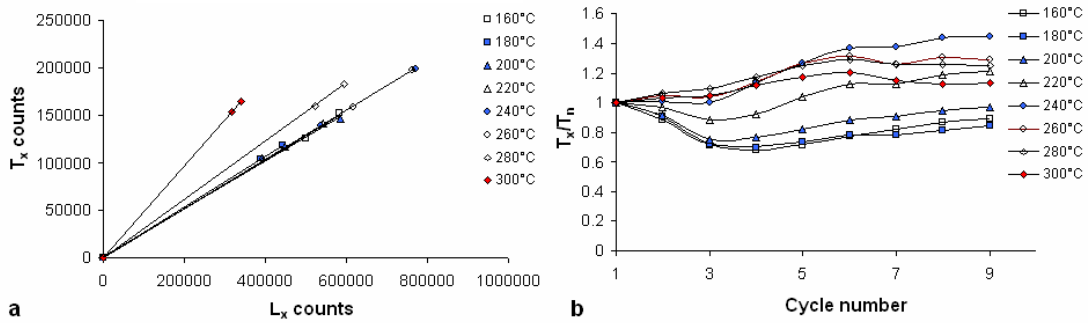
Sample RCC 7 2mm mask size (un-etched material)



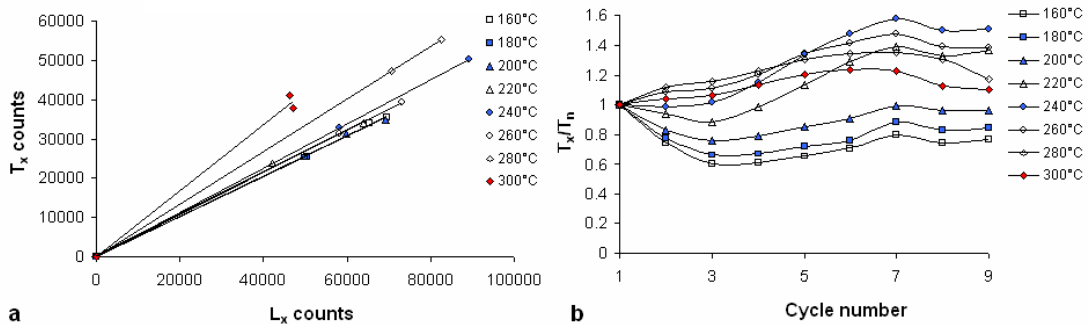
Sample RCC 7 2mm mask size (etched material)



Sample RCC 8 5mm mask size (un-etched material)



Sample RCC 8 2mm mask size (un-etched material)



Sample RCC 8 2mm mask size (etched material)

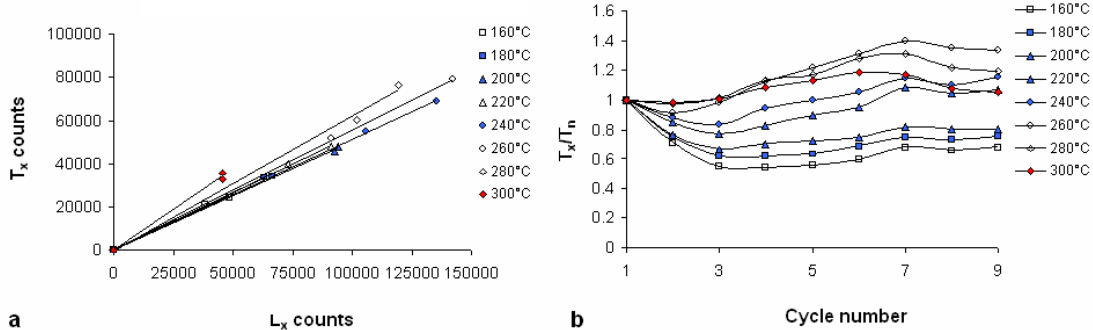
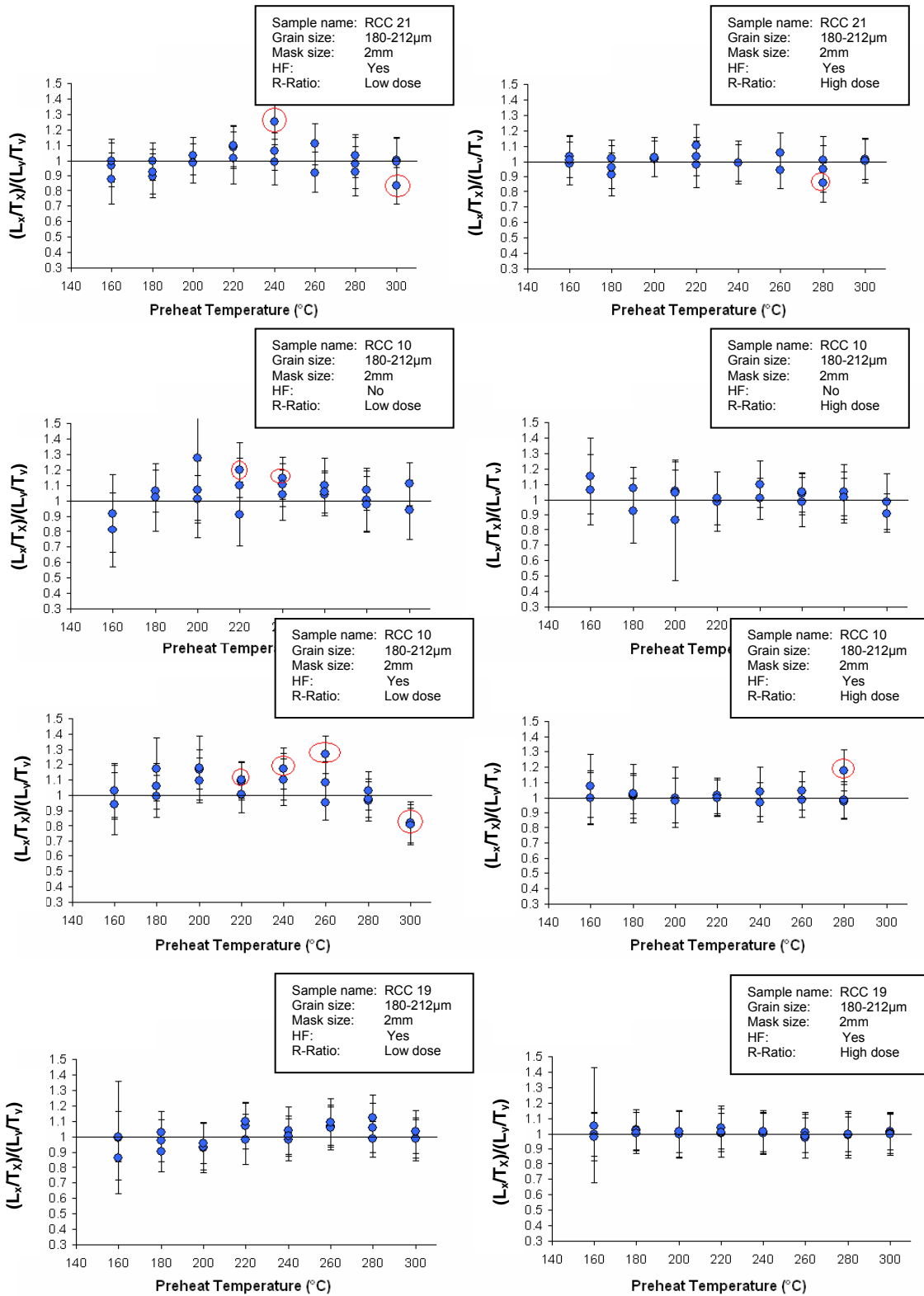
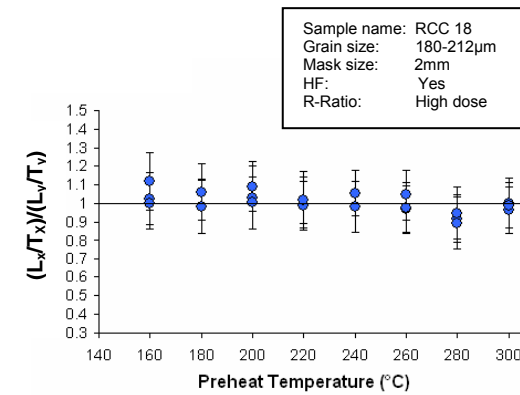
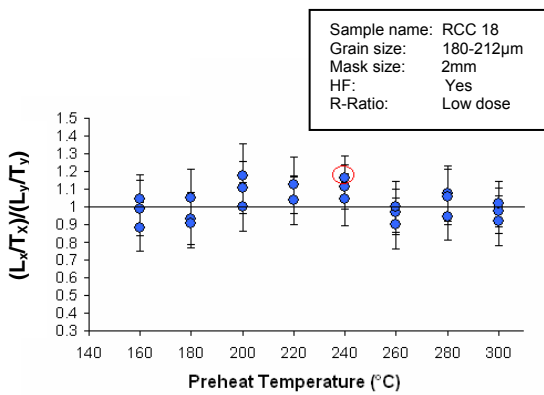
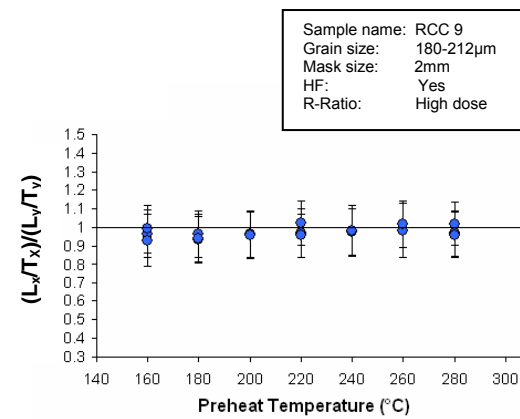
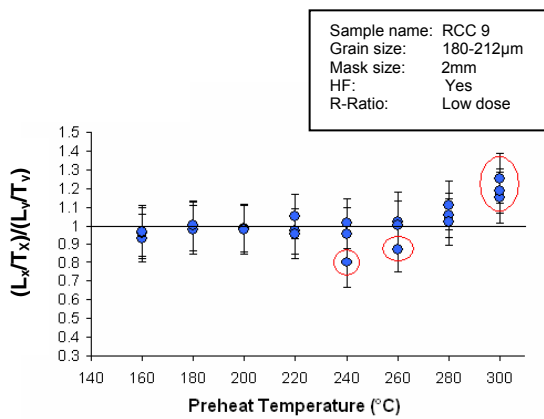
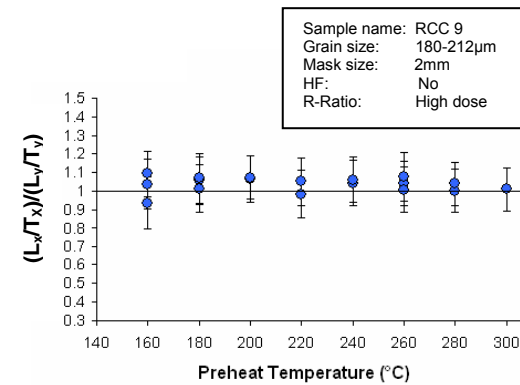
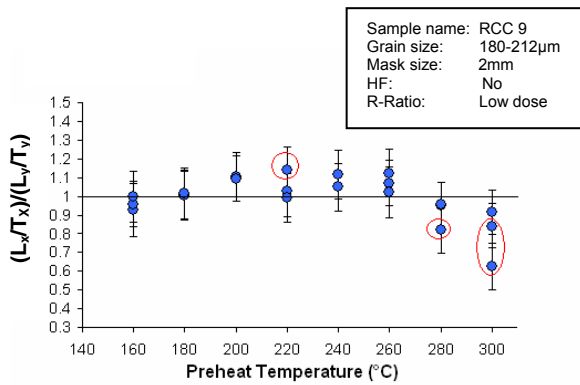
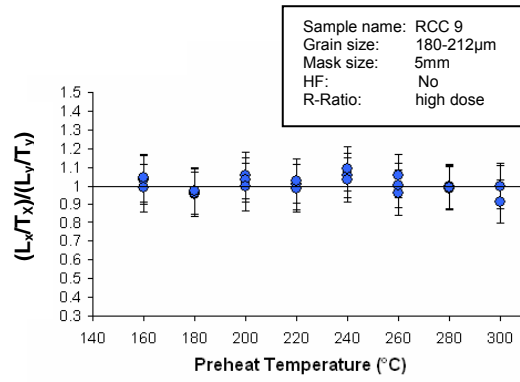
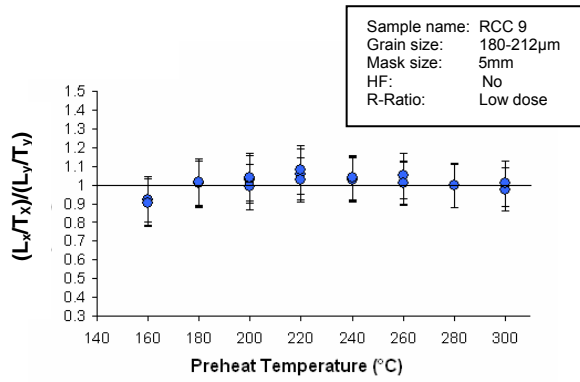


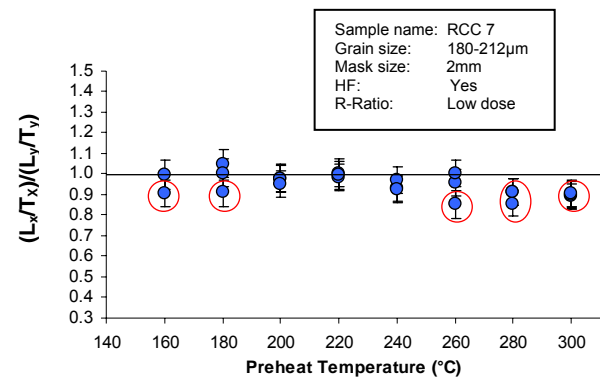
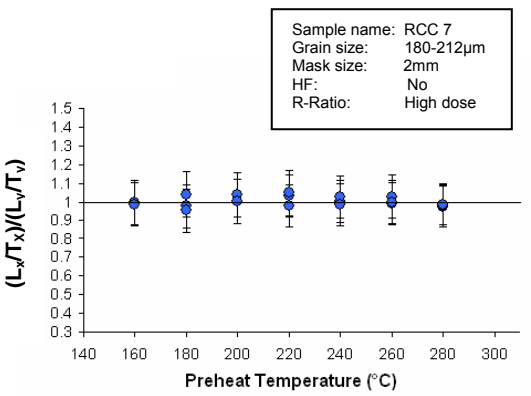
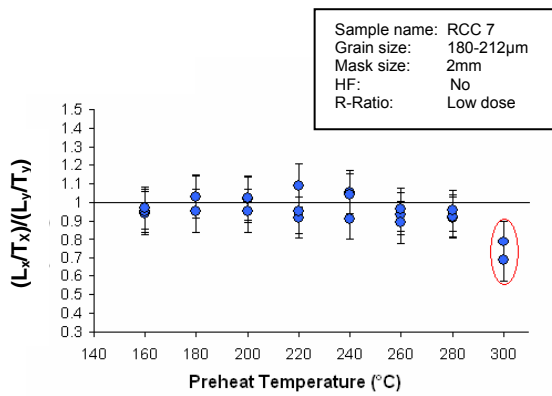
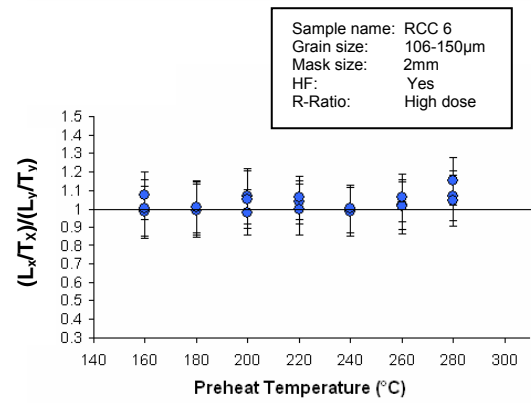
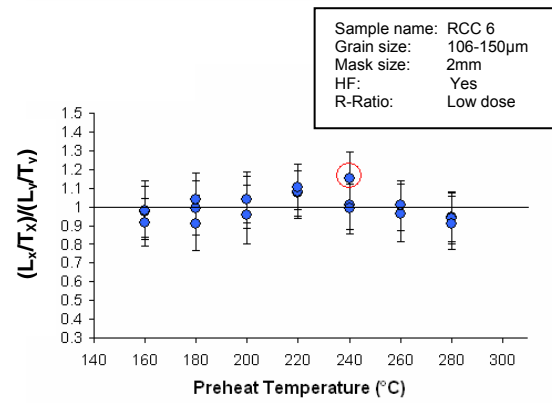
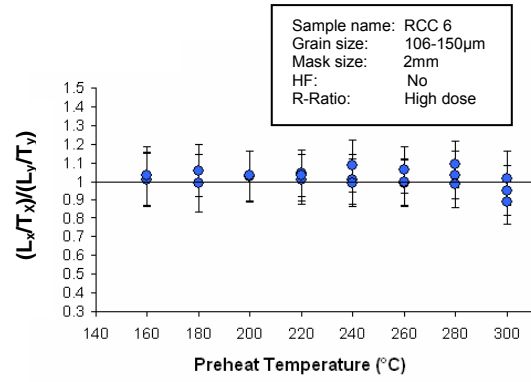
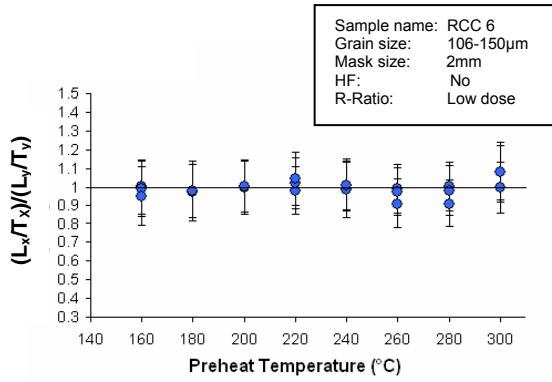
Figure 5. 4 Sensitivity changes monitored by the relationship between L_x/T_x and T_x/T_n vs. SAR cycle number. The checks are performed on aliquots using large (5mm) and small (2mm) mask sizes. The repeated dose points representing L_x/T_x values were obtained through recycling low dose data points. The 300°C values generally deviate from the main trend due to thermal depletion of the L_x measurement. The values of T_x are normalized to T_n , the lower preheat temperatures show a decrease in sensitivity for the first few measurement cycles. The higher preheat temperatures have an increase in sensitivity for the first few measurement cycles.

5.2.5 Recycling Ratio (R-Ratio) test

The values in figure 5.4 increase and decrease by between 25% and 35% typical of a SAR measurement cycle (Jacobs *et al.*, 2003a). For the above samples it can be assumed that sensitivity changes are corrected successfully. To check the validity of this assumption the SAR protocol makes use of the Recycling Ratio test (R-Ratio) (Murray & Wintle, 2000). The R-ratio is similar to the IR OSL depletion ratio test and uses a $[(L_2/T_2)/(L_1/T_1)]$ ratio to determine the degree of change in sensitivity. Two R-Ratio tests were performed on all the samples using the ratio $[(L_2/T_2)/(L_1/T_1)]$ to determine the rejection criteria. The first R-Ratio tests were performed using a low dose generally first administered at the beginning of the SAR measurement cycle, where one would expect to find the most sensitivity changes taking place. The second set of R-Ratios is taken from recycled points which were given a high dose. The results of these experiments are presented in figure 5.5 below. Note that the dataset does not include aliquots that were rejected using the IR-OSL depletion ration test. Most of the aliquots pass this test indicating good recycling behaviour.







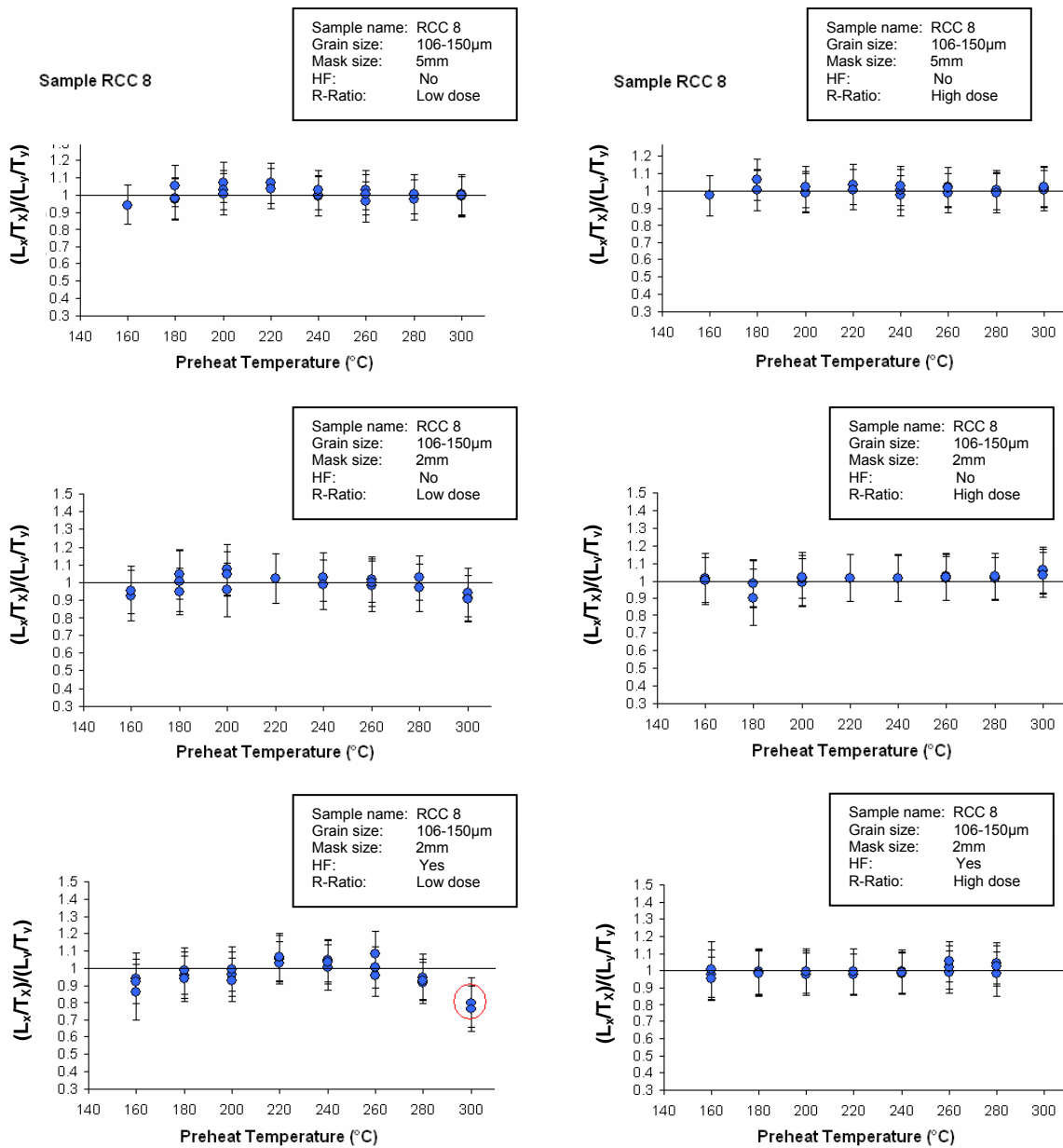


Figure 5.5 Low and high dose recycling ratio (R-Ratio) tests performed on aliquots using different mask sizes. 24 aliquots were divided into eight groups of three and measured at different preheat temperatures. The ratio is given as $[(L_2/T_2)/(L_1/T_1)]$. No aliquots which were rejected by the IR-OSL depletion ratio test are shown.

5.2.6 Recuperation

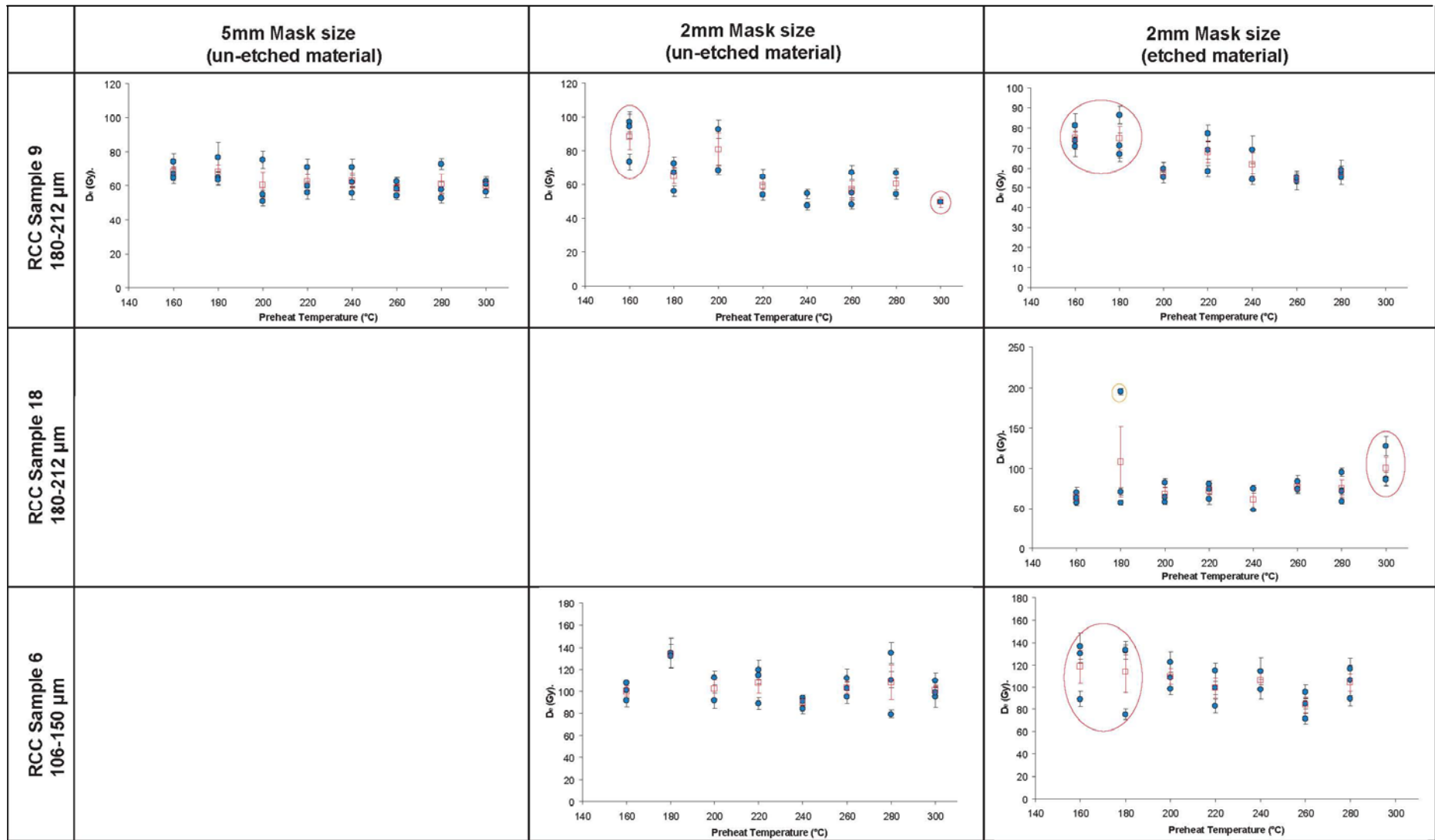
The effects of recuperation or ‘charge transfer’ could result in unacceptable variability in D_e values (Aitken & Smith, 1988) i.e. re-trapping of the charge that has remained in traps from the previous measurement and is induced by heat treatment applied to the

sample during a standard laboratory measurement protocol. Recuperation is likely to be minimal when using the conventional SAR protocol as all measurement cycles are carried out at 125°C (Murray & Wintle, 2000). Unwanted charge transfer is generally produced by traps that are emptied at higher preheat temperatures. The reliability of the corrected SAR growth curve is therefore reliant on minimal charge transfer between regenerative points (Murray & Wintle, 2000). The addition of a zero dose regenerative point visually demonstrates whether the curve is fitted through zero. A test for recuperation is used in this study by plotting the ratio between the zero dose and natural measurement and plotting the ratio as a percentage of the natural ($\{L_5/T_5\}/\{L_1/T_1\}$), all values that are greater than 5% (Murray & Olley, 2002) are rejected. No samples from RCC had recuperation values greater than 1.5%.

5.2.7 D_e versus T – Preheat Plateau

A plateau of D_e versus preheat temperature has been used in this study to ensure that reliable D_e values have been obtained for all the RCC samples. Isothermal decay curves obtained from Australian quartz using preheat ranges between 160°C and 280°C have demonstrated that the initial natural OSL signal is derived from a single trap (Wintle & Murray, 1998). The ability of the SAR protocol (Murray & Wintle, 2000) to correct for sensitivity changes is demonstrated by using a preheat range between 160°C and 300°C, if the same D_e values are obtained for all the accepted aliquots for which sensitivity changes have been corrected. In figure 5.6 the results for preheat plateaus are plotted; in most of the samples the lower and higher preheat ranges have been rejected. In a well behaved sample the charge transfer is evident at lower preheat temperatures and charge depletion occurs at higher preheat temperatures. Note that all samples in figure 5.6 do not include aliquots that have been rejected by previous rejection criteria.

	5mm Mask size (un-etched material)	2mm Mask size (un-etched material)	2mm Mask size (etched material)
RCC Sample 21 180-212 μm			
RCC Sample 10 180-212 μm			
RCC Sample 19 180-212 μm			



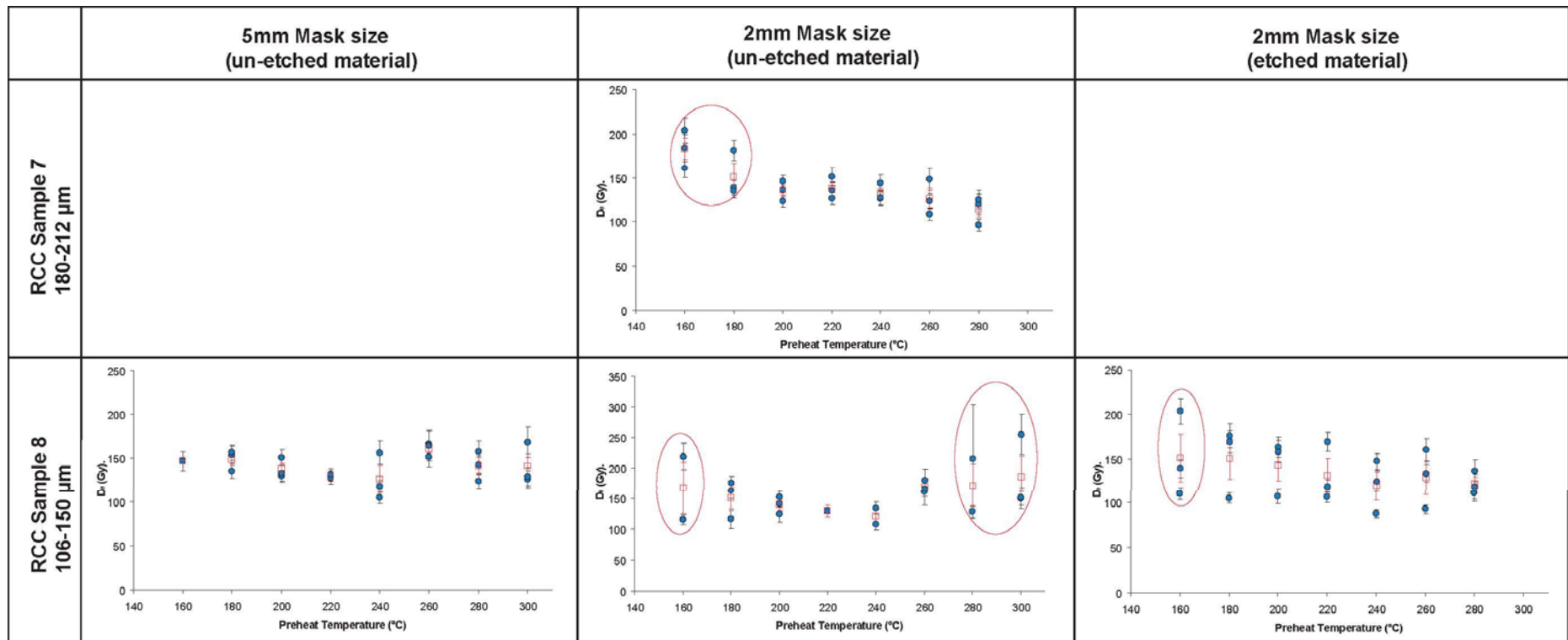


Figure 5. 6 Preheat Plateau results for RCC samples. 24 aliquots were divided into eight groups of three and measured at different preheat temperatures. The plot shows the relationship between D_e vs $Temperature$. No aliquots that were rejected by previous rejection criteria are shown.

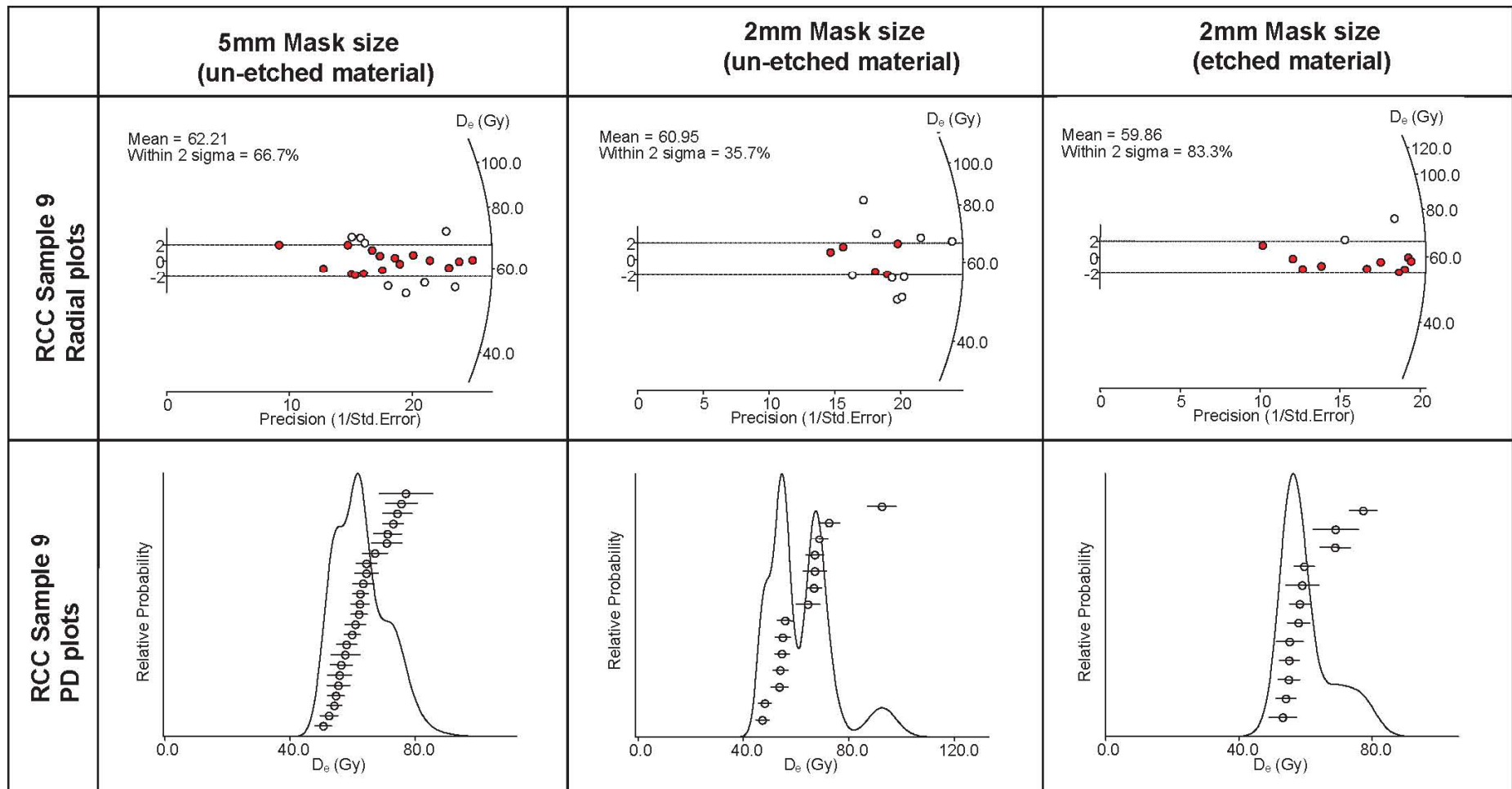
5.3 Analysis of D_e values

Figure 5.7 and table 5.3 present the results for D_e values after all SAR criteria have been met. These values are plotted as radial plots and probability density plots. Some of D_e measurements reflect large overdispersion values that need to be explained. A potential answer to such large overdispersion could be attributed to either sample mixing or to the large percentage of feldspar grains (not detected using the IR-OSL test) present in the samples (up to 60% composition in certain layers). The IR-OSL depletion ratio tests that were applied to samples RCC 6-10 using un-etched material measured on a large 5mm mask size resulted in some samples that were completely rejected either due to feldspar contamination or bad recycling behaviour. It was therefore assumed that once feldspar contaminated aliquots were rejected the remaining aliquots would be acceptable after all the other SAR tests were performed. On all the samples a central age model is suggested due to the general scatter in distribution.

	5mm Mask size (un-etched material)	2mm Mask size (un-etched material)	2mm Mask size (etched material)
RCC Sample 21 Radial plots			<p>Mean = 20.16 Within 2 sigma = 44.4%</p>
RCC Sample 21 PD plots			

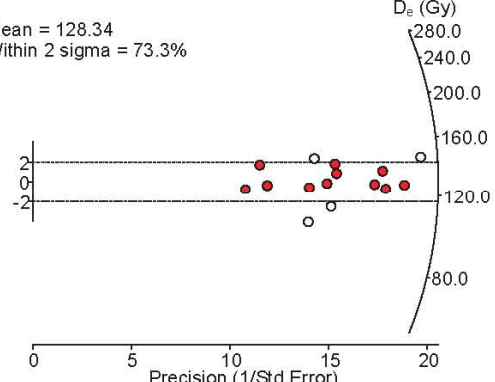
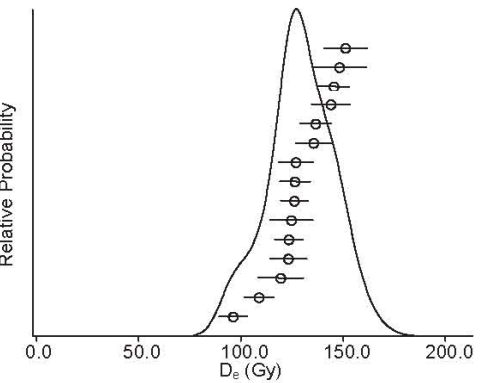
	5mm Mask size (un-etched material)	2mm Mask size (un-etched material)	2mm Mask size (etched material)
RCC Sample 10 Radial plots		<p>Mean = 25.25 Within 2 sigma = 45.5%</p>	<p>Mean = 27.38 Within 2 sigma = 61.5%</p>
RCC Sample 10 PD plots			

	5mm Mask size (un-etched material)	2mm Mask size (un-etched material)	2mm Mask size (etched material)
RCC Sample 19 Radial plots			<p>Mean = 65.40 Within 2 sigma = 86.7%</p>
RCC Sample 19 PD plots			



	5mm Mask size (un-etched material)	2mm Mask size (un-etched material)	2mm Mask size (etched material)
RCC Sample 18 Radial plots			<p>Mean = 68.95 Within 2 sigma = 47.4%</p>
RCC Sample 18 PD plots			

	5mm Mask size (un-etched material)	2mm Mask size (un-etched material)	2mm Mask size (etched material)
RCC Sample 6 Radial plots		<p>Mean = 103.45 Within 2 sigma = 63.6%</p>	<p>Mean = 99.14 Within 2 sigma = 64.3%</p>
RCC Sample 6 PD plots			

	5mm Mask size (un-etched material)	2mm Mask size (un-etched material)	2mm Mask size (etched material)
RCC Sample 7 Radial plots		<p>Mean = 128.34 Within 2 sigma = 73.3%</p> 	
RCC Sample 7 PD plots			

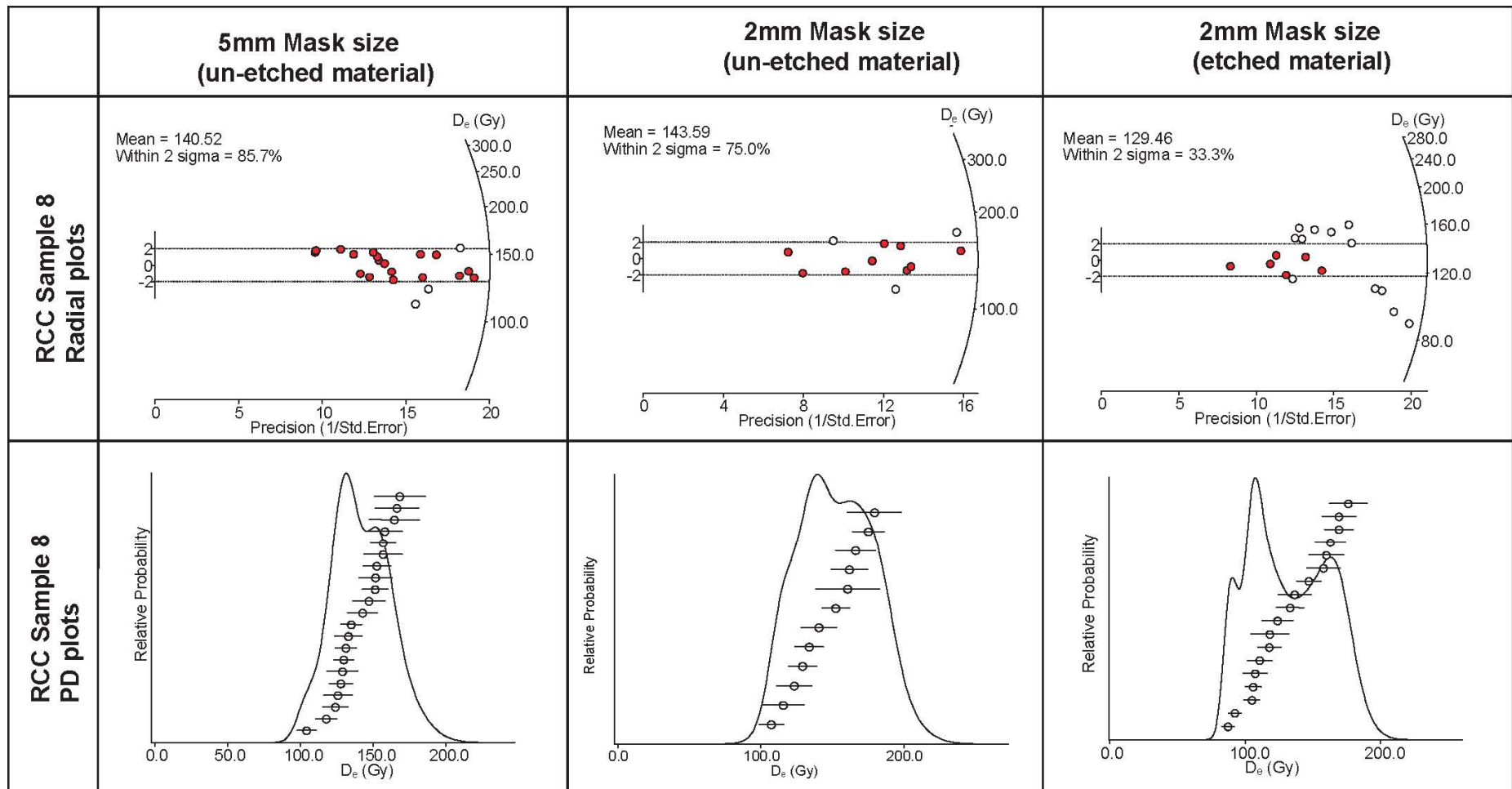


Figure 5.7 Radial plots and PD plots showing the D_e distributions for the RCC samples. A central age model is suggested for all samples based on the general scatter in distribution.

Table 5.3 Summary of D_e values obtained from RCC samples, measured in Pretoria.

Sample name	Sample affinities	D_e (Gy) values	Overdispersion	Comment
RCC 21	2mm mask size Etched	20.2 ± 0.8	15.8%	Mixed population or internal feldspar contamination
RCC 10	2mm mask size Un-etched	25.1 ± 2.0	25.2%	Mixed population or internal feldspar contamination
RCC 10	2mm mask size etched	27.5 ± 1.1	13.8%	Decreased scatter possibly due to feldspar elimination
RCC 19	2mm mask size etched	64.6 ± 1.6	7.2%	Good population distribution; however, does not correlate to known ^{14}C age
RCC 9	5mm mask size Un-etched	61.9 ± 1.4	9.8%	Good population distribution
RCC 9	2mm mask size Un-etched	61.0 ± 2.8	15.6%	Mixed population or internal feldspar contamination
RCC 9	2mm mask size etched	59.7 ± 2.0	9.4%	Decreased scatter possibly due to feldspar elimination
RCC 18	2mm mask size etched	68.8 ± 2.6	15.3%	Mixed population or internal feldspar contamination
RCC 6	2mm mask size Un-etched	102.7 ± 3.1	12.7%	Good population distribution
RCC 6	2mm mask size etched	98.5 ± 4.0	12.9%	Good population distribution
RCC 7	2mm mask size Un-etched	128.6 ± 3.8	9.1%	Good population distribution
RCC 8	5mm mask size Un-etched	139.3 ± 3.7	9.8%	Good population distribution; however, there is a large D_e range
RCC 8	2mm mask size Un-etched	143.9 ± 5.7	13.4%	Good population distribution; however, there is a large D_e range
RCC 8	2mm mask size etched	129.2 ± 5.7	20.7%	Mixed population or internal feldspar contamination

6 DOSE RATE ANALYSIS

6.1 Introduction

Little work has recently been published on the determination of the dose-rate but the use of TSAC as a reliable method has been under debate (Jensen & Prescott, 1983; Wintle & Dijkmans, 1988; Zöller & Pernicka, 1989). This is due to problematic 'overcounting' that occurs when using TSAC. In this study a comparison between TSAC, field gamma spectrometer measurements (FGS), and high resolution gamma spectrometer measurements (HRGS) (performed in Denmark by A. S. Murray) has been made. The use of different dose-rate determinations has been made to determine if it is possible to reproduce the dose-rate using different methods. These methods (TSAC and FGS) are the primary dose-rate evaluation methods used at the Pretoria laboratory.

6.2 Thorium and Uranium analysis

The possibility of disequilibrium in the U and Th series could not be ruled out at RCC due to the suggestion that the sediments were deposited through fluvial processes (Butzer, 1984a). Within the Th and U series are the gaseous elements ^{219}Rn , ^{220}Rn and ^{222}Rn that may escape a porous sample matrix, leading to disequilibrium in the decay chains (Aitken, 1985). Previous studies (Woodborne & Vogel, 1997) suggest that discrepancies, possibly attributed to the migration of uranium, could have lead to disequilibrium in the U series. However, a large contribution from ^{40}K to the dose rate makes the effects of Th and U to the total environmental dose rate negligible. Without the aid of high resolution gamma spectra to test for disequilibrium, a general indicator is taken as a typical ratio of ~3.4 between Th and U concentrations (ppm) (Murray & Aitken, 1988). Table 6.1, Figure 6.1, and figure 6.2 below show the Th/U ratio for all the RCC samples.

Table 6. 1 Th and U ppm comparisons. Samples are given in sequence.

Sample Name	Th ppm	U ppm	Th/U ratio	Technique
RCC 17	3.77 ± 0.12	0.82 ± 0.84	4.61	FGS
RCC 22	3.31 ± 0.04	1.33 ± 0.05	2.50	TSAC
RCC 21	3.33 ± 0.12	0.85 ± 0.04	3.92	FGS
RCC 20	3.14 ± 0.46	1.39 ± 0.05	2.25	TSAC
RCC 10	3.43 ± 0.39	1.26 ± 0.04	2.73	TSAC
RCC 10	3.71 ± 0.12	1.01 ± 0.04	3.68	FGS
RCC 10	3.09 ± 0.08	1.32 ± 0.04	2.34	TSAC 2
RCC 19	4.22 ± 0.57	1.45 ± 0.06	2.91	TSAC
RCC 9	4.09 ± 0.74	1.40 ± 0.08	2.92	TSAC
RCC 9	4.10 ± 0.09	1.50 ± 0.03	2.73	TSAC 2
RCC 18	4.29 ± 0.13	1.13 ± 0.05	3.79	FGS
RCC 16	5.05 ± 0.15	1.30 ± 0.04	3.87	TSAC
RCC 16	3.26 ± 0.14	1.10 ± 0.05	2.97	FGS
RCC 6	3.34 ± 0.68	1.33 ± 0.07	2.51	TSAC
RCC 6	3.36 ± 0.08	1.39 ± 0.03	2.42	TSAC 2
RCC 15	5.80 ± 0.25	1.53 ± 0.07	3.78	TSAC
RCC 15	3.64 ± 0.14	1.29 ± 0.06	2.82	FGS
RCC 14	5.55 ± 0.21	1.61 ± 0.06	3.45	TSAC
RCC 14	3.63 ± 0.17	1.44 ± 0.07	2.52	FGS
RCC 7	6.44 ± 1.19	1.46 ± 0.11	5.11	TSAC
RCC 7	6.47 ± 0.18	1.41 ± 0.03	5.30	TSAC 2
RCC 13	6.15 ± 0.24	1.27 ± 0.07	5.61	TSAC
RCC 13	3.63 ± 0.18	2.03 ± 0.08	1.79	FGS
RCC 12	4.27 ± 0.21	1.59 ± 0.06	2.69	TSAC
RCC 12	3.91 ± 0.18	0.95 ± 0.06	4.11	FGS
RCC 8	6.24 ± 0.78	1.80 ± 0.08	4.01	TSAC
RCC 8	4.91 ± 0.12	0.65 ± 0.02	6.55	TSAC 2
RCC 11	4.09 ± 0.20	1.08 ± 0.06	3.78	TSAC
RCC 11	3.85 ± 0.15	1.19 ± 0.05	3.22	FGS

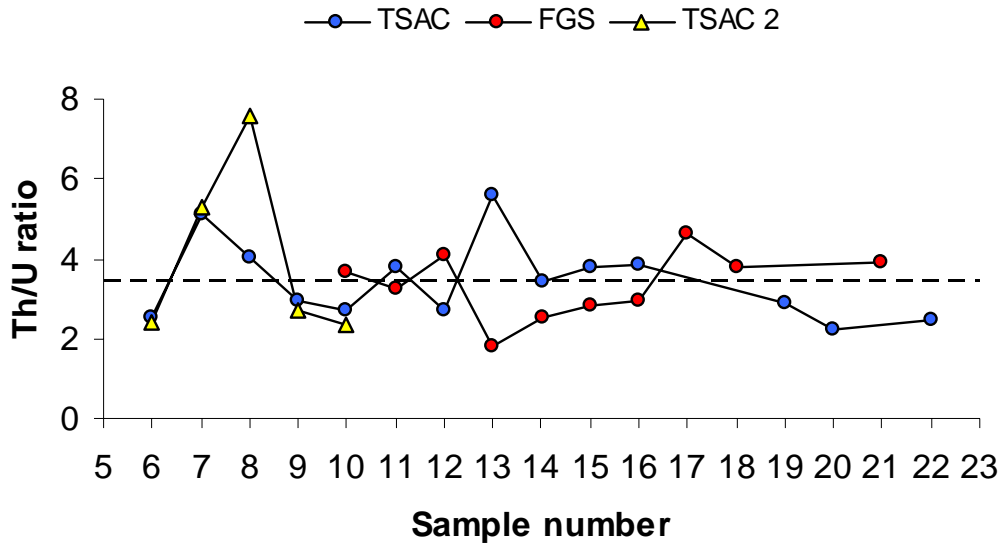


Figure 6. 1 Th/U ratios for RCC samples, the data is plotted in numerical order, where the numbers indicate the sample name. All the samples have good ratios. However, discrepancies between TSAC and FGS occur between samples RCC 8 and RCC 13.

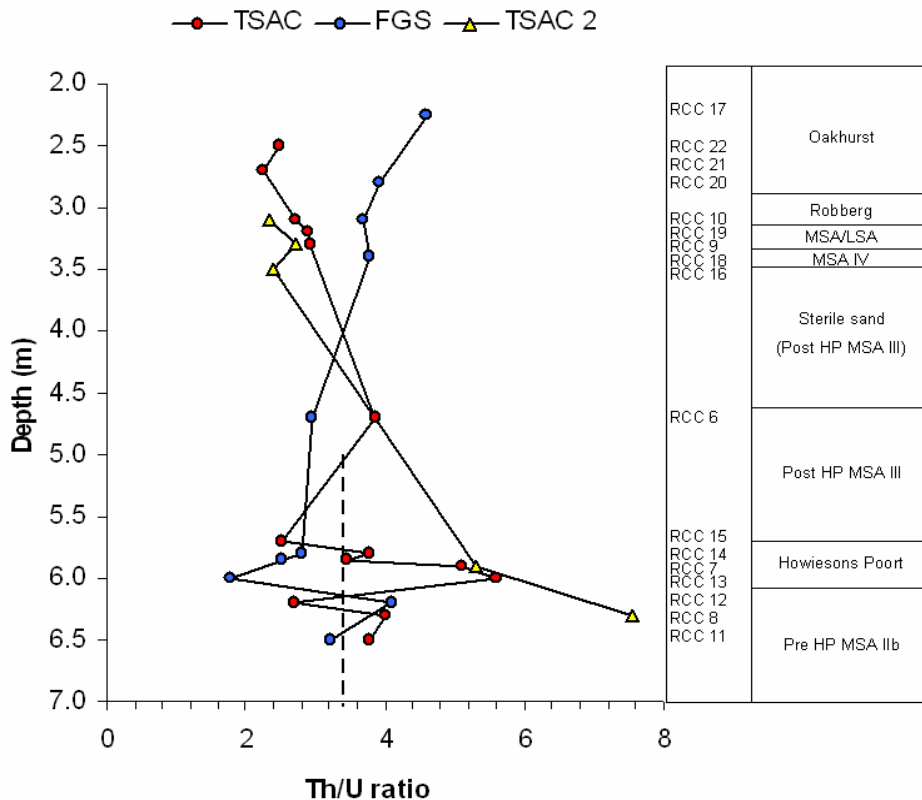


Figure 6. 2 Th/U ratios for RCC samples, the data is plotted according to depth. The spread at ~ 6m is largely attributed to discrepancies between TSAC and FGS for samples RCC 8 and RCC 13, associated with high intensity occupation during the HP whereby hearths could have played a role in potassium migration .

6.3 Potassium analysis

The average contribution of ^{40}K to the total dose rate for all samples from RCC is 65% and is predominantly produced from the decay of high potassium feldspars found throughout the site. The distribution of ^{40}K is complex due to the complexity and spatial arrangement of potassium distributions and the large numbers of hearths present in the archaeological record (Wadley, 1991). Estimates of K% were obtained from XRF and FGS. The ratios between these two techniques are given by FGS/XRF and are shown in table 6.2. Ratios could only be obtained for samples RCC 10-18 and RCC 21 because only one technique was used to obtain the K% for the others. The ratios are generally consistent with an average of $0.86 \pm 0.13\%$ indicating discrepancies between various low resolution techniques. This implies that the distribution of ^{40}K is probably inhomogeneous and that no single technique would give a true representation of K% that can be used to estimate beta and gamma dose rates.

Table 6. 2 Ratios of %K from XRF and FGS measurements.

Sample Name	%K FGS	%K XRF	K ratio (FGS/XRF)
RCC 17	1.45	1.89	0.77
RCC 22		1.59	
RCC 21	1.17	1.55	0.75
RCC 20		1.46	
RCC 10	1.20	1.45	0.83
RCC 19		1.55	
RCC 9		1.76	
RCC 18	1.26	1.72	0.73
RCC 16	1.22	1.34	0.91
RCC 6		1.26	
RCC 15	1.14	1.48	0.77
RCC 14	1.18	1.31	0.89
RCC 7		1.66	
RCC 13	1.02	1.26	0.81
RCC 12	1.33	1.15	1.15
RCC 8		1.23	
RCC 11	1.17	1.22	0.95

6.4 Dose-rates for Rose Cottage Cave

The average contribution from alpha, beta and gamma radiation are presented in table 6.3 and figure 6.3. In the table references to TSAC and TSAC2 include measurements of K done using XRF. TSAC2 refers to a second set of data measured by Dr. S. Woodborne. The average Alpha contribution is 1.7% of the total dose rate. The average beta contribution 62.6%, and the average contribution from gamma radiation is 35.6%. Furthermore the alpha contribution is negligible on etched samples. This implies that if there is a possibility of disequilibrium in the U/Th decay series it becomes almost redundant due to the high contribution from ^{40}K to the total dose rate. It is therefore very difficult to obtain the 'correct' dose-rate based on K% measurements. For the RCC samples the dose rates were chosen according to the technique that gave the best Th/U ratio, and in cases where two measurements of K% were done, two results are given.

Table 6. 3 Fractional components of dose-rates to Rose Cottage Cave.

Sample Name	Alpha contribution	Beta contribution	Gamma contribution	Technique
RCC 17	1.3	64.6	34.2	FGS
RCC 22	1.3	64.7	34.0	TSAC
RCC 21	1.4	64.7	33.8	FGS
RCC 20	1.4	64.2	34.3	TSAC
RCC 10	1.4	64.1	34.5	TSAC
RCC 10	1.6	63.9	34.5	FGS
RCC 10	1.4	64.4	34.2	TSAC 2
RCC 19	1.5	63.2	35.3	TSAC
RCC 9	1.3	64.4	34.3	TSAC
RCC 9	1.4	64.2	34.4	TSAC 2
RCC 18	1.6	62.1	36.3	FGS
RCC 16	1.7	61.4	36.9	TSAC
RCC 16	1.5	63.4	35.1	FGS
RCC 6	2.4	64.1	33.5	TSAC
RCC 6	2.0	65.0	33.0	TSAC 2
RCC 15	1.8	61.0	36.2	TSAC
RCC 15	1.8	63.0	35.2	FGS
RCC 14	1.9	60.2	36.9	TSAC
RCC 14	1.8	63.0	35.2	FGS
RCC 7	1.8	60.5	36.7	TSAC
RCC 7	1.8	60.5	36.7	TSAC 2
RCC 13	2.0	58.6	39.4	TSAC
RCC 13	2.2	60.7	36.0	FGS
RCC 12	1.9	60.6	36.5	TSAC
RCC 12	1.5	64.5	34.0	FGS
RCC 8	3.3	56.6	39.1	TSAC
RCC 8	2.2	62.2	35.5	TSAC 2
RCC 11	1.6	62.3	36.1	TSAC
RCC 11	1.7	63.1	35.2	FGS

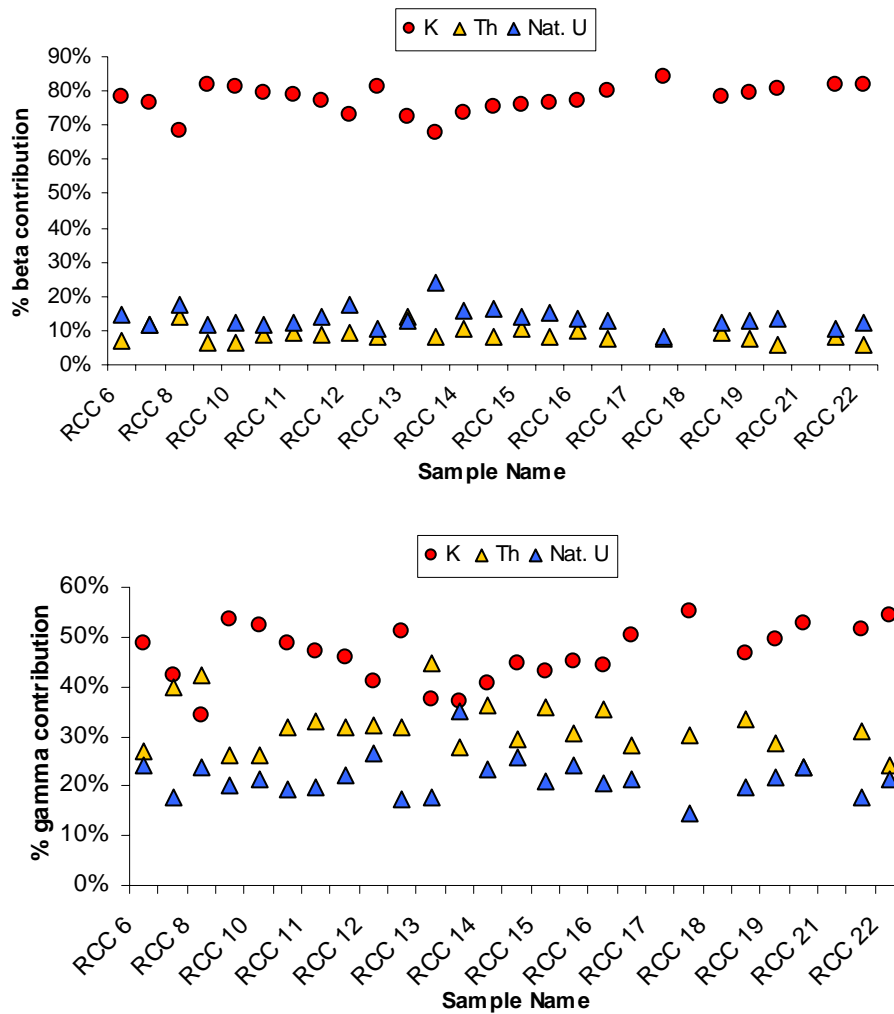


Figure 6.3 Contribution of ^{40}K , ^{232}Th and natural U to the Beta and gamma dose rates of Rose Cottage Cave.

Dose rates were calculated according to Adamiec & Aitken (1998) (see Appendix C) and are corrected for moisture content unless FGS measurements were done. Figure 6.4 below summarises the dose-rates obtained for RCC using all the available techniques, and demonstrates the scatter in dose-rate when using these various techniques. Table 6.4 illustrates the dose-rates obtained using the best Th/U ratio and both (when available) measurements of K%. Note the moisture content and cosmic ray contribution were both estimated to be approximately 5 ± 0.05 for all samples. It should be noted that comparisons using the measured moisture content relating to between 1.5% and 2.4% were done, but 5% moisture was chosen for the site's history as it is assumed that RCC was in general wetter in the past compared to today (Wadley *et al.*, 1992).

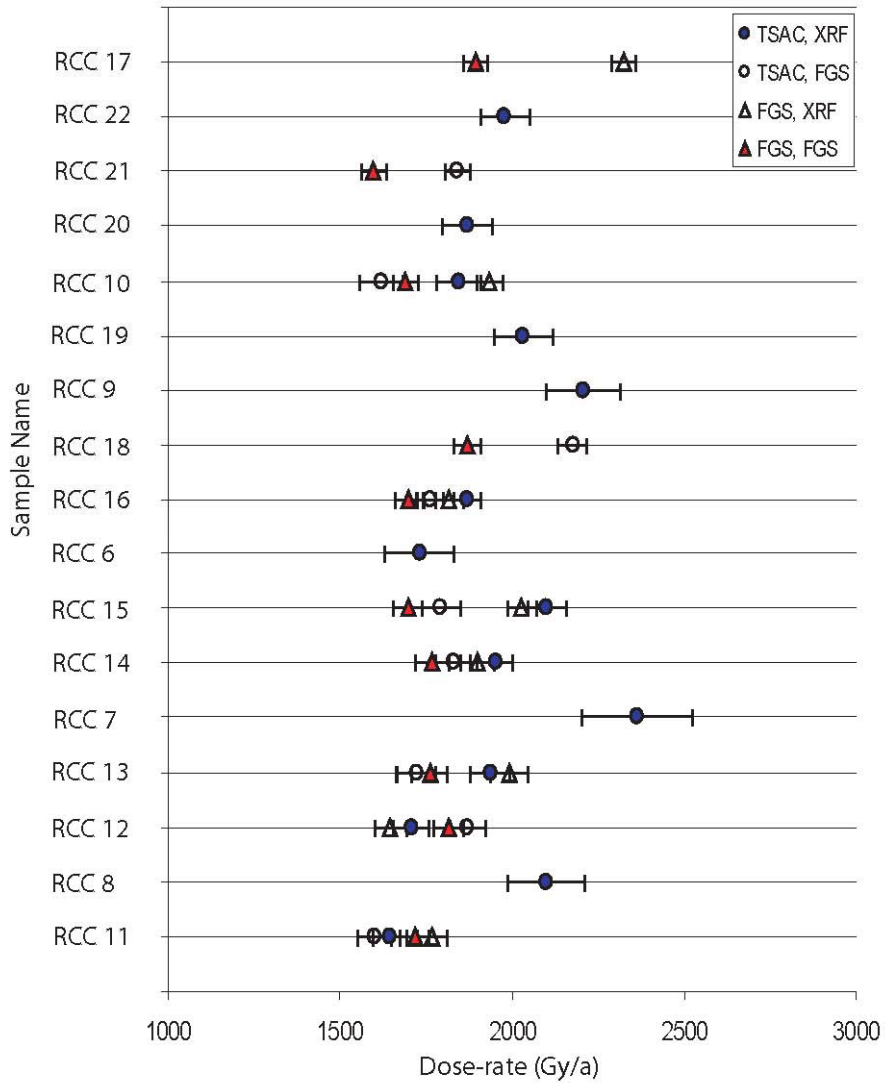


Figure 6. 4 Dose-rates obtained for RCC using all the available techniques, demonstrating the scatter in dose-rates when using various techniques. TSAC, XRF stands for all measurements done using TSAC with values for K% obtained by XRF. TSAC, FGS stands for all measurements done using TSAC with values for K% from FGS measurements. FGS, XRF stands for all measurements done using a FGS, using values for K% obtained by XRF. FGS, FGS stands for all measurements done using a FGS.

Table 6. 4 Dose-rates obtained for RCC using the best Th/U ratio and both (when available) measurements of K%.

Sample Name	Dose-rate TSAC, XRF	Dose-rate TSAC, FGS	Dose-rate FGS, XRF	Dose-rate FGS, FGS
RCC 21				1596.94 ± 35.65
RCC 10			1936.28 ± 36.97	1691.03 ± 36.97
RCC 19	2033.15 ± 86.09			
RCC 9	2206.88 ± 106.90			
RCC 18				1869.33 ± 40.29
RCC 16	1870.47 ± 39.82	1762.48 ± 39.82		
RCC 6	1731.30 ± 101.80			
RCC 15	2102.46 ± 56.52	1794.04 ± 56.52		
RCC 14	1951.75 ± 50.03	1829.94 ± 50.03		
RCC 7	2365.05 ± 161.53			
RCC 13	1936.53 ± 56.24	1721.82 ± 56.24		
RCC 12			1646.37 ± 46.22	1816.74 ± 46.22
RCC 8	2098.73 ± 112.96			
RCC 11			1768.19 ± 43.32	1716.46 ± 43.32

Note: TSAC, XRF stands for all measurements done using TSAC with values for K% obtained by XRF. TSAC, FGS stands for all measurements done using TSAC with values for K% from FGS measurements. FGS, XRF stands for all measurements done using a FGS, using values for K% obtained by XRF. FGS, FGS stands for all measurements done using a FGS.

7.0 RESULTS, DISCUSSION AND CONCLUSION

7.1 Results

Table 7.1 summarises the final D_e values and dose-rates which were chosen to calculate the depositional age of the RCC sediments. The dose-rates were chosen according to the technique which gave the best Th/U ratio and include both XRF and FGS estimates of %K. Therefore two dose-rates are presented representing those chosen from table 6.4 in chapter 6. It is believed that the D_e measurements are probably correct. Therefore any deviation from correct ages is associated with problems intrinsic to the dosimetry of RCC. This is evident in chapter 6, where it was noted that no two techniques could return the same dose-rates.

The D_e values for samples RCC 21, 19, 18 and 7 were a straightforward choice as only one mask size was either used or accepted after all SAR protocol rejection criteria were performed. D_e values for samples RCC 11-16 were measured in Denmark and the values were obtained by Andrew Murray. Some of the RCC samples are believed to still be contaminated by feldspars (as is shown by single grain measurements done on sample RCC 21, shown later in this chapter), these samples such as RCC 10 have higher D_e values for un-etched material. However, this is only an assumption as significant fading could have occurred in the un-etched material. The lowest D_e value was used in age calculations. The remainder of the samples were chosen as 2mm mask size, etched material due to the fact that they either passed the IR-OSL depletion ratio test exceptionally well or they yielded the lowest D_e values.

Table 7. 1 D_e values and Dose-rates chosen according OSL criteria to be used in age determination for Rose Cottage Cave.

Sample Name	Sample affinities	D_e values	Dose rate 1	Dose rate 2	Comment
RCC 21	2mm mask size, etched, FGS	20.2 ± 0.8	1597.94 ± 35.65		The only values that were obtained
RCC 10	2mm mask size, un-etched, FGS	25.1 ± 2.0	1936.28 ± 36.97	1691.03 ± 36.97	Lowest D_e value was chosen, due to feldspar contamination. Dose rate values were chosen according to Th/U ratios.
RCC 19	2mm mask size, etched, TSAC	64.4 ± 1.6	2033.15 ± 86.09		The only values that were obtained
RCC 9	2mm mask size, etched, TSAC	59.7 ± 2.0	2207.88 ± 106.90		Lowest D_e value was chosen, due to feldspar contamination. Dose rate values were chosen according to Th/U ratios.
RCC 18	2mm mask size, etched, FGS	67.8 ± 2.6	1869.33 ± 40.29		The only values that were obtained
RCC 16	>5mm mask size, TSAC	65 ± 3	1870.47 ± 39.82	1762.48 ± 39.82	D_e values were obtained by A. Murray. Dose rate values were chosen according to Th/U ratios
RCC 6	2mm mask size, etched, TSAC	97.5 ± 4.0	1731.30 ± 101.80		Lowest D_e value was chosen, due to feldspar contamination. Dose rate values were chosen according to Th/U ratios.
RCC 15	>5mm mask size, TSAC	130 ± 3	2102.46 ± 56.52	1794.04 ± 56.52	D_e values were obtained by A. Murray. Dose rate values were chosen according to Th/U ratios
RCC 14	>5mm mask size, TSAC	122 ± 3	1951.75 ± 50.03	1829.94 ± 50.03	D_e values were obtained by A. Murray. Dose rate values were chosen according to Th/U ratios
RCC 7	2mm mask size, un-etched, TSAC	127.6 ± 3.8	2365.05 ± 161.53		The D_e values were the only values that were obtained. Dose rate values were chosen according to Th/U ratios
RCC 13	>5mm mask size, TSAC	133 ± 2	1936.53 ± 56.24	1721.82 ± 56.24	D_e values were obtained by A. Murray. Dose rate values were chosen according to Th/U ratios
RCC 12	>5mm mask size, FGS	122 ± 4	1646.37 ± 46.22	1816.74 ± 46.22	D_e values were obtained by A. Murray. Dose rate values were chosen according to Th/U ratios
RCC 8	2mm mask size, etched, TSAC	129.2 ± 6.7	2097.73 ± 112.96		Lowest D_e value was chosen, due to feldspar contamination. Dose rate values were chosen according to Th/U ratios.
RCC 11	>5mm mask size, FGS	158 ± 7	1767.19 ± 43.32	1716.46 ± 43.32	D_e values were obtained by A. Murray. Dose rate values were chosen according to Th/U ratios

The values from table 7.1 can be used to calculate the ages for RCC by using the age equation and are presented in table 7.2. These results are compared to the RCC radiocarbon chronology as well as to previous luminescence studies performed at the site in figure 7.1. These include luminescence dates obtained by S. Woodborne using TL techniques and OSL dates performed by Andrew Murray. If the results correlate to both the radiocarbon chronology and the existing luminescence chronology, then a coherent MSA chronology is feasible. Figure 7.2 presents a more detailed comparison between OSL and radiocarbon and identifies miscorrelations, as well as a comparison between OSL and previous luminescence studies performed at the site.

Table 7. 2 Preliminary results for Rose Cottage Cave.

Sample name	Sample layer	Archaeological affiliation	Age 1 (ka)	Age 2 (ka)
RCC 21	H	Oakhurst	12.6 ± 0.8	
RCC 10	DB	Robberg	13.0 ± 1.3	14.8 ± 1.5
RCC 19	G	MSA/LSA transition	31.7 ± 2.0	
RCC 9	RU	MSA IV	27.0 ± 2.1	
RCC 18	CD	MSA IV	36.8 ± 2.1	
RCC 16	Lyn	'Sterile sands'	34.8 ± 2.3	36.9 ± 2.5
RCC 6	CLY	Post-HP MSA III	56.9 ± 5.3	
RCC 15	ANN	Post-HP MSA III	61.8 ± 3.0	72.5 ± 3.8
RCC 14	ETH	HP	62.5 ± 3.1	66.7 ± 3.4
RCC 7	BER	HP	54.4 ± 5.0	
RCC 13	EMC	HP	67.7 ± 2.9	77.2 ± 3.6
RCC 12	KUA	Pre-HP MSA IIb	74.1 ± 4.0	67.2 ± 3.8
RCC 8	KUA	Pre-HP MSA IIb	61.6 ± 6.2	
RCC 11	LEN	Pre-HP MSA IIb	89.4 ± 6.0	92.0 ± 6.2

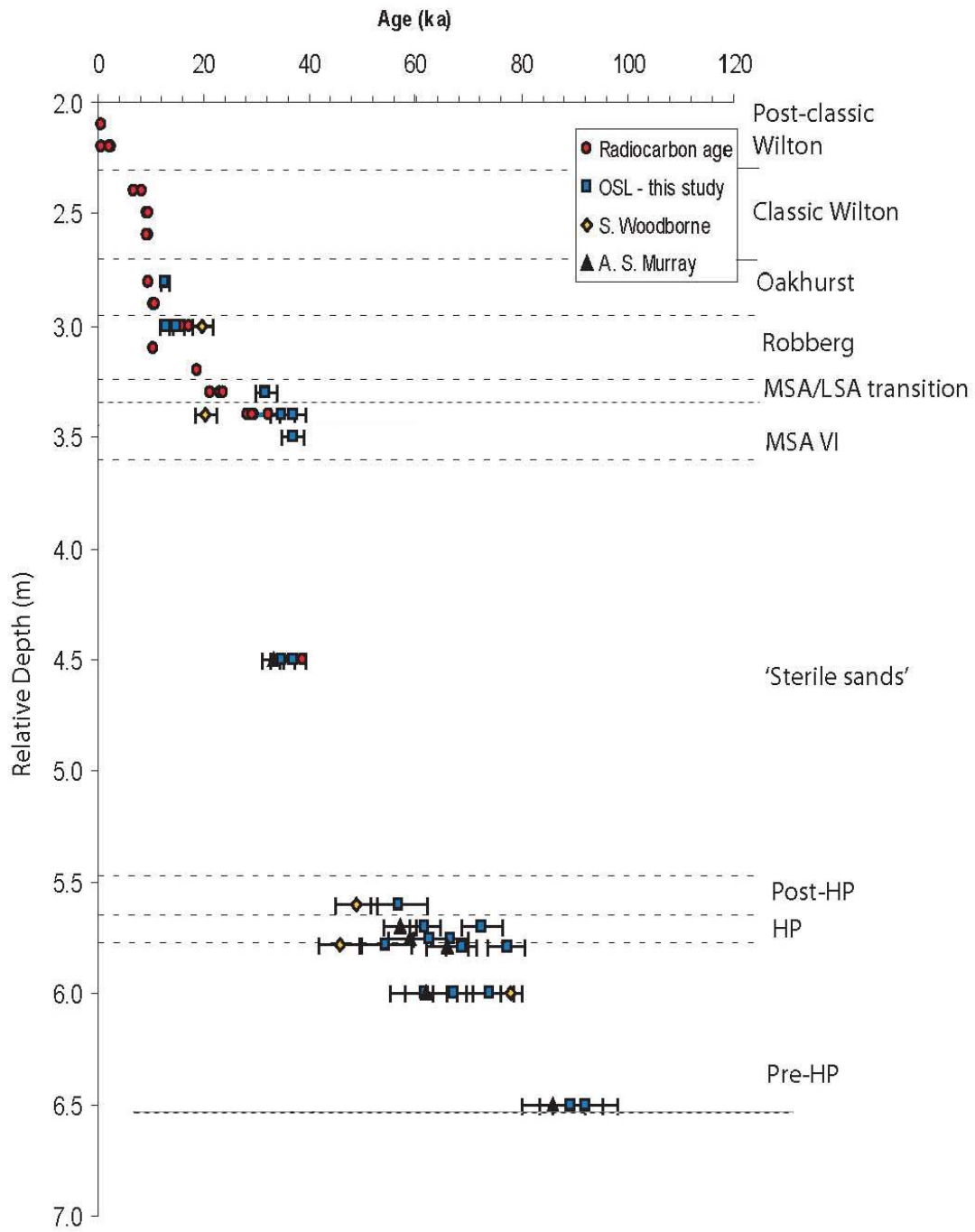


Figure 7. 1 Comparison between OSL dating and other dating techniques performed at RCC.

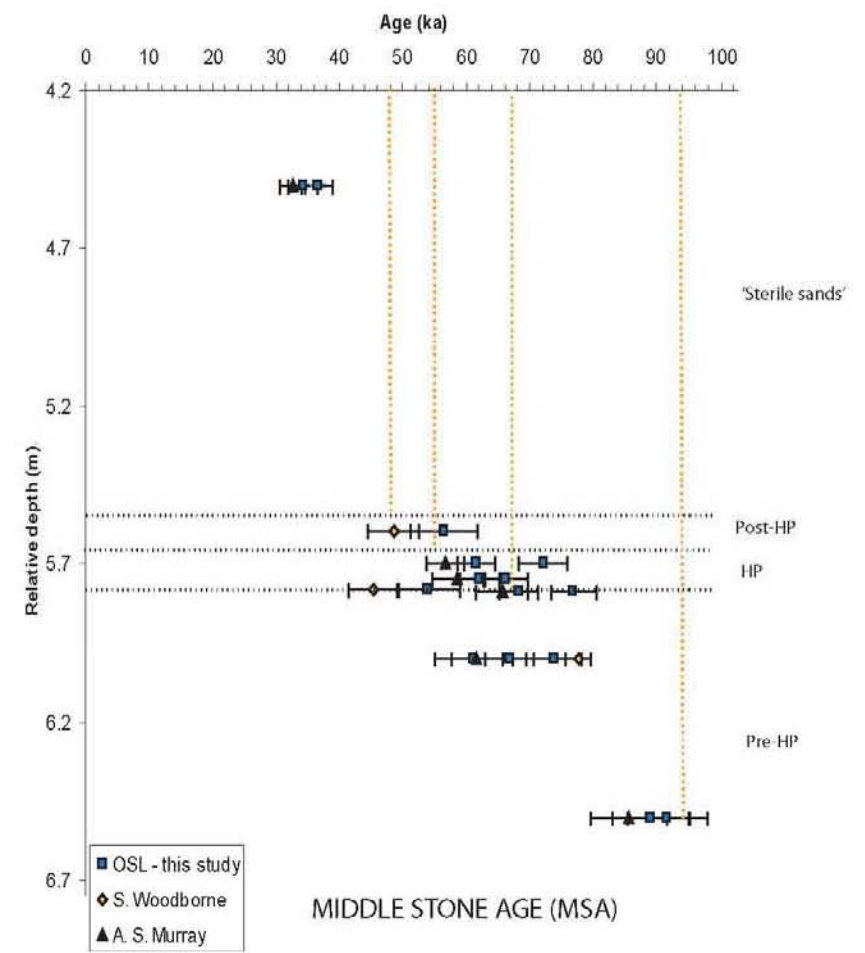
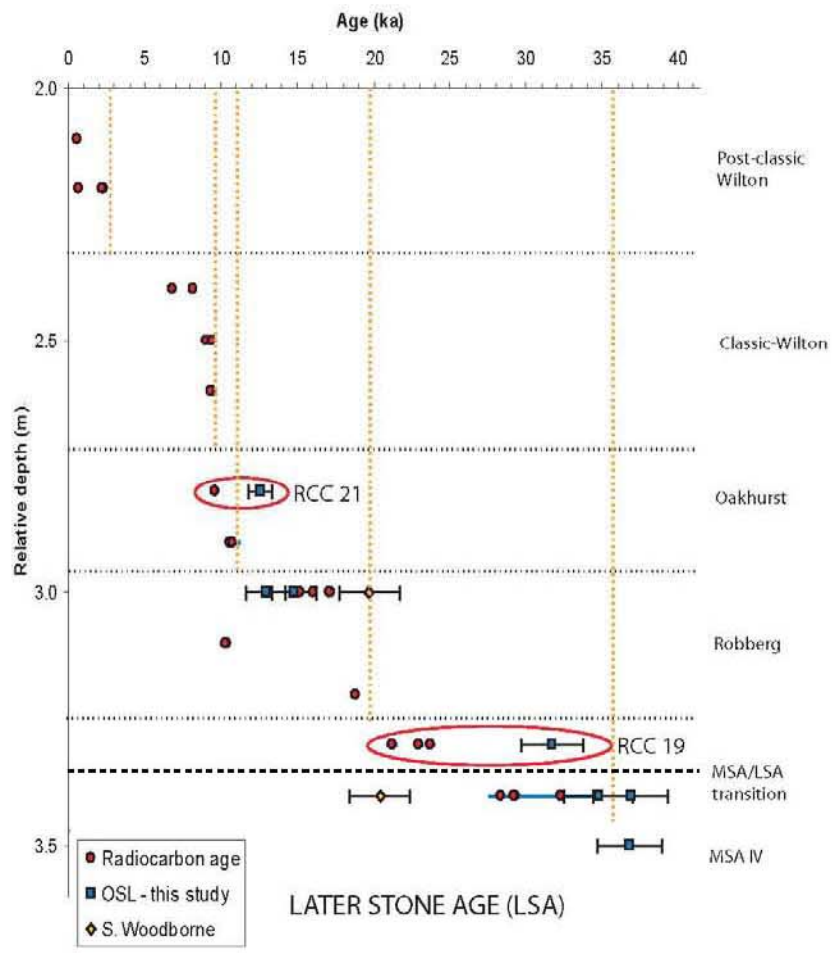


Figure 7.2 Age sequence for RCC. The vertical dashed lines represent the most probable ages for the lithostratigraphy of RCC. Note that sample RCC 21 and sample RCC 19 do not correlate with the existing radiocarbon chronology.

7.1.1 Resolving age discrepancies between OSL and radiocarbon

From figure 7.2 it can be seen that sample RCC 21 and sample RCC 19 do not correlate to the existing radiocarbon age chronology. Sample RCC 21 was selected to perform single grain analysis in an attempt to resolve the discrepancies in age correlation on the basis of incorrect D_e determination in the forgoing analysis. It was found during single grain analysis that there was a total rejection of over 50% of grains due to feldspar contamination. However, the grains were first put through rejection criteria defined by Jacobs *et al.*, (*in press*) that eliminated 23% of the feldspar contaminated population, after this elimination a further 27% of the grains were rejected due to feldspar contamination alone. It was also found that for sample RCC 21, 20% of the grains were responsible for the 'light' produced when averaging out single aliquots. The analysis is available on request in the form of a Microsoft excel spreadsheet. The analysis did not form part of this study and was only done as a test to resolve discrepancies in sample RCC 21. Two radial plots for sample RCC 21 of all the grains versus the accepted grains are presented in figure 7.3 below.

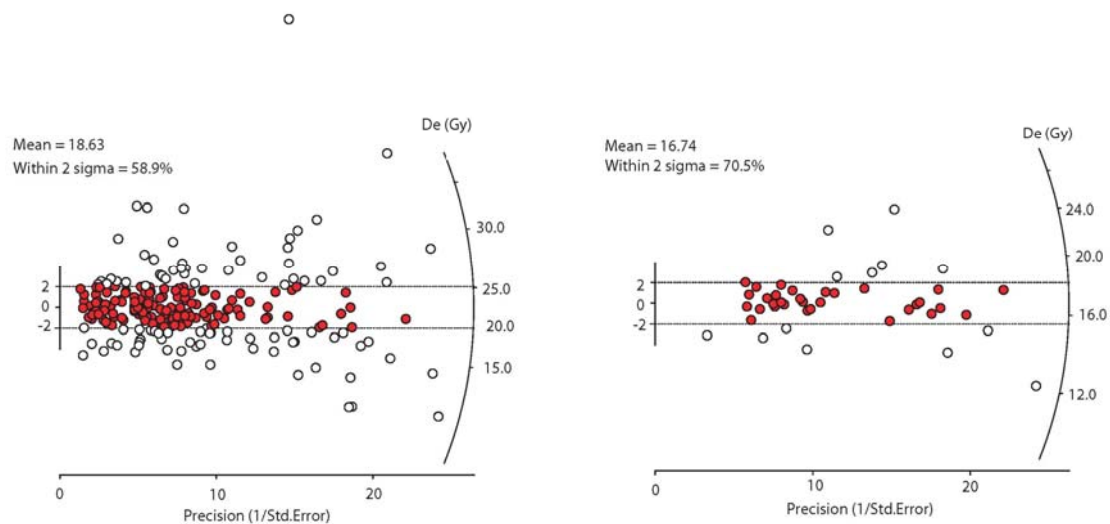


Figure 7.3 Radial plots showing all the grains from sample RCC 21 (right) and the accepted grains of sample RCC 21 (left).

From figure 7.3 it is clear that the radial plot on the left returns the same D_e value obtained using a single aliquot. In the plot on the right, grains that were

giving higher D_e values have been rejected. This is due to feldspar contamination not detected when using a single aliquot approach. It is important to note that the single aliquot measurements were performed on HF etched material, emphasising the importance of single grain analysis when dealing with a potassium rich site such as RCC. The new age values when using a central age model with a D_e value of 17 ± 1 Gy for RCC 21 becomes 10.6 ± 0.8 thousand years. This shifts the OSL value for RCC 21 to correlate perfectly with the radiocarbon age.

In most instances feldspar contamination will result in scattered D_e values. Sample RCC 19 appears to have a single population with minimal scatter around the central value (overdispersion = 7.2%). For this reason it was assumed not to be feldspar contaminated in contrast to RCC 21 (where the single aliquot analysis gave an overdispersion value of 15.8%). The fact that radiocarbon ages associated with sample RCC 19 are all consistent, suggests the OSL age is erroneous. The most likely scenario for the erroneous age would be that layer mixing occurred during sample collection either as a result of the sample tube penetrating more than one layer, or through the misidentification of the layer. From figure 7.2 it can be seen that RCC 19 yields the same date as the (calibrated) radiocarbon analyses from layers Ru, Dc and Dy (stratified below). This may be the result of localised turbation (such as pit digging) that would elevate older sediments to the surface without necessarily zeroing the OSL signal. Alternatively the dosimetry surrounding sample RCC 19 is possibly incorrect and single grain analysis may be necessary to clarify this. The conclusion on the basis of the radiocarbon comparison is that RCC 19 is erroneous either as a result of dosimetry, mis-sampling, or through a taphonomic process. Further analyses can be done to clarify this, but for the immediate discussion it is recommended that sample RCC 19 be excluded from the age chronology.

7.2 Discussion

When OSL dating an archaeological cave site it is important to apply strict rejection criteria in order to exclude any contamination of the samples. It has been demonstrated (Fullagar *et al.*, 1996; Roberts *et al.*, 1998, 1999) that ages can be overestimated due to either partial bleaching, or unbleached grains that contaminate the site due to roof or wall spalling. The possible forms of sedimentary contamination at RCC are:

- Cave roof or wall spalling
- Sample mixing
- Feldspar contamination
- Partial bleaching due to water lain sediments.

It is more than likely that the majority of the deposition at RCC is from aeolian origin as opposed to Butzer's (1984a, 1984b) original observations as no evidence for partial bleaching exists, and large accumulations of sand were deposited in a very short time period. The possibility of sample mixing however could be a major source of inaccuracy at RCC. This is easily discernable through cross-checking results with established chronologies and observing overdispersion values when performing D_e analysis. Although RCC samples present scatter in D_e values, it has been shown by single grain analysis that this is more probably attributed to feldspar contamination as opposed to layer mixing. It is more than likely that inaccuracies in ages are attributed to dosimetry as apposed to D_e evaluation.

Little research has gone into dose-rate evaluation in recent years. At RCC there is an existing chronology to check whether OSL ages are correct using the available dose-rate determination methods in South Africa. This could have a large impact on other OSL dated sites where no correlation record exists. To illustrate this point, the moisture content for RCC was measured today to be between 1 and 3%. However, an average of 5% moisture content was assumed for the site. The problems associated with no uniformity of K% estimates (possibly due to scattered feldspar depositions) create a second concern. There is no way of knowing when doing standard analysis, whether the right K% is

being used. Figure 7.4 below demonstrates how moisture content and estimates of K affects a sample that is older than 40ka. In the example a sample having 7.44 ± 1.19 pmm Th, and 1.46 ± 1.66 ppm U was chosen using a D_e value of 150 Gy. The graph represents the different ages that can be obtained by adjusting the moisture content from between 1% and 20% and by using two values of K (1% and 1.5%).

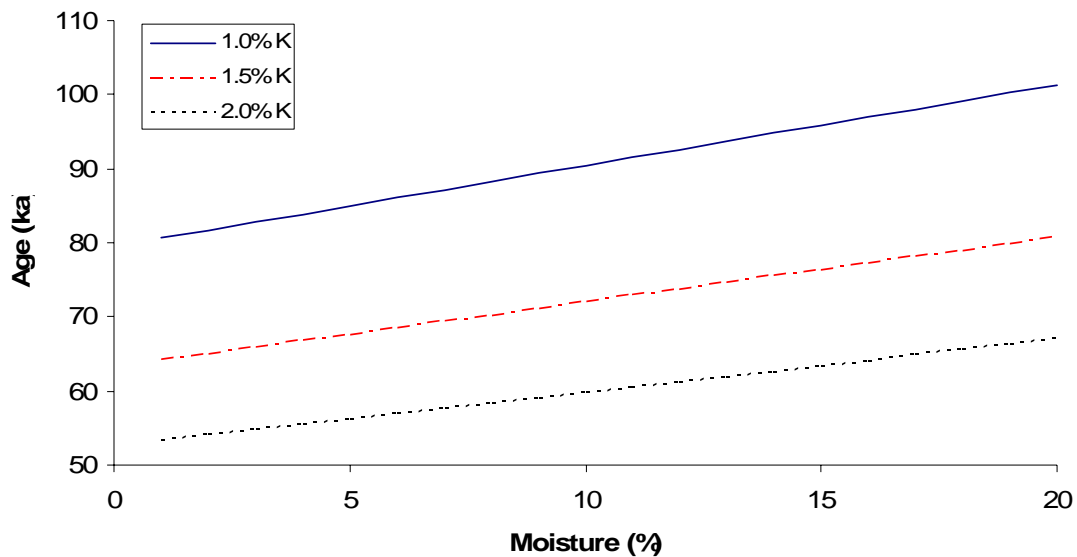


Figure 7.4 The effects of moisture content and %K on a sample.

The fact that there is a consistent OSL chronology at RCC assumes that the K% and moisture content estimates are generally correct. The causes of inconsistencies in K% are of great concern and are not understood at RCC. Two scenarios present themselves: the measurements of K were done with an incorrectly calibrated FGS; the dynamics of K change spatially to such an extent that all measurements do not represent the true K% of the dated sample. It should be noted that the age ranges obtained for RCC are the most probable and to fine tune these results further study will need to be conducted focusing on the dosimetry. Using the obtained values however, it is possible to correlate archaeological events at RCC to environmental changes.

The most probable ages for RCC, presented in table 7.3, reflect combined OSL and radiocarbon dates that have been calibrated and presented in years before AD 2005. The values in table 7.3 are rounded to the nearest 500 years

and exclude outliers from both the radiocarbon and OSL chronology. The transition between the Robberg and MSA/LSA transition at RCC is clearly defined at 20 ka. The final MSA at RCC is currently dated to 27 ka while the MSA/ELSA transition at BC is placed at 41 ka (calibrated relative to AD 2001) (Grun & Beaumont, 2001). It is unlikely that the RCC 19 date of 31.7ka (MSA/LSA transition) can be correct in the context of the other OSL dates stratified above and below it as well as the radiocarbon dates, but a literal acceptance of this date would shift the MSA/LSA transition at RCC closer to the age range defined at BC. If it is shown that RCC 19 is a mixture of MSA/LSA transition deposits with MSA IV deposits, then the date is an overestimation of the MSA/LSA, and the radiocarbon chronology will stand. The issue then becomes a typological debate around the MSA/LSA vs. the ELSA. With this in mind it is important to check other lines of evidence for potential mixing of sediments in some areas of RCC at this time.

Table 7. 3 Most probable age ranges for the Rose Cottage Cave sequence.

Archaeological affiliation	Probable age range (calendar years relative to AD 2005)
Post-Classic Wilton	< 3 000 years ago
Classic-Wilton	3 000 years ago – 8 500 years ago
Oakhurst	8 500 years ago – 10 500 years ago
Robberg	10 500 years ago – 20 000 years ago
MSA/LSA transition	20 000 years ago – 27 000 years ago
MSA IV	>27 000 years ago – 36 000 years ago
'Sterile sands'	>36 000 years ago – 48 000 years ago
Post-HP MSA III	48 000 years ago - 55 000 years ago
HP	55 000 years ago – 68 000 years ago
Pre-HP MSA IIb	68 000 years ago – 94 000 years ago

7.3 Conclusion and recommendations

Most of this thesis was concerned with applying standard OSL measurement procedures using the SAR protocol to the Stone Age layers at RCC. The protocol along with standardised single grain measurements have been two of the most significant developments in OSL dating in recent years. The SAR protocol has been applied successfully to a variety of different samples (Murray & Olley, 2002) and was not problematic at RCC. There are, however, still contentious issues surrounding dosimetry studies. Standardised measurement procedures need to re-look at the dosimetry. The HP dates for RCC are consistent with the emerging HP chronology from the rest of the country. Table 7.4 presents the final results obtained from the RCC sequence after single grain analysis was performed on sample RCC 21.

Table 7. 4 Results for Rose Cottage Cave.

Sample name	Sample layer	Archaeological affiliation	D _e Method	Age 1 (ka)	Age 2 (ka)
RCC 21	H	Oakhurst	Single Grain	10.6 ± 0.8	
RCC 10	DB	Robberg	SAR	13.0 ± 1.3	14.8 ± 1.5
RCC 19*	G	MSA/LSA transition	SAR	31.7 ± 2.0	
RCC 9	RU	MSA IV	SAR	27.0 ± 2.1	
RCC 18	CD	MSA IV	SAR	36.8 ± 2.1	
RCC 16	Lyn	'Sterile sands'	SAR	34.8 ± 2.3	36.9 ± 2.5
RCC 6	CLY	Post-HP MSA III	SAR	56.9 ± 5.3	
RCC 15	ANN	Post-HP MSA III	SAR	61.8 ± 3.0	72.5 ± 3.8
RCC 14	ETH	HP	SAR	62.5 ± 3.1	66.7 ± 3.4
RCC 7	BER	HP	SAR	54.4 ± 5.0	
RCC 13	EMC	HP	SAR	67.7 ± 2.9	77.2 ± 3.6
RCC 12	KUA	Pre-HP MSA IIb	SAR	74.1 ± 4.0	67.2 ± 3.8
RCC 8	KUA	Pre-HP MSA IIb	SAR	61.6 ± 6.2	
RCC 11	LEN	Pre-HP MSA IIb	SAR	89.4 ± 6.0	92.0 ± 6.2

*Sample RCC 19 is believed to be erroneous and should not be used until further analysis is done.

It is recommended that further studies are performed at RCC dealing with dosimetry issues and the dating feldspars from the site. It is also recommended that further analysis be performed on sample RCC 19. RCC offers an excellent opportunity for those who wish to study feldspars. This is now possible due to a coherent OSL correlation dataset.

APPENDIX A: RADIOCARBON AGE CHRONOLOGY OF ROSE COTTAGE CAVE.

Below is a summary of 46 ¹⁴C analyses done at Rose Cottage Cave. Note a total of 49 samples were submitted of which there was too little sample for 3 of the analyses. Most of the analyses were done on charcoal.

- Pta = the analysis code of the Pretoria Radiocarbon Laboratory (South Africa).
- Grn = the analysis code of the Groningen Radiocarbon Laboratory (Germany).
- Sr = the analysis code of the Radiocarbon Laboratory in Salisbury Rhodesia (Zimbabwe, Lab. does not exist anymore).

* The descriptions are those given by the submitter.

** Analysis numbers 7796 and 7763 were not assigned to any layer

Analysis No.	Description	Position	Submitter	Age Yrs B. P.	Calibrated date (1 sigma range)
Pta-2076	Wilton	60 cm	Butzer, K. W	8640 ± 100	7716 (7595) 7564 BC
Pta-1417	'Orange Sand"	Layer 6a	Butzer, K. W	23400 ± 200	23714 (23714) 23660 BC
Pta-1416	'Orange Sand"	Layer 6a	Butzer, K. W	22700 ± 240	23377 (23215) 23054 BC
Pta-350	Potsherd	34 cm (Fh)	Mason, R. J	610 ± 50	AD 1312 – 1358, 1385 (1403) 1417
GrN-5298	Wilton 3 (Pottery)	20-25 cm (Le)	Mason, R. J	1100 ± 30	AD 963 (992) 1015
Grn-5299	Wilton 2	36-46 cm (Ld)	Mason, R. J	6850 ± 45	5728 (5706) 5659 BC
Pta-211	Pre-Wilton	135 cm (Jf)	Mason, R. J	29430 ± 520	33274 (32379) 30870 BC
Grn-5300	ELSA	176 cm (Jf)	Mason, R. J	25640 ± 220	25430 (25259) 25095 BC
Pta-0354	B 'Orange Sand"	325 cm (Hc)	Mason, R. J	>40950	-
Pta-0213	B 'Orange Sand'	330 cm (Hd)	Mason, R. J	>50200	-

	Upper Magosian				
Pta-0001	Upper Magosian	366 (Hd)	Mason, R. J	36100 ± 2000	42095 (40731) 38089 BC
Pta-0214	Upper Magosian	378 cm (Ie)	Mason, R. J	>42500	-
Sr-0116	Upper Magosian	378 cm	Mason, R. J	>48000	-
Pta-0231	Upper Magosian	380 cm	Mason, R. J	>48400	-
Pta-6839	Donga	20 cm	Smith, J	3 ± 10	-
Pta-6843	Donga	70 cm	Smith, J	1590 ± 70	AD 423 (534) 597
Pta-3360	Donga	100 cm	Scott, L	2310 ± 50	391 (377) 357, 290 – 229 BC
Pta-7120	Post-Classic Wilton	Level Mn (192 cm)	Wadley, L	85 ± 5	-
Pta-6788	Post-Classic Wilton	Level Mn	Wadley, L	500 ± 50	AD 1421 (1436) 1456
Pta-5622	Post-Classic Wilton	Level A	Wadley, L	680 ± 50	AD 1291 (1304) 1397
Pta-7117	Post-Classic Wilton	Level A2 (219cm)	Wadley, L	2240 ± 60	373 (348, 308, 212) 180 BC
Pta-5934	Classic-Wilton	Level Pt (210 cm)	Wadley, L	5970 ± 70	4848 (4792) 4719 BC
Pta-6783	Classic-Wilton	Level Pt (224 cm)	Wadley, L	7630 ± 80	6237 (6206) 6071 BC
Pta-7122	Oakhurst	Level Ja (247 cm)	Wadley, L	8160 ± 70	7174 (7075) 7055 BC
Pta-5600	Oakhurst	Level jaG (268 cm)	Wadley, L	8380 ± 70	7513 (7462) 7323 BC
Pta-7287	Oakhurst	Level Ph (252 cm)	Wadley, L	8350 ± 70	7489 (7433, 7419, 7351) 7300 BC
Pta-5560	Oakhurst	Level H (281 cm)	Wadley, L	8614 ± 38	7598 (7588) 7577 BC
Pta-5599	Oakhurst	Level O (285 cm)	Wadley, L	9250 ± 70	8539 (8432, 8360, 8337) 8294 BC
Pta-7288	Robberg	Level Lb (278 cm)	Wadley, L	9340 ± 80	8625 (8557) 8442 BC
Pta-7275	Robberg	Level Lb (278 cm)	Wadley, L	9560 ± 70	9124 – 8991, 8910 (8789) 8737 BC

Pta-5593	Robberg	Level Db (322 cm)	Wadley, L	12690 ± 120	13334 (13176) 13018 BC
Pta-5601	Robberg	Level Db (352 cm)	Wadley, L	13360 ± 150	14222 (14049) 13864 BC
Pta-7290	Robberg	Level Be	Wadley, L	14320 ± 120	15291 (15153) 15015 BC
Pta-6195	Robberg	Level Wal (354 cm)	Wadley, L	15700 ± 40	16789 (16740) 16694 BC
Pta-7390	MSA/LSA	Level G (297 cm)	Wadley, L	17800 ± 180	19362 (19155) 18948 BC
Pta-7289	MSA/LSA	Level G/G2	Wadley, L	19600 ± 220	21121 (20963) 20748 BC
Pta-5598	MSA/LSA	Level G/G2	Wadley, L	20600 ± 250	21921 (21735) 21549 BC
Pta-6303	MSA IV	Level J/Ru (344 cm)	Wadley, L	26900 ± 550	26878 (26315) 25827 BC
Pta-6202	MSA IV	Level Ru (343 cm)	Wadley, L	27800 ± 1700	32510 (27309) 25621 BC
Pta-7126	MSA IV	Level Ru (364 cm)	Wadley, L	27700 ± 480	27894 (27177) 26632 BC
Pta-7184	MSA IV	Level Ru (364 cm)	Wadley, L	28800 ± 450	31957 (30298) 28238 BC
Pta-5596	MSA IV	Level Dc (350 cm)	Wadley, L	27200 ± 350	26996 (26610) 26270 BC
Pta-7805	'Orange sand'	Level Dy (340 cm)	Wadley, L	30800 ± 200	34599 (34375) 34143 BC
Pta-7796*	'Orange sand'	Level (354 cm)	Wadley, L	32900 ± 910	37680 (36609) 35650 BC
Pta-5592	'Orange sand'	Level Ge (374 cm)	Wadley, L	31300 ± 900	35868 (34925) 33900 BC
Pta-7763*	'Orange sand'	383-389 cm	Wadley, L	30800 ± 200	34599 (34375) 34143 BC

Source: QUADRU Database, CSIR, Pretoria, South Africa.

The radiocarbon age (Age Yrs B.P.) are reported in conventional radiocarbon years using a half-life of 5568 years given in years BP, i.e. before AD 1950 and are corrected for isotopic fractionation. Calibrated dates were calculated with the Pretoria programme (Talma & Vogel, 1993) which was updated in 2000. The 1 sigma range is given, with the most probable date between brackets.

APPENDIX B: GRAIN SIZE DISTRIBUTIONS OF RCC SAMPLES.

Below is a summary of grain size distribution for 0.5m intervals from the RCC sequence. The sedimentary interpretation is given by Butzer (1984b) for all material at the same depth. Note these distributions are representations of the sedimentary mixture after pre-treatment was performed on the material.

DEPTH	SAMPLE NAME	GRAIN SIZE DISTRIBUTION (µm)	SEDIMENTARY INTERPRETATION (BUTZER, 1984)
2.0	RCC 17		Organic silty sand produced from spring influx
2.5	RCC 21		Organic silty sand produced from spring influx
3.0	RCC 19		Organic silty sand produced from spring influx
3.5	RCC 18		Silty sand produced from spring influx with subangular to angular roof spall
4.5	RCC 16		Subangular to angular roof spall
5.0	RCC 14		Angular roof spall
5.5	RCC 12		
6.0	RCC 11		

APPENDIX C

Radioactivity and dose-rate data.

C.1 TSAC calculations

Alpha particles are emitted isotropically therefore many of the alpha decays will not interact with the scintillant. The equation that expresses the measured alpha activity $\dot{\alpha}$ (Bq/kg) of a sample relative to the total alpha activity is given by

$$\dot{\alpha} = \frac{1}{4} fAR\rho nC \times 10^{-4} \text{ (Adamiec \& Aitken, 1998)}$$

Equation C1

Where:

f is the electronic threshold fraction

A is the area of the screen (1385 mm²)

$R\rho$ is the average alpha emission range per density ($\mu\text{g mm}^2$)

n is the effective number of alpha emissions

C is the activity per unit mass of the parent (Bq/kg)

The value of $R\rho$ is determined from the energy of the alpha emission. High energy alphas will obviously have a longer range than low energy alphas in a material of any given density (Aitken, 1985). The value is calculated by averaging the range of each alpha in the decay sequence. This assumes that all alphas in the decay chain contribute equally to the $\dot{\alpha}$ dose which will only happen when the decay chain is in equilibrium. Alternate calculations can be made for samples that are not in equilibrium, but this was not done in this study as it requires appropriate knowledge of the disequilibrium. As a result the calculated parent activity is not accurate where disequilibrium occurs. The reported TSAC values are therefore the full chain equivalent parent activity that would give rise to the measured alpha activity.

The value of R differs between the Th and U chains. The average alpha range for the Th chain in equilibrium is 67.4 μm and for the U chain in equilibrium is 57.1 μm (Adamiec & Aitken, 1998). Where TSAC is done using the pairs technique, the calculation of the full chain parent activity takes this into account. The threshold fraction (f) relates the efficiency of the detector and is determined by the low level discriminator setting of the photomultiplier. This is typically 0.85 for the Th series. Because of the different average energy, the equivalent value is 0.82 for the U series (Aitken, 1985). The *effective alpha range* can then be calculated as the ratio between $R\rho$ and f (Aitken, 1985). Equation C1 can therefore be rewritten as

$$\dot{\alpha} = (\text{effective range} \times n \frac{1}{4} AC \times 10^{-4})$$

Equation C2

Combining the contribution of the U and Th decay chains to the total detected alpha count gives the equation

$$\dot{\alpha} = (67.4 \times 6 \times 0.25 \times A \times C_h \times 10^{-4}) + (57.1 \times 8 \times 0.25 \times A \times C_u \times 10^{-4})$$

Equation C3

Where:

C_h is the Th full chain activity and

C_u is the U full chain activity.

This can be simplified to give the equation

$$\alpha = (0.1191c_h \times 10^{-4}) + (0.1302c_u \times 10^{-4})$$

Equation C4

Equation C4 expresses the alpha count rate that is measured on a 42 mm diameter screen in terms of the contribution of Th and U. The contribution of the Th series can be calculated from the slow pair's count. The probability of

two random alpha events, which are not “true pairs” derived from ^{216}Po is a function of the count rate of the sample, and of the duration ‘coincidence window’ circuitry (Aitken, 1985). The random pair’s probability can then be calculated according to equation C5

$$P_r = \dot{\alpha}^2 t^{-ks} \quad (\text{Aitken, 1985})$$

Equation C5

Where:

$\dot{\alpha}^2$ is the raw count rate (cts/ks)² and

t^{-ks} is the coincidence time per kilo second (ks)

The true pairs are a measurement of the actual pairs occurring from the Th chain. If \dot{d} is used for the total observed pairs then the true pairs rate is given by

$$\dot{p} = \dot{d} - P_r$$

Equation C6

The probability of recording true pairs is dependant on the duration of the coincidence window, and the lifetime (λ) of fast emitting alpha nuclei. The formula used to express the pairs probability is

$$Pp = 1 - \exp(-\lambda t) \quad (\text{Aitken, 1985})$$

Equation C6.1

Where:

λ is the lifetime of ^{216}Po (0.209 s) and

t is the coincidence window.

This can be simplified to give a pairs probability of 76% by substituting values into equation C6.1 with

$$Pp = (1 - \exp^{(-0.4 \div 0.209)}) - (1 - \exp^{(-0.02 \div 0.209)}) = 0.7611$$

Equation C6.2

The pair's count rate for the Th series can now be calculated by using equation C7

$$\dot{P}h = \frac{0.7611}{12} A \times 62.39 \left(1 + \frac{0.5(82 - 72.5)}{71.26} \right) \div 1000000 = \mathbf{0.0058}$$

(after Aitken, 1985)

Equation C7

Where:

$\dot{P}h$ is the pairs count rate for the Th series

0.7611 is the pair's probability taken from equation 3.5

A is the counting area of the screen (1385cm²)

62.39 is the effective alpha range for ²²⁰Rn

82 and 72.5 are the average alpha ranges for ²¹⁶Po and ²²⁰Rn respectively

71.26 is the effective alpha range for ²¹⁶Po.

It is now possible to calculate the total Th and U count. The U contribution is calculated by subtracting the total Th counts from the observed count rate.

The total Th counts are given by equation C8

$$Ch = p \frac{\dot{\alpha}}{\dot{P}h}$$

Equation C8

To convert the parent specific alpha count rates to ppm the counts are divided by the corresponding alpha activity of 1 ppm of the parent. The count rate (ks⁻¹) for 1 ppm of parent for a 42 mm diameter scintillator has been calculated by Adamiec & Aitken (1998) and correspond to 0.483 for the Th series and 1.67 for the U series.

C.2 Radioactive Decay chains

Figures C.1, C.2 and C.2 below are schematic representations of the Th and U decay series. The y-axis, titled “A”, is the atomic number. MeV represents the energy emitted per disintegration; figures are after Ivanovich & Harmon, 1982 and Adamiec & Aitken, 1998.

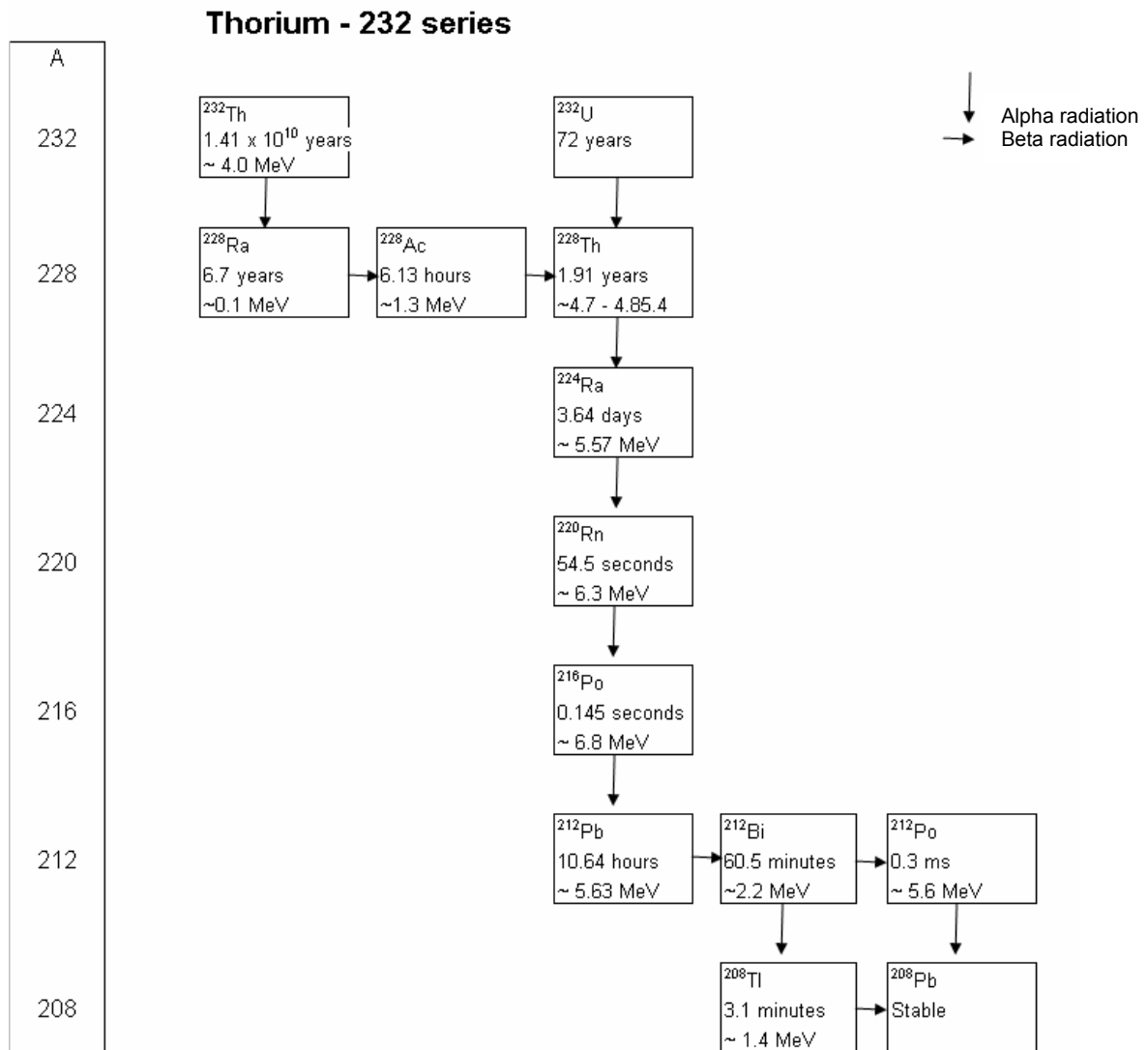


Figure C.1 Energy release and decay series for ^{232}Th .

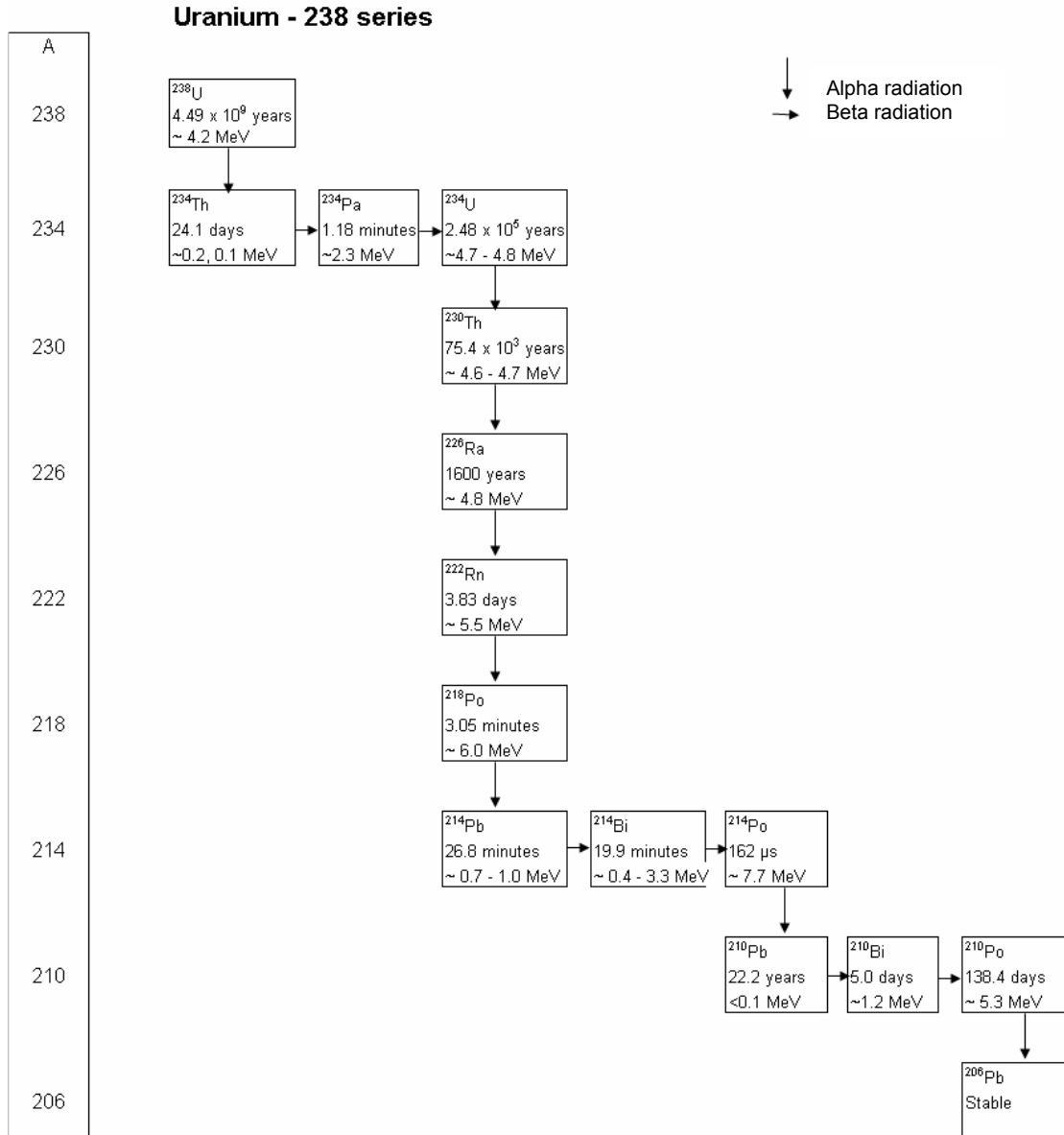


Figure C.2 Energy release and decay series for ^{238}U .

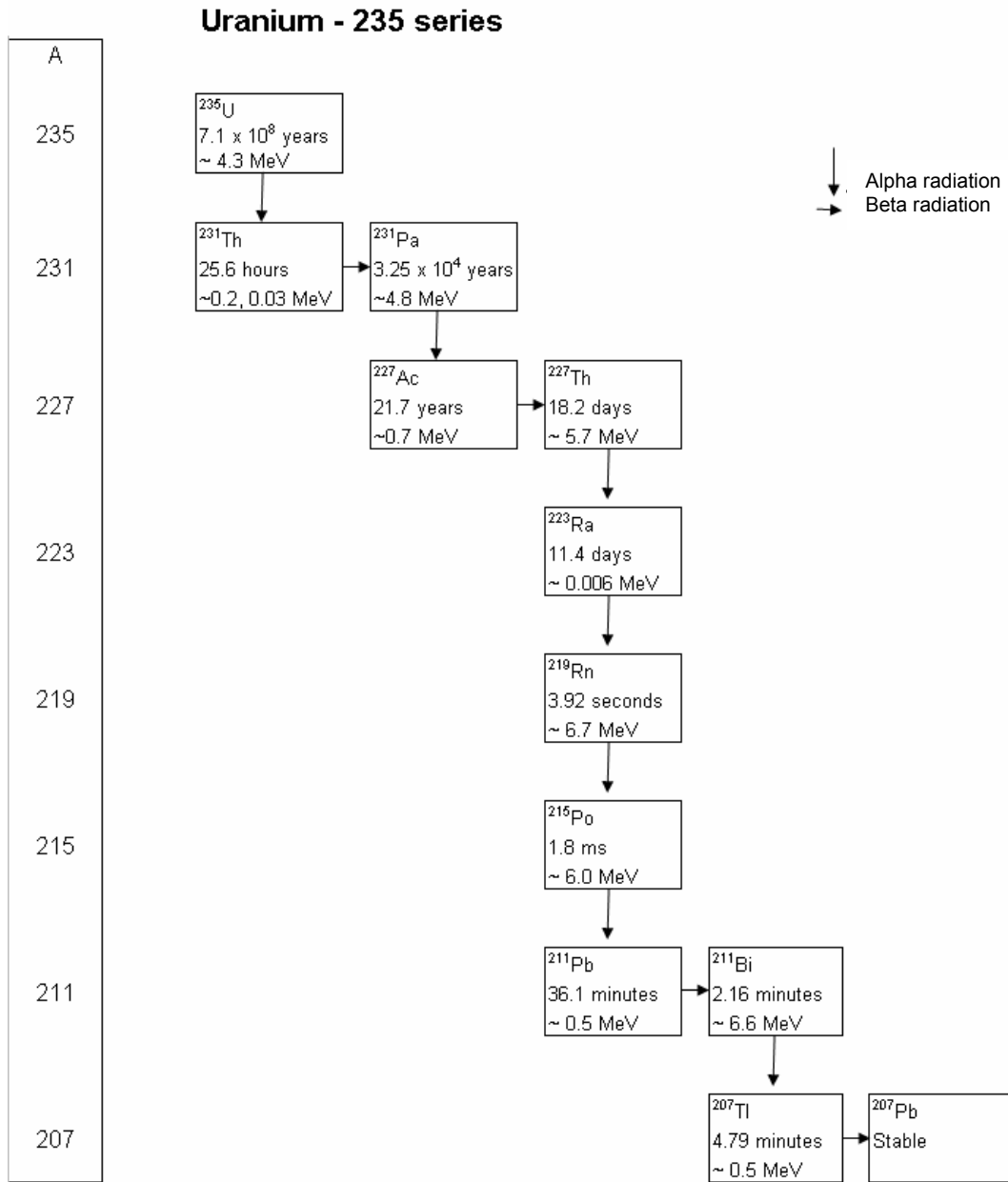


Figure C.3 Energy release and decay series for ^{235}U .

BIBLIOGRAPHY

Adamiec, G. and Aitken, M. J. (1998). Dose-rate conversion factors: update. *Ancient TL*, **16**, 37-49.

Aitken, M. J. (1985). *Thermoluminescence Dating*, Academic Press, London.

Aitken, M. J. (1998). *An Introduction to Optical Dating*, Oxford University Press, Oxford.

Aitken, M. J. and Smith, B. W. (1988). Optical dating: recuperation after bleaching. *Quaternary Science Reviews*, **7**, 387-393.

Avery, D. M. (1997). Micromammals and the Holocene environment of Rose Cottage Cave. *South African Journal of Science*, **93**, 445-448.

Bailey, R. M. (2000). Circumventing possible inaccuracies of the single aliquot regeneration method for the optical dating of quartz. *Radiation Measurements*, **32**, 233-246.

Bailey, R. M. (2003a). Paper I: The use of measurements-time dependant single-aliquot equivalent-dose estimates from quartz in the identification of incomplete signal resetting. *Radiation Measurements*, **37**, 673-683.

Bailey, R. M. (2003b). Paper II: The interpretation of measurement-time-dependant single-aliquot equivalent-dose estimates using predictions from a simple empirical model. *Radiation Measurements*, **37**, 685-691.

Bailey, R. M., Singarayer, J. S., Ward, S. and Stokes, S. (2003). Identification of partial resetting using D_e as a function of illumination time. *Radiation Measurements*, **37**, 511-518.

Bailey, R. M., Smith, B. W. and Rhodes, E. J. (1997). Partial Bleaching and the decay form characteristics of quartz OSL. *Radiation Measurements*, **27**, 123-136.

Beaumont, P. B. (1978). Border Cave. MA Thesis: University of Cape Town.

Bell, W. T. (1980). Alpha dose attenuation in quartz grains for thermoluminescence dating. *Ancient TL*, **12**, 4-8.

Binneman, J. (1997). Usewear traces on Robberg bladelets from Rose Cottage Cave. *South African Journal of Science*, **93**, 479-481.

Bird, M. I., Fifield, L. K., Santos, G. M., Beaumont, P. B., Zhou, Y., di Tada, M. L. and Hausladen, P. A. (2003). Radiocarbon dating from 40 to 60 ka BP at Border Cave, South Africa. *Quaternary Science Reviews*, **22**, 943-947.

Bøtter-Jensen, L. (1997). Luminescence techniques: instrumentation and methods. *Radiation Measurements*, **27**, 749-768.

Bøtter-Jensen, L., Anderson, C. E., Duller, G. A. T. and Murray, A. S. (2003). Developments in radiation, stimulation and observation facilities in luminescence measurements. *Radiation Measurements*, **37**, 535-541.

Bøtter-Jensen, L., Buler, E., Duller, G. A. T. and Murray, A. S. (2000). Advances in luminescence instrument systems. *Radiation Measurements*, **32**, 523-528.

Bøtter-Jensen, L. and Duller, G. A. T. (1992). A new system for measuring optically stimulated luminescence from quartz samples. *Nuclear Tracks and Radiation Measurements*, **20**, 549-553.

Bray, H. E., Bailey, R. M. and Stokes, S. (2002). Quantification of cross-irradiation and cross-illumination using a Risø Da-15 reader. *Radiation Measurements*, **35**, 275-280.

Butzer, K. W. (1984a). Late Quaternary environments in South Africa. In *Late Cainozoic Palaeoclimates of the Southern Hemisphere*(Ed, Vogel, J. C.) Balkema, Rotterdam, pp. 225-264.

Butzer, K. W. (1984b). Archaeology and Quaternary environments in the interior of southern Africa. In *Southern African Prehistory and Palaeoenvironments*(Ed, Klein, R. G.) Balkema, Rotterdam.

Clark, A. M. B. (1997a). The MSA/LSA transition in southern Africa: new technological evidence from Rose Cottage Cave. *South African Archaeological Bulletin*, **52**, 113-121.

Clark, A. M. B. (1997b). The final Middle Stone Age at Rose Cottage Cave: a distinct industry in the basutolian ecozone. *South African Journal of Science*, **93**, 449-458.

Clark, A. M. B. (1999). Late Pleistocene technology at Rose Cottage Cave: A Search for Modern Behaviour in an MSA context. *African Archaeological Review*, **16**, 93-120.

Clark, J. D. (1959). *The Prehistory of Southern Africa*, Penguin Books, London.

Clark, J. D. (1969). *The Kalambo Falls Prehistoric Site, I*, Cambridge University Press, Cambridge.

Deacon, H. J. (1983). Another Look at the Pleistocene Climates of South Africa. *South African Journal of Science*, **79**, 325-328.

Deacon, H. J. and Deacon, J. (1999). *Human Beginnings in South Africa, Uncovering the secrets of the Stone Age*, David Phillips, Cape Town.

Deacon, J. (1990). Weaving the fabric of Stone Age research in southern Africa. In *A history of African archaeology*(Ed, Robertshaw, P. T.) James Currey, London, pp. 39-58.

Duller, G. A. T. (1991). Equivalent dose determination using single aliquots. *Nuclear Tracks and Radiation Measurements*, **18**, 371-378.

Duller, G. A. T. (2003). Distinguishing quartz and feldspar in single grain luminescence measurements. *Radiation Measurements*, **37**, 161-165.

Engela, R. (1995). Space, material culture and meaning in the late Pleistocene and early Holocene at Rose Cottage Cave. MA Thesis: University of the Witwatersrand.

Esterhuysen, A. B. (1996). Palaeoenvironmental reconstruction from Pleistocene to present: an outline of charcoal from the eastern Free State and Lesotho. MA Thesis: University of the Witwatersrand.

Esterhuysen, A. B. and Smith, J. M. (2003). A comparison of charcoal and stable carbon isotope results for the Caledon River Valley, southern Africa, for the period 13 500 - 5000 YR BP. *South African Archaeological Bulletin*, **58**, 1-5.

Feathers, J. K. (2002). Luminescence dating in less than ideal conditions: case studies from Klasies River Mouth and Duinefontein, South Africa. *Journal of Archaeological Science*, **29**, 177-194.

Feathers, J. K. and Bush, D. A. (2000). Luminescence dating of Middle Stone Age deposits at Die Kelders. *Journal of Human Evolution*, **38**, 91-119.

Fleming, S. J. (1966). Study of thermoluminescence of crystalline extracts from pottery. *Archaeometry*, **9**, 170-173.

Fleming, S. J. (1970). Thermoluminescent dating: refinement of the quartz inclusion method. *Archaeometry*, **15**, 13-30.

Fleming, S. J. (1979). *Thermoluminescence techniques in archaeology*, Clarendon Press, Oxford.

Fullagar, R. L., Price, D. M. and Head, L. M. (1996). Early human occupation in northern Australia: archaeology and thermoluminescence dating of Jimmium rock-shelter, Northern Territory. *Antiquity*, **70**, 751-753.

Galbraith, R. F. (1988). Graphical Display of Estimates Having Differing Standard Errors. *Technometrics*, **30**, 271-281.

Galbraith, R. F. (1990). The Radial Plot: Graphical Assessment of Spread in Ages. *Nuclear Tracks and Radiation Measurements*, **17**, 207-214.

Galbraith, R. F. (1994). Some Applications of Radial Plots. *Journal of American Statistical Association*, **89**, 1232-1242.

Galbraith, R. F. (1998). The trouble with 'probability density' plots of fission track ages. *Radiation Measurements*, **29**, 125-131.

Galbraith, R. F., Roberts, R. G., Laslett, G. M., Yoshida, H. and Olley, J. M. (1999). Optical dating of single and multiple grains of quartz from Jimmium rock shelter, northern Australia: Part I, Experimental design and statistical models. *Archaeometry*, **41**, 339-364.

Goodwin, A. J. H. (1935). A commentary on the history and present position of South African prehistory. *Bantu Studies*, **9**, 291-417.

Goodwin, A. J. H. and Van Riet Lowe, C. (1929). The Stone Age cultures of South Africa. *Annals of the South African Museum*, **27**, 1-289.

Grün, R. and Beaumont, P. B. (2001). Border Cave revisited: a revised ESR chronology. *Journal of Human Evolution*, **40**, 467-482.

Grün, R., Shackleton, N. J. and Deacon, H. J. (1990). Electron-spin resonance dating from Klasies River Mouth Cave. *Current Anthropology*, **32**, 427-432.

Harper, P. T. N. (1997). The Middle Stone Age sequence at Rose Cottage Cave: a search for continuity and discontinuity. *South African Journal of Science*, **93**, 470-475.

Herries, A. and Latham, L. (2002). 'Environmental Archaeomagnetism': evidence for climatic change during the later Stone Age using the magnetic susceptibility of cave sediments from Rose Cottage Cave, South Africa. In *RESEARCHING AFRICA'S PAST. New Contributions from British Archaeologists* (Eds, Mitchell, P., Haour, A. and Hobart, J.) Oxford University Press, Oxford.

Holmgren, K., Lee-Thorp, J. A., Cooper, G. R. J., Lundblad, K., Partridge, T. C., Scott, L., Sithaldeen, R., Talma, A. S. and Tyson, P. D. (2003). Persistent millennial-scale climate variability over the past 25,000 years in Southern Africa. *Quaternary Science Reviews*, **22**, 2311-2326.

Huntley, D. J., Godfrey-Smith, D. I. and Thewalt, M. L. W. (1985). Optical dating of sediments. *Nature*, **313**, 105-107.

Huntley, D. J., Hurren, J. T. and Prescott, J. R. (1993). The stranded beach-dune sequence of south-east South Australia: A test of thermoluminescence dating, 0-800 ka. *Quaternary Science Reviews*, **12**.

Ivanovich, M. and Harmon, R. S. (1982). *Uranium Series Disequilibrium. Applications to Environmental Problems*, Clarendon Press, Oxford.

Jacobs, Z. (2004). Development of luminescence techniques for dating Middle Stone Age sites in South Africa. PhD Thesis: University of Aberystwyth, Aberystwyth

Jacobs, Z., Wintle, A. G. and Duller, G. A. T. (2003a). Optical dating of dune sand from Blombos Cave, South Africa: I - multiple grain data. *Journal of Human Evolution*, **44**, 599-625.

Jacobs, Z., Duller, G. A. T. and Wintle, A. G. (2003b). Optical dating of dune sand from Blombos Cave, South Africa: II - single grain data. *Journal of Human Evolution*, **44**, 613-625.

Jacobs, Z., Duller, G. A. T. and Wintle, A. G. (*in press*). Interpretation of single grain D_e distributions and calculation of D_e . *Radiation Measurements*.

Jain, M., Murray, A. S. and Bøtter-Jensen, L. (2003). Characterisation of blue-light stimulated luminescence components in different quartz samples: implications for dose measurements. *Radiation Measurements*, **37**, 441-449.

Jensen, H. E. and Prescott, J. R. (1983). The thick-source alpha particle counting technique: comparison with other techniques and solutions to the problem of overcounting. *PACT*, **9**, 25-35.

Klein, R. G. (1974). Environment and subsistence of prehistoric man in the southern Cape Province, South Africa. *World Archaeology*, **5**, 249-284.

Lamothe, M., Balescu, S. and Auclair, M. (1994). Natural IRSL intensities and apparent luminescence ages of single feldspar grains extracted from partially bleached sediments. *Radiation Measurements*, **23**, 555-562.

Leakey, L. S. B. and Solomon, J. D. (1929). East African archaeology. *Nature*, **124**, 9.

Libby, W. F., Anderson, E. C. and Arnold, J. R. (1949). Age determination by radiocarbon content: world wide assay of natural radiocarbon. *Science*, **109**, 227-208.

Malan, B. D. (1952). In *Proceedings of the Pan-African Congress on Prehistory, 1947* Philosophical Library, New York.

Mason, R. J. (1962). *Prehistory of the Transvaal: a record of human activity*, Witwatersrand University Press, Johannesburg.

Mason, R. J. (1969). Tentative interpretations of new radiocarbon dates for stone artefact assemblages from Rose Cottage Cave, O.F.S. and Bushman Rock Shelter, Transvaal. *South African Archaeological Bulletin*, **24**, 57-59.

Mason, R. J. (1989). *South African Archaeology 1922-1988: Archaeological Research Unit*, University of the Witwatersrand, Johannesburg.

McCormac, F. G., Hogg, A. G., Blackwell, P. G., Buck, C. E., Higham, T. F. G. and Reimer, P. J. (2004). SHCAL04 Southern Hemisphere Calibration, 0-11.0 CAL KYR BP. *Radiocarbon*, **46**, 1087-1092.

McFee, C. J. and Tite, M. S. (1994). Investigations into the thermoluminescence properties of single quartz grains using an imaging photon detector. *Radiation Measurements*, **23**, 355-360.

Mejdahl, V. (1979). Thermoluminescence dating: beta-dose attenuation in quartz grains. *Archaeometry*, **21**, 61-73.

Mejdahl, V. (1985). Thermoluminescence dating of partially bleached sediments. *Nuclear tracks*, **10**, 4-6.

Milankovitch, M. (1941). Canon of Insolation and the Ice Age Problem. *Royal Academy of Serbia*, **133**, 633.

Miller, G. H., Beaumont, P. B., Deacon, H. J., Brooks, A. S., Hare, P. E. and Jull, A. J. T. (1999) Earliest modern humans in South Africa dated by isoleucine epimerization in ostrich eggshell. *Quaternary Science Reviews*, **18**, 1537-1548.

Mitchell, P. J. (1994) Understanding the MSA/LSA transition: the pre-20 000 BP assemblages from new excavations at Sehonghong rock-shelter, Lesotho. *Southern African Field Archaeology*, **3**, 15-25.

Mitchell, P. J., Parkington, J. E. and Wadley, L. (1998). A tale from three regions: The archaeology of the Pleistocene/Holocene transition in the western Cape, the Caledon Valley and the Lesotho Highlands, southern Africa. *Quaternary International*, **49/50**, 105-115.

Murray, A. S. and Aitken, M. J. (1988). Analysis of low-level naturally occurring radioactivity in small samples for use in thermoluminescence dating using high resolution gamma spectrometry. *International Journal of Applied Radiation Isotopes*, **39**, 145-158.

Murray, A. S. and Mejdahl, V. (1999). Comparison of regenerative-dose single-aliquot and multiple-aliquot (SARA) protocols using heated quartz from archaeological sites. *Quaternary Science Reviews (Quaternary Geochronology)*, **18**, 223-229.

Murray, A. S. and Olley, J. M. (2002). Precision and accuracy in the optically stimulated luminescence dating of sedimentary quartz: a status review. *Geochronometria*, **21**, 1-16.

Murray, A. S. and Roberts, R. G. (1998). Measurement of the equivalent dose in quartz using a regenerative-dose single aliquot protocol. *Radiation Measurements*, **29**, 503-515.

Murray, A. S., Roberts, R. G. and Wintle, A. G. (1997). Equivalent dose measurement using a single aliquot of quartz. *Radiation Measurements*, **27**, 171-184.

Murray, A. S. and Wintle, A. G. (1999a). Isothermal decay of optically stimulated luminescence in quartz. *Radiation Measurements*, **30**, 119-125.

Murray, A. S. and Wintle, A. G. (1999b). Sensitisation and stability of quartz OSL: Implications for interpretation of dose-response curves. *Radiation Protection Dosimetry*, **84**, 427-432.

Murray, A. S. and Wintle, A. G. (2000). Luminescence dating of quartz using an improved Single-Aliquot Regenerative-dose protocol. *Radiation Measurements*, **32**, 57-73.

Murray, A. S. and Wintle, A. G. (2003). The single-aliquot regenerative-dose protocol: potential for improvements in reliability. *Radiation Measurements*, **37**, 377-381.

Pillans, B., Chappel, J. and Naish, T. R. (1998). A review of the Milankovitch climate beat: template for Plio-Pleistocene sea-level changes and sequence stratigraphy. *Sedimentary Geology*, **122**, 5-21.

Plug, I. and Engela, R. (1992). The macrofaunal remains from recent excavations at Rose Cottage Cave, Orange Free State. *South African Archaeological Bulletin*, **47**, 16-25.

Prescott, J. R. and Hutton, J. T. (1994). Cosmic ray contributions to dose rates for luminescence and ESR dating: large depths and long-term time variations. *Radiation Measurements*, **23**, 497-500.

Roberts, R. G., Bird, M., Olley, J., Galbraith, R. F., Lawson, E., Laslett, G., Yoshida, H., Jones, R., Fullagar, R. L., Jacobsen, G. and Hua, Q. (1998).

Optical and radiocarbon dating Jinmium rock shelter in northern Australia. *Nature*, **393**, 358-362.

Roberts, R. G., Galbraith, R. F., Olley, J., Yoshida, H. and Laslett, G. (1999). Optical dating of single and multiple grains of quartz from jinmium rock shelter, northern Australia: Part II, Results and implications. *Archaeometry*, **41**, 365-395.

Roberts, R. G., Spooner, N. A. and Questiaux, D. G. (1994). Palaeodose underestimates caused by extended-duration preheats in the optical dating of quartz. *Radiation Measurements*, **23**, 647-653.

Scott, L. (1989). Late Quaternary vegetation history and climatic change in the eastern Orange Free State, South Africa. *South African Journal of Botany*, **55**, 107-116.

Scott, L., Anderson, J. M. and Anderson, H. (1997). In *The vegetation of Southern Africa* (Eds, Cowling, R. M. and Richardson, D.) Cambridge University Press, Cambridge.

Scott, L., Steenkamp, M. and Beaumont, P. B. (1995). Palaeoenvironmental conditions in South Africa at the Pleistocene-Holocene transition. *Quaternary Science Reviews*, **14**, 937-947.

Singer, R. and Wymer, J. (1982). *The Middle Stone Age at Klasies River Mouth in South Africa*, University of Chicago Press, Chicago.

Spooner, N. A., Prescott, J. R. and Hutton, J. T. (1988). The effect of illumination wavelength on the bleaching of the thermoluminescence (TL) of quartz. *Quaternary Science Reviews*, **7**, 325-329.

Stokes, S. (1992). Optical dating of young (modern) sediments using quartz: results from a selection of depositional environments. *Quaternary Science Reviews*, **11**, 153-159.

Stokes, S., Colls, A. E. L., Fattahi, M. and Rich, J. (2000). Investigations of the performance of quartz single aliquot D_e determination procedures. *Radiation Measurements*, **32**, 585-594.

Stokes, S., Ingram, S., Aitken, M. J., Sirocko, F., Anderson, R. and Leuschner, D. (2003). Alternative chronologies for Late Quaternary (Last Interglacial-Holocene) deep sea sediments via optical dating of silt-sized quartz. *Quaternary Science Reviews*, **22**, 925-941.

Stuiver, M. and Polach, A. (1977). Discussion: Reporting of ^{14}C Data. *Radiocarbon*, **19**, 355-363.

Stuiver, M., Reimer, P. J. and Braziunas, T. F. (1998a). High-precision radiocarbon age calibration for terrestrial and marine samples. *Radiocarbon*, **40**, 1127-1151.

Stuiver, M., Reimer, P. J., Bard, E., Beck, J. W., Burr, G. S., Hughen, K. A., Kromer, B., McCormac, G., van der Plicht, J. and Spurk, M. (1998b). IntCal98 radiocarbon age calibration, 24,000-0 cal BP. *Radiocarbon*, **40**, 1041-1083.

Talma, A. S. and Vogel, J. C. (1992). Late Quaternary Palaeotemperatures derived from a speleothem from Cango Cave, Cape Province, South Africa. *Quaternary Research*, **37**, 203-213.

Talma, A. S. and Vogel, J. C. (1993). A simplified approach to calibrating ^{14}C dates. *Radiocarbon*, **35**, 317-322.

Thorp, C. R. (1997). The indigenous ceramics from Rose Cottage Cave and their place in the regional ceramic sequence. *South African Journal of Science*, **93**, 465-470.

Thorp, C. R. (2000). *Hunters-gatherers and farmers: an enduring frontier in the Caledon Valley, South Africa*, British Archaeological Reports, Oxford.

Tribolo, C. (2003). Apport des methodes de la luminescence a la chronologie des techno-facies du Middle Stone Age associes aux premiers hommes modernes du Sud De L'Afrique. D Phil: L'Universite Bordeaux I.

Tyson, P. D., Odada, E. O. and Partridge, T. C. (2001). Late Quaternary environmental change in southern Africa. *South African Journal of Science*, **97**, 139-150.

Tyson, P. D. and Partridge, T. C. (2000). Evolution of Cenozoic climates. In *The Cenozoic of Southern Africa*(Eds, Partridge, T. C. and Maud, R. R.) Oxford University Press, New York, pp. 371-387.

Van der Plicht, J., Beck, J. W., Bard, E., Baillie, M. G. L., Blackwell, P. G., Buck, C. E., Friedrich, M., Guilderson, T. P., Hughen, K. A., Kromer, B., McCormac, F. G., Bronk Ramsey, C., Reimer, P. J., Remmele, S., Richards, D. A., Southon, J. R., Stuiver, M. and Weyhenmeyer, C. E. (2004). NOTCAL04 – Comparison/Calibration ¹⁴C records 26-50 CAL KYR BP. *Radiocarbon*, **46**, 1225-1238.

Van Zinderen Bakker, E. (1976). The evolution of late Quaternary palaeoclimates of southern Africa. *Palaeoecology of Africa*, **9**, 160-202.

Vogel, J. C. (1985). Further attempts at dating the Taung Tufas. In *Hominid Evolution*(Ed, Tobias, P. V.) Alan R. Liss, New York, pp. 189-194.

Vogel, J. C. (2000). Radiometric dates for the Middle Stone Age in South Africa. In *Humanity from African Naissance to Coming Millennia*(Eds, Tobias, P. V., Raath, M. A., Moggi-Cecchi, J. and Doyle, G. A.) University of Florence Press, Florence, pp. 261-268.

Vogel, J. C. and Beaumont, P. B. (1972a). Revised radiocarbon chronology for the Stone Age in South Africa. *Nature*, **237**, 50-51.

Vogel, J. C. and Beaumont, P. B. (1972b). On a new radiocarbon chronology for Africa south of the equator. *African Studies*, **30**, 63-89.

Wadley, L. (1991). Rose Cottage Cave: Background and a preliminary report on the recent excavations. *South African Archaeological Bulletin*, **46**, 125-130.

Wadley, L. (1995). Review of dated Stone Age sites recently excavated in the eastern Free State, South Africa. *South African Journal of Science*, **91**, 574-579.

Wadley, L. (1996). The Robberg levels of Rose Cottage Cave: technology, environments and spatial analysis. *South African Archaeological Bulletin*, **51**, 64-74.

Wadley, L. (1997). Rose Cottage Cave: archaeological work 1987 to 1997. *South African Journal of Science*, **93**, 439-444.

Wadley, L. (2000). The early Holocene layers of Rose Cottage Cave, eastern Free State: technology, spatial patterns and environment. *South African Archaeological Bulletin*, **55**, 18-31.

Wadley, L., Esterhuysen, A., B and Jeannerat, C. (1992). Vegetation changes in the eastern Orange Free State: the Holocene and later Pleistocene evidence from charcoal studies at Rose Cottage Cave. *South African Journal of Science*, **88**, 558-563.

Wadley, L. and Harper, P. (1989). Rose Cottage Cave revisited: Malan's Middle Stone Age collection. *South African Archaeological Bulletin*, **44**, 23-32.

Wadley, L. and Vogel, J. C. (1991). New dates from Rose Cottage Cave, Ladybrand, eastern Orange Free State. *South African Journal of Science*, **87**, 605-607.

Wadley, L. and Jacobs, Z. (2004). Sibudu Cave, KwaZulu-Natal: Background to the excavations of Middle Stone Age and Iron Age occupations. *South African Journal of Science*, **100**, 145-151.

Wallinga, J., Murray, A. S., Duller, G. A. T. and Törngvist, T. E. (2001). Testing optically stimulated luminescence dating of sand-sized quartz and feldspar from fluvial deposits. *Earth and Planetary Science Letters*, **193**, 617-630.

Williamson, B. S. (1997). Down the microscope and beyond: microscopy and molecular studies of stone tool residues and bone samples from Rose Cottage Cave. *South African Journal of Science*, **93**, 458-464.

Wintle, A. G. (1997). Luminescence Dating: Laboratory Procedures and Protocols. *Radiation Measurements*, **27**, 769-817.

Wintle, A. G. (1999). Optical dating in southern Africa. *South African Journal of Science*, **95**, 181-185.

Wintle, A. G. and Dijkmans, J. W. A. (1988). Dose rate comparisons of sands for thermoluminescence dating. *Ancient TL*, **6**, 15-17.

Wintle, A. G. and Murray, A. S. (1998). Towards the development of a preheat procedure for OSL dating of quartz. *Radiation Measurements*, **29**, 81-94.

Wintle, A. G. and Murray, A. S. (1999). Sensitivity changes in quartz. *Radiation Measurements*, **30**, 107-118.

Woodborne, S. and Vogel, J. C. (1997). Luminescence dating at Rose Cottage Cave: A progress report. *South African Journal of Science*, **93**, 467-470.

Zimmerman, J. (1971). The radiation-induced increase of thermoluminescence sensitivity of fired quartz. *Journal of Physics C: Solid State Physics*, **4**, 3277-3291.

Zöller, L. and Pernicka, E. (1989). A note on overcounting in alpha counters and its elimination. *Ancient TL*, **7**, 11-13.